



HAL
open science

Subduction of oceanic lithosphere in the Alps: Selective and archetypal from (slow-spreading) oceans

Philippe Agard

► **To cite this version:**

Philippe Agard. Subduction of oceanic lithosphere in the Alps: Selective and archetypal from (slow-spreading) oceans. *Earth-Science Reviews*, 2021, 214, pp.103517. 10.1016/j.earscirev.2021.103517 . insu-03402292

HAL Id: insu-03402292

<https://insu.hal.science/insu-03402292>

Submitted on 13 Feb 2023

HAL is a multi-disciplinary open access archive for the deposit and dissemination of scientific research documents, whether they are published or not. The documents may come from teaching and research institutions in France or abroad, or from public or private research centers.

L'archive ouverte pluridisciplinaire **HAL**, est destinée au dépôt et à la diffusion de documents scientifiques de niveau recherche, publiés ou non, émanant des établissements d'enseignement et de recherche français ou étrangers, des laboratoires publics ou privés.



Distributed under a Creative Commons Attribution - NonCommercial 4.0 International License

1
2 **Subduction of oceanic lithosphere in the Alps:**
3 **selective and archetypal from (slow-spreading) oceans**

4
5 P. Agard

6
7 ¹Sorbonne Université, CNRS-INSU, Institut des Sciences de la Terre Paris,
8 ISTeP UMR 7193, F-75005 Paris

9
10
11
12 **Abstract**

13 *The Alps are amongst the best subduction archives in the world, with abundant*
14 *blueschists and eclogites preserving fragments of mantle, gabbros, thinned continental*
15 *margin and pelagic sediments partly within their pre-collisional architecture. But to what*
16 *extent is the Alpine record representative of the subduction of oceanic lithosphere*
17 *worldwide? What is its significance, merits and limits for understanding subduction (and*
18 *exhumation) dynamics? This contribution shows that this record is neither exceptional nor*
19 *atypical but rather exemplifies the fate of relatively short-lived and small, slow-spreading and*
20 *slowly closing North Atlantic-type oceans (in this case a ~400-700 km-wide domain closed*
21 *over 60 Ma, at ~1 cm/a), whose subducting slabs do not reach below the Mantle Transition*
22 *Zone. Subducted fragments experienced conditions typical of mature subduction worldwide*
23 *and show no sign of significant tectonic overpressure. Contrasts in rock recovery with time*
24 *and space outline distinct subduction dynamics. During the first half of the subduction lifetime*
25 *(~30 Ma), no subducted oceanic fragments were recovered. A marked difference is observed*
26 *between metasediment- and mafic/ultramafic-dominated units (S and MUM units).*
27 *Underplating of S units took place intermittently and preferentially at ~30-40 km depth. The*
28 *MUM units of the Western Alps deeply subducted to ~80 km were only recovered late, i.e.*
29 *within a few Ma at most before continental subduction and initially lied close to the margin. At*
30 *the scale of the orogen, the recovery of subducted fragments allows to recognize four distinct*
31 *sectors and demonstrates a strong influence of initial margin architecture and/or continental*
32 *subduction. Whilst typical of subduction zone thermal regimes, the subduction archive*
33 *appears to selectively preserve slow-spreading oceans and/or hyperextended margins.*

37 **1. Introduction: what sort of 'oceanic' subduction in the Alps?**

38

39 Subduction of oceanic lithosphere into the mantle is a key driver of plate
40 tectonics (Forsyth and Uyeda, 1975; Ricard et al., 1993; Conrad and Lithgow-
41 Bertelloni, 2002; Coltice et al., 2019) and a major seismic and volcanic hazard.
42 Understanding processes acting along the subduction plate boundary, such as
43 mechanical coupling or fluid migration, is a prerequisite for elucidating subduction
44 dynamics, element and fluid transfer to subarc depths or risk assessment (e.g.,
45 Stern, 2002 and references therein).

46 The subduction of oceanic lithosphere (coined as 'oceanic subduction' in the
47 following) mostly happens at depths beyond reach for sampling and observation.
48 Basic geometries are only accessible down to a few km by seismic imaging (e.g.,
49 Calahoranno et al., 2008; Shillington et al., 2015); monitoring of displacements and
50 earthquakes provides limited time series (typically 1-100 yrs; Chlieh et al., 2011;
51 Bedford et al., 2013); interpretation of geophysical measurements is commonly
52 equivocal when assessing material behavior and constraining rheology (e.g., Vp/Vs
53 ratios and lithology: Audet and Burgmann, 2014; magnetotelluric data and fluids:
54 Wannamaker et al., 2014). A complementary approach is to use samples exhumed
55 from fossil subduction zones (e.g., Jolivet et al., 2003; Chopin, 2003; Bebout, 2007),
56 which mostly originate from the downgoing plate (or 'slab'; Agard et al., 2018).

57 The Alps is one of the best such locations worldwide: subducted remnants
58 (blueschists and eclogites) are comparatively abundant and well-preserved (Goffé et
59 al., 2004); metamorphic reworking of these remnants by later collision has been only
60 moderate, except in some parts of the Central Alps; active topography makes up for
61 many good exposures (Sternai et al., 2019). Two centuries of detailed structural
62 investigations have shown, in addition, that major units and paleogeographic
63 domains have not been tremendously offset with respect to former convergence
64 directions (e.g., Schmid et al., 2017). The Alpine belt is moreover small enough that
65 its whole structure can be envisioned in 3D and lateral variations be investigated in
66 tight connection to geophysical imaging (e.g., Schmid and Kissling, 2000; Hétyenyi et
67 al., 2018; Kästle et al., 2019). Alpine subducted fragments thus seem ideal probes to
68 study deep subduction processes, or to reconstruct the initial subduction geometry.

69 The Alps are in fact intimately associated with the birth of subduction ideas
70 (Ampferer and Hammer, 1911), and one Alpine study even coined the term (Amstutz,

71 1951; White et al., 1970). Effective recognition of past oceanic subduction in the Alps
72 came from petrological investigations ~50 years ago, shortly after the advent of plate
73 tectonics. Building on studies conducted in the Western United States, early authors
74 associated the presence of relict metamorphic minerals making up blueschists and
75 eclogites (e.g., glaucophane, lawsonite, sodic pyroxene) to former subduction (Ernst,
76 1971, 1975; Dal Piaz et al., 1972; Michard, 1977; Dal Piaz and Ernst, 1978).

77 The search for deeply buried rocks, yet maintained relatively cold, i.e.
78 equilibrated under high pressure low temperature conditions (HP-LT), intensified in
79 the 80s (e.g., Goffé and Chopin, 1986; Pognante and Kienast, 1987) and culminated
80 with the discovery of coesite in continent-derived fragments, which revealed the
81 existence of deep continental subduction (Chopin, 1984). A tectono-metamorphic
82 overview of the Alps was published in 2004 (Handy and Oberhänsli, 2004;
83 Oberhänsli and Goffé, 2004) and partly updated a few years later (Bousquet et al.,
84 2008; Berger and Bousquet, 2008; Agard et al., 2009. Beltrando et al., 2010;
85 Bousquet et al. 2012).

86 Lithostratigraphic and petrological studies have shown, in parallel, that these
87 subducted remnants once belonged to a slow-spreading ocean (Lemoine et al.,
88 1970, 1984, 1987; Lagabriele and Cannat, 1990) whose margins are relatively well-
89 preserved (Manatschal and Müntener, 2009; Mohn et al., 2011, 2012; Lagabriele et
90 al., 2015). Paleogeographic reconstructions (Dercourt et al., 1986; Stampfli and
91 Marchant, 1997; Vissers et al., 2013; van Hinsbergen et al., 2020) and tomographic
92 studies investigating the presence, number and polarity of slabs, or potential tear
93 faults and slab breakoff events (Lippitsch et al., 2003; Handy et al., 2010; Kästle et
94 al., 2019), place important constraints on the subduction history (Handy et al., 2010).

95 But to what extent is the Alpine example representative of subduction dynamics
96 worldwide? Subduction of the Alpine ocean is special in a number of ways: a
97 relatively small ~500 km wide domain characterized by Atlantic type, slow-spreading
98 oceanic lithosphere disappeared between Europe and Adria, leaving no volcanic arc
99 behind and trench sediments quite different from Peri-Pacific subduction zones
100 today.

101 How much and what sort of 'oceanic subduction' prevailed in the Alps? Has the
102 picture changed since the 2004 overview (Handy and Oberhänsli, 2004; Berger and
103 Bousquet, 2008)? While many studies have improved our understanding of
104 subduction processes, some issues still need clarification and/or new areas of

105 contention have emerged (i.e., the possibility of tectonic overpressures, the issue of
106 representativity, processes of mélangé formation or the role of tectonic inheritance;
107 Balestro et al., 2015; Yamato and Brun, 2017; Luisier et al., 2019; Moulas et al.,
108 2019; McCarthy et al., 2018).

109 The aim of the present study is to evaluate what is left of the Alpine oceanic
110 lithosphere, what the Alpine record tells us about subduction and/or exhumation
111 dynamics, to assess major differences along the belt and the role of tectonic
112 inheritance and examine the new insights gained over the last decade on processes
113 acting along the plate interface (e.g., report of fossil earthquakes, fingerprinting of
114 fluid-rock interactions). The ensuing, short-lived continental subduction is only
115 mentioned here to the extent it affected the fate of subducted oceanic fragments.

116

117

118 **2. Petrological and geodynamic context**

119

120 Oceanic fragments bearing diagnostic subducted-related HP-LT mineral
121 assemblages are found within the core of the entire Alpine orogen, from the Ligurian
122 Alps to the Rechnitz window, from Genova to Vienna (Fig. 1). They are found in the
123 Liguro-Piemont and Valais domains (Upper and Lower Penninic, respectively), two
124 former oceanic domains merging to the east but separated in the Western and
125 Central Alps by a continental fragment (Briançonnais, or 'Middle-Penninic'; see Fig. 1
126 for the definition of Western, Central and Eastern Alps used here). The schematic
127 cross-section illustrates the structural organization of the major paleogeographic
128 domains recognized in the belt, from the Austro-Alpine units on top to the European
129 units below (Fig. 1b). A detailed account of the architecture of the Alps or of the
130 evolution of ideas on the Alpine orogeny is beyond the scope of the present study
131 (e.g., for a selective 'tour': Argand, 1924; Debelfmas and Lemoine, 1970; Tricart,
132 1984; Froitzheim et al., 1996; Stampfli et al., 1998; Rosenbaum & Lister, 2005;
133 Schmid et al., 2004, 2017; Nagel, 2008; Manzotti et al., 2014).

134

135

136 *2.1. Evidence for subduction of oceanic lithosphere*

137

138 Owing to its importance for characterizing the subduction of oceanic lithosphere,
139 a brief outline of HP-LT metamorphic rocks is given here (see chapter 3 for details)
140 before recalling available first-order paleogeographic and geodynamic constraints.

141 As noted by Dal Piaz and Ernst (1978), Alpine subducted oceanic fragments are
142 dominated by 'Mesozoic calc-schists, greenstones and serpentized peridotites'.
143 Subduction of such rocks, deeply buried under cool conditions, produces a distinctive
144 metamorphic mineralogy, e.g., lawsonite, sodic clinopyroxene ('omphacite'), blue
145 amphibole (glaucofan and 'crossite'), garnet, in metamafic rocks; ferro-magnesian
146 carpholite, lawsonite, chloritoid, garnet, talc, coesite in metasedimentary rocks;
147 antigorite, titanite-clinohumite, titanite-chondrodite in metaperidotites. Noteworthy, the
148 names antigorite and eclogite, now commonly associated with HP-LT environments,
149 were born in the Alps (Hauy, 1822; Godard, 2001).

150 Following early reports of HP-LT metamorphism in the Alps (e.g., Kienast and
151 Velde, 1970; Dal Piaz et al., 1972; Goffé et al., 1973), a first overview of their
152 mineralogy and distribution was provided forty years ago (26th Int. Geol. Congress;
153 Saliot et al., 1980). It was soon realized that, in the case of the Western Alps, the
154 intensity of HP-LT metamorphism increases towards the southeast. This distribution
155 of metamorphosed oceanic units in the Western Alps, from blueschist to transitional
156 blueschist-eclogite to eclogite facies (Fig. 2b), advocates for southeast-directed
157 subduction of oceanic lithosphere below the Adriatic plate. The same fossil
158 subduction zone is exposed in the Central and Eastern Alps, indicating subduction
159 below the Austroalpine and South Alpine domains; Fig. 1c). It is therefore relatively
160 easy to bridge the gap, geometrically, between the present-day architecture and the
161 subduction history (compare Figs. 1b and 1c).

162 A distinct record of late Cretaceous intracontinental subduction, unrelated to the
163 closing of the Alpine ocean, is documented in the Eastern Alps through volumetrically
164 small HP-LT remnants in the Saualpe, Koralpe and Porhoje (Fig. 1a). These reached
165 peak burial between 105-90 Ma (Froitzheim et al., 1996; Miller and Thöni, 1997;
166 Thöni, 1999; Faryad and Hoinkes, 2003; Stüwe and Schuster 2010). In the broader
167 Alpine region, Jurassic high pressure metamorphism is also found in the Western
168 Carpathians and the Dinarides, where it is generally thought to result from the
169 closure of the westward closing westernmost sector of the Neotethys, the
170 Vardar/Meliata/Sava ocean (Stampfli and Borel, 2002; van Hinsbergen et al., 2020;
171 Schmid et al. 2020, see § 2.3).

172

173

174 *2.2. Oceanic material: types and peculiarities*

175

176 Sedimentary and magmatic features show that the Liguro-Piemont and Valais
177 domains were small ocean basins (Auzende et al., 1983; Lemoine et al., 1986)
178 characterized by extensive ocean-continent transition domains (OCT; e.g., in the
179 Central Alps: Err-Plata; Manatschal and Nievergelt, 1997; Mohn et al., 2011), with a
180 series of larger continental fragments in between (e.g., from the largest to the
181 smallest: Briançonnais, Sesia Zone, Emilius, Pilonnet; Dal Piaz et al., 2001; Manzotti
182 et al., 2014). Information from lithostratigraphy, paleogeography, magmatic petrology
183 and kinematics (§ 2.3) is provided in figure 3. Figure 3a combines these data into a
184 schematic view of the initial status of the Alpine domain prior to subduction (key
185 locations as in Figs. 1a and 2).

186

187

188 *2.2.1. Sedimentary cover: lithostratigraphic constraints*

189 Systematic lithostratigraphic studies, mostly in the 1970s and 1980s, recognized
190 pre-rift (Triassic), syn-rift (early to mid-Jurassic) and post-rift series in the Liguro-
191 Piemont and Valais oceanic domains and their adjacent continental margins
192 (Lemoine et al., 1986). The two former types, overall carbonate-dominated, are found
193 on the stretched portions of the European and Adria margins, in the OCT domain and
194 in extensional allochthons (Fig. 3a). Post-rift sediments are found almost across the
195 entire domain, mainly as calcschists and flysch deposits, whereby it is often uncertain
196 which of these post-rift sediments were deposited on a truly oceanic substratum and
197 which on the adjacent continental margin. Unmetamorphosed, or little
198 metamorphosed equivalents are found in the Prealps (Fig. 1a; Gets and Simme
199 nappes; Ricou and Siddans, 1986; Stampfli et al., 1998) and in the Flysch nappes
200 (e.g., Winkler et al., 1985; Merle, 1982).

201 Sediments truly deposited on ophiolitic seafloor, which make up the Schistes
202 Lustrés and Bündnerschiefer complexes (Elter, 1971), comprise radiolarian cherts,
203 shales, pelagic limestones and calcschists (Figs. 4a-f). These pelagic metasediments
204 range from the Callovo-Oxfordian (e.g., De Wever and Caby, 1981) to the early
205 Paleocene but are volumetrically mostly Cretaceous in age (Fig. 3b; Caron, 1977;

206 Lemoine et al., 1984; Lemoine and Polino, 1984). Their average thickness prior to
207 subduction ranges between 200 and ~400 m (Lemoine et al., 1984; Lemoine and
208 Polino, 1984; Lemoine and Tricart, 1986; Michard et al., 1996).

209 They commonly exhibit syntectonic cm- to km-scale detrital intercalations (Figs.
210 4d,e; Tricart et al., 1982; Dumont et al., 1984; Lagabrielle et al., 1985), particularly in
211 Late Jurassic and Early Cretaceous beds (Elter, 1971; Tricart and Lemoine, 1991).
212 Ophiolitic pebbles or hm-scale fragments (Polino and Lemoine, 1984; Le Mer et al
213 1986) are common in oceanic metasediments (Balestro et al., 2014; Corno et al.,
214 2019), though not evenly distributed (see § 3). Large hm-/km-sized carbonate
215 (commonly Triassic in age; Tricart et al., 1982; Fig. 4g) or continental fragments
216 found within the Schistes Lustrés and Bündnerschiefer, in both the Liguro-Piemont
217 and Valais domains, mark the transition between the continent and the ocean (e.g.,
218 'Prepiemont' domain; Elter, 1971; Tricart et al., 1982; Tricart and Lemoine, 1986).
219 Large bodies are commonly interpreted as extensional allochtons from the stretched
220 continental margin (Beltrando et al., 2014 and references therein).

221 Flysch-type deposits represent the other main type of oceanic sediments (e.g.,
222 Helminthoid or Prättigau flyschs; Merle, 1982; Merle and Brun, 1984; Mueller et al.,
223 2020) and range from the late Cretaceous to the Paleocene (Trümpy, 1960, 2006).
224 They are interpreted as trench sediments and mark the existence of an accretionary
225 margin associated with oceanic subduction (see Fig. 6 of Handy et al., 2010 for a
226 recent compilation).

227 Alpine sediments are dominated by carbonates, calcschists and pelites,
228 commonly organic-rich (Fig. 4a). This feature appears largely specific to Tethyan
229 rocks, as opposed to the more 'mafic' metagraywackes from the circum-Pacific
230 (Maruyama et al., 1996). Present-day analogues of Alpine-type sediments are being
231 deposited in the Sunda region for example (see discussion in Epstein et al., 2019).

232

233

234 *2.2.2. Oceanic crust/lithosphere: mafic and ultramafic material*

235 'Ophiolitic' fragments of oceanic crust/lithosphere are relatively abundant in the
236 Liguro-Piemont domain (Fig. 2c) and sparser in the Valais domain. The Alpine
237 lithosphere was early on recognized as made of extensive amounts of exhumed
238 mantle and discontinuous patches of crust (Lagabrielle, 1987; Lemoine et al., 1987)
239 directly overlain by ophicarbonates and sediments (Fig. 4h; Tricart et al., 1982), with

240 noticeable differences between sections (Fig. 3b; e.g., Queyras and Monviso; Tricart
241 and Lemoine, 1991). These characteristics are at odds with the Penrose type
242 lithosphere (1972) exemplified by the Semail ophiolite (Nicolas, 1989).

243 The importance of mantle exhumation, asymmetric rifting, slow spreading Atlantic-
244 type lithosphere was acknowledged by Lemoine et al. (1986; for a historical
245 perspective see Lagabriele, 2009) and later authors (Lagabriele and Cannat, 1990;
246 Lagabriele and Lemoine, 1997; Cannat et al., 1997, 2009; Manatschal and
247 Müntener, 2009). Concepts of mantle exhumation and formation of oceanic core-
248 complexes in fact partly derive from Alpine examples (e.g., mega-mullions: Tricart
249 and Lemoine, 1986; mantle exhumation: Trommsdorff et al., 1993).

250 Peridotites are for the most part variably serpentized, partly refertilized abyssal
251 type lherzolites (Barnes et al., 2014), compositionally intermediate between
252 oceanic/asthenospheric and sub-continental mantle (e.g., Malenco, Central Alps;
253 Lanzo, Western Alps; McCarthy and Müntener, 2015; Picazo et al., 2016). Basalts
254 and gabbros show a typical MORB-type affinity (e.g., Chalot-Prat et al., 2003),
255 although ridge-type magmatism was probably limited in the Alpine ocean. Alpine
256 gabbros essentially cluster between ~165 and 150 Ma (Bortolotti and Principi, 2005;
257 Manatschal and Müntener, 2009).

258 Some (almost) unmetamorphosed fragments from the eastern Central Alps allow
259 to map out the OCT domain (e.g., Err-Plata; Froitzheim et al., 1996; Manatschal and
260 Nievergelt, 1997), identify oceanic core-complexes or the transition from initial
261 extension to necking and rifting/spreading stages (e.g., Mohn et al., 2011), assess
262 the paleogeographic position of some Alpine massifs (e.g., Tasna as stretched
263 margin to OCT on the Briançonnais side, and Err-Platta near Adria; Mohn et al.,
264 2012; Fig. 3) and assign them to specific portions of the seafloor (e.g., Chenaillet as
265 near mid-oceanic; Manatschal et al., 2011; Lagabriele et al., 2015). The comparison
266 between unmetamorphosed protoliths and those having experienced blueschist
267 and/or eclogite facies conditions may be used to study oceanic processes
268 (petrogenesis, interactions between magmatism and tectonics, hydrothermal
269 alteration) or disentangle the effects of subduction-related transformations, (e.g.,
270 Chalot-Prat et al., 2003; Bucher and Grapes, 2009; Tartarotti et al., 2011; Lafay et
271 al., 2013; see § 5).

272

273

274 *2.3. Geodynamic setting: boundary conditions for oceanic subduction*

275

276 Plate kinematics reconstructions (Dercourt et al., 1986; Dewey et al., 1989;
277 Stampfli et al., 1998; Rosenbaum et al., 2002; Handy et al., 2010; Vissers et al.,
278 2013; van Hinsbergen et al., 2020), though different in detail, place bounds on the
279 Alpine ocean in terms of size and duration:

280 — The Alpine oceanic was ~400-700 km wide (Stampfli et al., 1998; Vissers et
281 al., 2013; Fig. 3c) and comprised, in its southern part, the Valais domain to the west
282 and the Liguro-Piemont domain to the east, separated by the ~100-150 km wide
283 Briançonnais continental fragment (including its stretched Prepiemont or sub-
284 Briançonnais margins; Lemoine et al., 1986). The Liguro-Piemont domain was ~300-
285 400 km wide (Stampfli et al., 1998; e.g., their Fig. 14) and partly floored by refertilized
286 sub-continental mantle (Manatschal and Müntener, 2009; Picazo et al., 2016). The
287 SW branch of the Valais (hereafter termed Valaisan, for clarity) was 50-200 km wide
288 only, and represented a strongly stretched margin and/or OCT first affected by
289 Jurassic rifting. It lacked ophiolitic material except in portions (e.g., Internal Valais
290 Versoyen units) extended further during the early Cretaceous (> 130 Ma; Loprieno et
291 al., 2011). The NE portions of the Valais and Liguro-Piemont oceans were
292 respectively larger and smaller than their SW portions.

293 — Slow opening of the ocean occurred between 170 and ~120 Ma (< 2cm/a;
294 Vissers et al., 2013; Fig. 3d). The age cluster of the Liguro-Piemont gabbros (~165-
295 150 Ma) suggests that either subsequent magmatism was insignificant and/or that all
296 oceanic lithosphere formed between 150 and 120 Ma, be it 'normal' or slow-
297 spreading, was subducted. The Alpine seafloor did not resemble the thick, Pacific-
298 type crust with stratified 'ocean plate stratigraphy' (Kusky et al., 2014) but rather, in
299 terms of size and constitution, parts of the North Atlantic such as between Greenland
300 and Norway.

301 — The onset of subduction is poorly constrained and its locus even less so (see
302 Fig. 3a). It is usually dated by the deposition of the first flysch-type sediments. It is
303 considered to lie within 110-80 Ma, and may have started somewhat earlier in the
304 east (Trumpy, 1960; Lemoine et al., 1986; Wagreich, 2001; Handy et al., 2010). We
305 herein consider it to be ~100-95 Ma based on the presence of well-dated
306 Cenomanian-Turonian flysch (Stampfli et al., 1998). No subduction-related magmatic

307 arc formed in the Alps (Stampfli et al., 1998; McCarthy et al., 2018). Collision started
308 at 34-32 Ma in the Western Alps (Simon-Labric et al., 2009; Beltrando et al., 2009).

309 — Metamorphic ages associated with the subduction of oceanic lithosphere
310 range from Cretaceous to Eocene (Handy and Oberhänsli, 2004; Berger and
311 Bousquet, 2008). Most of them lie between 60 and 35 Ma. Some older (Cretaceous)
312 ages are presently disregarded as biased (by excess argon for example), while some
313 correspond to the paleogeographically distinct Eoalpine domain (Froitzheim et al.,
314 1996). Episodes of continental subduction are documented for the Sesia Zone (75-65
315 Ma), the Briançonnais and the Internal Basement Complexes (i.e., Monte Rosa,
316 Grand Paradiso and Dora Maira; ~42-35 Ma). Further details and their significance
317 are addressed below.

318 — Since 400-700 km of lithosphere (including the Briançonnais fragment; Vissers
319 et al., 2013) was subducted within ~60 Ma (from 100-95 to 40-35 Ma), the subduction
320 rate was ~1 cm/a (see also Schmid et al., 1997). Independent, rough petrological
321 constraints yield 0.5-1 cm/a (Lapen et al., 2003). A minimum of ~200-300 km of this
322 subduction was truly oceanic in the Liguro-Piemont domain (for a similar estimate:
323 Manzotti et al., 2014), although this amount varied along strike due to the obliquity of
324 Alpine subduction (Handy et al. 2010). It is plausible that the Alpine slab never
325 reached the 660 km mantle discontinuity and that slab dynamics, and any slab
326 retreat, was confined to small-scale convection (e.g., Royden and Faccenna, 2018).

327

328

329 **3. Oceanic fragments in the Western Alps: contrasting modes of subduction** 330 **and recovery**

331

332 Due to the absence of a strong collision-related metamorphic overprint, contrary
333 to parts of the Central Alps (Engi et al., 2004; Berger et al., 2005; Keller et al. 2005;
334 Fig. 2b), subducted HP-LT oceanic fragments are best preserved in the Western Alps
335 (Goffé et al., 2004). This metamorphic record is examined first and then compared to
336 that of the Central and Eastern Alps (§ 4). The Ligurian Alps and Corsica, which
337 share many similarities, are not addressed here except in passing.

338 Two main types of tectono-metamorphic units can be recognized (Figs. 5-9),
339 dominated either by metamorphosed pelagic sediments (i.e., calcschists of the
340 Schistes Lustrés and Bündnerschiefer), hereafter called S units, or by mafic and

341 ultramafic bodies with only minor calcschists (Lagabrielle and Cannat, 1990),
342 hereafter called MUM units. Their respective, partly separate spatial distribution over
343 the Western Alps (Figs. 2c, 7a-b) reveals that these initial lithological contrasts (§
344 2.2) were amplified by later tectonics. A similar divide is observed in Corsica (Vitale-
345 Brovarone et al., 2013 and references therein).

346 In the Cottian Alps (Fig. 7a-d), dominantly metasedimentary blueschist-facies
347 units are located to the west, whereas large, mainly eclogitic mafic and ultramafic
348 bodies crop out to the east, next to the continental Dora Maira massif (e.g.,
349 Rocciavre, Monviso; Fig. 2c). Despite large spatial variations, available cross-
350 sections (e.g., Deville et al., 1992; Fudral, 1996; Lardeaux et al., 2006), map
351 compilations and personal observations provide rough indications on the relative
352 proportions of sediment to mafic/ultramafic rocks, around ~20:1 in S units and ~1:5 in
353 MUM units.

354

355

356 *3.1. Metasedimentary dominated (S) units from the Liguro-Piemont ocean, Western* 357 *Alps*

358

359 From south to north, the main exposures are found in the Queyras, Cottian,
360 Maurienne (Deville et al., 1992) and in somewhat lesser volumes in the Combin (or
361 'Tsaté'; Marthaler and Stampfli, 1989; Fig. 2c). They comprise intensely folded
362 calcschists and rare but diagnostic marbles (e.g., Crête de la Taillante: Fig. 4f) with
363 minor fragments of oceanic crust/mantle (Fig. 4i). The latter are mostly ultramafic but
364 in places large mafic bodies also exist (Fig. 5b; e.g., in Queyras: Pelvas d'Abries, Bric
365 Bouchet; Tricart et al., 1982; Lagabrielle et al., 2015; in Platta; Mohn et al., 2012).
366 Tectonic patterns are characterized by a composite, flat lying to gently west-dipping
367 schistosity with stretching mineral lineations trending N090 to N110 on average
368 (Fudral, 1996; Agard et al., 2001). Structural patterns indicate protracted stretching
369 and deformation parallel to subduction movements (e.g., Caby, 1973; Platt et al.,
370 1989; Rosenbaum and Lister, 2005).

371

372 *3.1.1. Contrasting P-T conditions for metasedimentary-dominated units (SW Alps):*

373 Each region evidences stacking of distinct several km-long, hm- to km-thick
374 tectonic units separated into upper, middle and lower units, based on lithology and

375 metamorphic grade (e.g., Lagabriele, 1987; OP1/OP2 units of Pognante, 1991).
376 Three or four units are recognized depending on latitude and authors (Fig. 7c; Fudral,
377 1996; Polino et al., 2002; Barfety et al, 2006; Plunder et al 2012; Lagabriele et al.,
378 2015).

379 - Upper S unit: This lawsonite- and/or Fe-Mg-carpholite-bearing blueschist facies
380 unit (Fig. 5c-e) is well preserved in the Queyras and Cottian Alps, or as discrete
381 klippen in the Maurienne area (Fig. 4c). It is commonly pelitic and rich in organic
382 matter (Fig. 4a). Subtle m-hm scale lithological differences influence the nature
383 and/or proportion of HP-LT mineralogy (e.g., lawsonite abundance; Lefeuvre et al.,
384 2020). Large km-scale carbonate fragments of Prepiemont origin found close to the
385 Briançonnais (Fig. 4g; Tricart et al., 1982) suggest that this unit initially lied close to
386 the OCT domain, unless they represent an uppermost, dismembered unit on top of
387 the nappe stack. The upper S unit contains minor mafic/ultramafic fragments and/or
388 tectonic slivers made of serpentinites, blueschist facies lawsonite-glaucophane-
389 bearing metabasalts and metagabbros (Fig. 5e) and deerite-bearing metacherts
390 (e.g., Lago Nero unit; Martin and Polino, 1984). P-T estimates range between 1.1
391 GPa - 330°C and 1.4 GPa - 350°C (Figs. 7e,f).

392 - Middle S unit: This lawsonite- to epidote-blueschist facies unit commonly
393 represents more than 50% of the Schistes Lustrés complex (Fig. 4c,d). It is
394 dominated by calcareous schists and almost pure pelagic metacarbonates (e.g.,
395 Grande Sassièrè, or Charbonnel-Rocciamelone unit in the Maurienne; Fudral et al.,
396 1987). Most of the Combin exposures also belong to this unit. It locally contains
397 detrital material, both oceanic and continental in origin. Sheared metaophiolitic
398 material (mainly serpentinite) can be found as dismembered tectonic horizons,
399 preferentially at the base of the unit. Metapelitic horizons contain chloritoid (Fig. 5g,h)
400 and lawsonite pseudomorphs. Garnet is generally absent and epidote is found in the
401 warmest portions only. P-T estimates are mostly in the range 1.5-2 GPa and 370-
402 450°C (Fig. 7e).

403 - Lower S unit: This lowermost unit is located immediately above the Gran
404 Paradiso (Le Bayon et al., 2006) or Dora Maira internal basement complex (Chopin,
405 1981). It is made of metasediments locally rich in volcanic debris and cherts,
406 overlying an ophiolitic 'basement' or interleaved with substantial mafic bodies (Fig.
407 7d). Metamorphic grade is eclogitic or transitional between blueschist and eclogite
408 facies and characterized by variably retrogressed chloritoid ± garnet ± epidote

409 assemblages. P-T estimates are in the range 2-2.3 GPa and 470-550°C (Fig. 7e).
410 Whether this unit represents the former cover of mafic/ultramafic dominated units
411 such as the Rocciavre and Monviso units (Fig. 7b) or a separate unit remains unclear
412 (see § 3.2). It is considered as one single unit in Maurienne (Villaron–Gran Uia;
413 Fudral, 1996) and two distinct ones in Queyras (Lagabrielle et al., 2015).

414 Estimates of peak pressure and temperature experienced by these units align
415 along a consistent P-T gradient of ~ 8°C/km in a P-T diagram, assuming lithostatic
416 pressure (Agard et al., 2001; Figs. 7e, 9a). In the Cottian Alps, these three units are,
417 from bottom to top, the Pietre Verde, Albergian/Cerogne-Ciantiplagna and Lago Nero
418 units (Fig. 5a; Caron, 1977; Polino et al., 2002; Burrioni et al., 2003; Corno et al.,
419 2019). The spatially restricted, unmetamorphosed ~150 Ma mafic and ultramafic
420 dominated Chenaillet unit (Fig. 7d; Mével et al., 1978; Costa and Caby, 2001;
421 Manatschal et al., 2011) overlies the Lago Nero unit. All ocean-derived units were
422 originally thrust on top of the Briançonnais and Prepiemont cover or basement units
423 and remained there in places (e.g., Combin or Maurienne, north and south of Ambin;
424 Fig. 7c,d). Backfolding of the Briançonnais, associated with the Mischabel and/or
425 Vanzone early collisional stages (Argand, 1924; Ballèvre et Merle, 1993; Bucher et
426 al., 2003), which varies considerably in dip and intensity along strike, also emplaced
427 continent-derived sediments from the Briançonnais margin above oceanic units (e.g.,
428 Cottian Alp; Figs. 7a,c; e.g., Michard et al. 2004).

429

430 *3.1.2. Nappe stacking of the S units*

431 The Schistes Lustrés metasediments were scraped off their underlying oceanic
432 crust/mantle during subduction (Deville et al., 1992; Agard, 1999; Schwartz, 2000)
433 and represent a deep accretionary complex (Marthaler and Stampfli, 1989), as for the
434 Franciscan complex (Platt, 1986; Dumitru et al., 2010). The stacking of these
435 metasedimentary units partly coincides with lithostratigraphic contrasts: the
436 metapelitic-rich upper S unit is mostly made of early Cretaceous metasediments,
437 whereas the middle S unit is mostly made of late Cretaceous calcschists (Fig. 3a;
438 Lemoine & Tricart, 1986; Deville et al., 1992).

439 While most fossil accretionary complexes show preferential
440 accretion/underplating at 30-40 km depth, thus close to the upper plate Moho (Agard
441 et al., 2018; e.g.: Willner, 2005; Angiboust et al., 2014), this occurs across a larger
442 depth range in the southern Western Alps. A rather continuous evolution of P-T

443 conditions is indeed observed in the Queyras, Cottian and Maurienne regions, from
444 1.2-1.3 GPa-350°C to ~2.0 GPa-500°C, as exemplified by the progressive eastward
445 increase of the phengitic substitution in carpholite- or chloritoid-bearing assemblages
446 (Agard et al., 2001a,b; Figs. 7d,e), and the consistent P-T estimates from dm-sized
447 mafic bodies scattered in the Schistes Lustrés complex (Schwartz, 2000) or in the
448 vicinity of former extensional allochthons (Corno et al., 2019).

449 Despite the stacking of distinct tectonic units, maximum temperatures (Fig. 7c)
450 increase fairly regularly across the Queyras, Cottian (Agard et al., 2001a; Beyssac et
451 al., 2002; Schwartz et al., 2013) and Maurienne units (Gabalda et al., 2009; Plunder
452 et al., 2012): they are commonly lower than 400 °C for the upper unit, between 400
453 and 500 °C for the middle unit, and greater than 500 °C for the lower unit (Fig. 7f). A
454 more restricted range of temperatures is observed for the Schistes Lustrés complex
455 west of Grivola (Bousquet, 2008) or in the Combin area (mostly 420-550°C; Negro et
456 al., 2013; Angiboust et al., 2014a). This absence of major P-T gaps across the
457 distinct units argues for early stacking, before their main exhumation stage, since a
458 more irregular temperature pattern would be expected otherwise (Plunder et al.,
459 2012).

460 The age of peak burial of the Schistes Lustrés complex clusters between 55 and
461 62 Ma, at least for the middle and upper S units, although prograde deformation
462 accompanying burial was largely erased (Agard et al., 2002). Early exhumation was
463 accompanied by east-vergent relative movements while subduction was still active
464 (D2 stage, 45-40 Ma; Agard et al., 2001a, 2002; see also Ghignone et al., 2020).
465 This was followed, at ~40-37 Ma, by west-vergent exhumation, associated with
466 exhumation of the Monviso and Dora Maira units (D3 stage; Agard et al., 2001a;
467 Plunder et al., 2012; Angiboust et al., 2014a). Some early tectonic contacts, notably
468 between the lower and middle S units, were reactivated through locally extensional
469 exhumation shear zones in the Queyras or Combin (Fig. 5a,b; Pognante, 1991;
470 Ballèvre et al., 1990; Ballèvre and Merle, 1993; Schwartz et al., 2009; Lagabrielle et
471 al., 2015).

472 Conceivably, structurally upper units may have been underplated earlier
473 (Bachmann et al., 2009a,b; Dumitru et al., 2010; Plunder et al., 2012; Menant et al.,
474 2020). More in-situ ages and P-T constraints are nevertheless needed to reconstruct
475 the Alpine accretionary wedge and correlate (stacks of) units from the southern
476 Queyras to the northernmost Combin. To the west of Grivola, peak burial conditions

477 were estimated between 48 and 44 Ma (Bucher et al., 2003; Villa et al., 2014). Age
478 constraints in the Combin/Tsaté area cluster around 42 to 37 Ma, and show a
479 complex spatial distribution (Dal Piaz et al., 2001; Reddy et al., 2003). Diachronous
480 juxtaposition and underplating of material detached from 25-35 km depth along the
481 Alpine subduction interface was documented there (Angiboust et al., 2014a).

482

483

484 *3.2 Mafic and Ultramafic dominated (MUM) units, Western Alps*

485

486 Large, km- to 10 km-long portions of mafic/ultramafic MUM material representing
487 portions of the top of the Liguro-Piemont 'slab' (Fig. 1c) are exposed in Monviso (Fig.
488 6a), around Gran Paradiso, north and south of the Aosta valley (Fig. 2c), as well as in
489 the Ligurian Alps (Fig. 1a; e.g., Beiga and Erro-Tobio units; Scambelluri et al., 1995)
490 or Corsica (Vitale-Brovarone et al., 2013). Such large-scale fragments are seldom
491 recovered from the Valais ocean. As for the Schistes Lustrés, these oceanic
492 fragments are composite, usually very deformed and crosscut by a number of shear
493 zones (Fig. 6a). Metasediments are subordinate and, although large variations exist
494 within tectonic slices or from massif to massif, the relative proportion of mafic and
495 ultramafic material is in first approximation roughly equivalent (Angiboust et al.,
496 2009). The description below illustrates the diversity of the MUM units (Figs. 6b-d;
497 further magmatic-related details in: Manatschal and Müntener, 2009; Beltrando et al.,
498 2014; Lagabrielle et al., 2015) and outlines some of their most important features,
499 from north to south.

500

501 — *Zermatt-Saas (N. Aosta valley):*

502 This MUM unit is well-exposed in Val Tournanche and Val d'Ayas (Italy), or near
503 Täsch, Pfulwe and Saas (Switzerland). These occurrences are characterized by a
504 number of hm- to km-scale tectonic duplications (Angiboust and Agard, 2010). The
505 Zermatt-Saas unit is generally underlying the Schistes Lustrés Combin units
506 (Ballèvre et Merle, 1993; Groppo et al., 2009), but the two units are tectonically
507 interleaved in places due to large-scale post-nappe emplacement refolding and/or
508 backthrusting (e.g., Ellero and Loprieno, 2017). Metamorphosed mafic rocks
509 comprise variably retrogressed eclogitic minerals, most commonly garnet,
510 clinopyroxene ± lawsonite pseudomorphs, glaucophane, talc, chloritoid depending on

511 the exact protolith chemistry and prior hydrothermal alteration on the seafloor (Fig.
512 6b,e; Angiboust and Agard, 2010). In particular, abundant, several cm-long lawsonite
513 pseudomorphs around former pillows, preserving evidence of seafloor hydration, are
514 found around Zermatt (e.g., near Britannia Hütte or Pfulwe pass; Figs. 6b,e).

515 Pressure and temperature estimates (by Raman spectroscopy of organic matter,
516 thermobarometry and thermodynamic modelling), were shown to be relatively
517 constant from Saas to south of the Aosta valley at ~2.5 GPa and 550°C (Angiboust et
518 al., 2009; Angiboust and Agard, 2010; Fig. 6b), consistent with earlier estimates for
519 the Zermatt area (Bucher et al., 2005; 2.8 GPa, 570°C). Similar conditions with
520 slightly higher temperature were inferred for the Allalin metagabbro (2.5 GPa, 600°C;
521 Bucher and Grapes, 2009) or some Valtournanche localities (2.55 GPa, 600°C;
522 Zanoni et al., 2016). In contrast, a small, hm-thick, 2 km² tectonic slice with coesite-
523 bearing metasediments indicative of higher, UHP conditions at ~2.8-3..2 GPa and
524 600°C (Reinecke, 1998; Groppo et al 2009; Frezzoti et al., 2011) was found in Lago
525 di Cignana (Reinecke, 1991, 1998; van der Klauw, 1997; Compagnoni and Rolfo,
526 2003). Nearby serpentinites hosting Ti-chondrodite indicate consistent with UHP
527 conditions (Luoni et al., 2018).

528 Based on Lu-Hf in garnet (Amato et al., 1999; Lapen et al., 2003; Skora et al.,
529 2015), Ar/Ar on phengite in garnet (Gouzu et al., 2006) and U/Pb on zircon (Rubatto
530 et al., 1998), most age constraints for peak burial cluster at 43 ± 4 Ma (see age
531 compilations in Berger and Bousquet, 2008; Rebay et al., 2018; Dragovic et al.,
532 2020), with indications for prograde growth around 49-48 Ma (Lapen et al., 2003;
533 Skora et al., 2015). One contrasting age at 65 Ma was obtained by Rebay et al.
534 (2018).

535

536 — *Avic (S. Aosta valley):*

537 Similar tectonic slices comprising horizons of mafic and ultramafic rocks are
538 found south of the Aosta valley (e.g., Val Clavalité, St Marcel; Angiboust and Agard,
539 2010). A remarkable, several km-long metaperidotite body with minor gabbros is
540 found in Monte Avic (Fig. 6c-d), where former oceanic structures are partly preserved
541 despite eclogite facies metamorphism (Tartarotti et al., 2011). Fewer P-T estimates
542 exist for the area (2.3 GPa, 545°C; Angiboust et al., 2009).

543 Below the Zermatt□Saas (MUM) unit and immediately overlying the Gran
544 Paradiso massif, the Grivola□Urtier unit (Dal Piaz et al., 2001; Tartarotti et al., 2019)

545 is made of metaflysch and calcschists envelopping blocks and slices of both mafic
546 and gneissic, continental derived material. This unit can be regarded as a former
547 OCT domain. In the Entrelor-Grivola unit, P-T conditions for MUM type slivers are 2.3
548 GPa, 550°C (Bousquet, 2008).

549

550 — *Rocciavre*:

551 The Rocciavre massif is a ~8 km long dominantly metagabbroic (gabbro-noritic)
552 massif surrounded by serpentinized peridotite, with Fe-Ti metagabbros showing
553 garnet-omphacite eclogitic parageneses similar to those found in Monviso (see
554 below). Pressure-temperature conditions, estimated prior to the advent of multi-
555 equilibrium techniques and thermodynamic modelling (Pognante 1991; Bouffette and
556 Caron, 1991), should however be reappraised. Given the similar mineralogy and
557 mineral compositions to other massifs, P-T conditions can be predicted to lie in the
558 range 2-2.5 GPa and 550°C ± 50°C.

559

560 — *Lanzo*

561 The Lanzo massif is a large, ~30 km long fragment of irregularly eclogitized
562 mantle. Whether this massif represents former sub-continental or oceanic mantle is
563 disputed. It was cut across by ~160 Ma dykes now eclogitized (Piccardo et al., 2010).
564 The massif was exposed on the seafloor as shown by the presence of thin sediment
565 horizons, ophicarbonates, and seafloor serpentinization (Lagabrielle et al., 1990;
566 Debret et al., 2013). It was subducted during Alpine subduction at around 55–46 Ma
567 (Rubatto et al., 2008). Metagabbros in metaperidotites, metasedimentary horizons
568 hosting kyanite-talc-chloritoid ± garnet assemblages and incipient antigorite de-
569 serpentinization indicate P-T conditions around 2–2.5 GPa and 550–620 °C (Kienast
570 and Pognante, 1988; Pelletier and Müntener, 2006; Debret et al., 2013). A similar
571 peridotite massif is found in the Ligurian Alps (Erro-Tobbio; e.g., Scambelluri et al.,
572 1995).

573

574 — *Monviso*

575 Since the seminal mapping of Lombardo (1978), the Monviso massif has been
576 extensively studied (Philipot, 1990; Cliff et al., 1998; Schwartz, 2000; Castelli et al.,
577 2002), particularly over the last decade (Groppo and Castelli, 2010; Angiboust et al.,

578 2011, 2012a,b; Locatelli et al., 2019a,b). A new map was recently published by
579 Locatelli et al. (2019a).

580 The Monviso ophiolitic massif contains two major units (Fig. 6a), the overturned
581 blueschist to eclogite facies Monviso unit on top with nicely preserved metapillows
582 (Fig. 6h), and the eclogitic Lago Superiore unit below. Both are dominantly made of
583 metaperidotites, metagabbros (mostly Mg-rich) and metabasalts (Lombardo, 1978).
584 In the 15 km long, 1.5-2 km-thick eclogitic Lago Superiore unit, one finds, from
585 bottom to top, a ~500m thick serpentinized basal peridotite unit (Gilio et al., 2020),
586 Mg-rich metagabbros, sills, dykes and a discontinuous layer of Fe-Ti metagabbros
587 hosting garnet, omphacite, abundant rutile (Fig. 6i), lawsonite pseudomorphs and
588 eclogite breccias (Fig. 8a,b). These are finally capped by metabasalts and a few
589 meters of metamorphosed calcschists at the very top.

590 The Lago Superiore unit is probably the most intact and best documented
591 eclogitized slab fragment reported so far in the world. Large-scale shear zones
592 formed prior to its detachment from the downgoing slab (e.g., Lower Shear Zone; Fig.
593 8c; Philippot and Kienast, 1989; Angiboust et al., 2011) host metagabbros brecciated
594 under eclogitic facies conditions, now mostly embedded in serpentinites, that
595 preserve evidence for brittle, possible seismic fracturing (Fig. 8d-f; Angiboust et al.,
596 2012a; Locatelli et al., 2019b). Progressive brecciation and fluid ingression (Locatelli
597 et al., 2019b), together with abundant omphacite veins (Spandler et al., 2011), allow
598 studying fluid migration pathways in the Lago Superiore unit (see chapter 5). P-T
599 estimates for this unit, around 2.6-2.7 GPa, 550-580°C (Locatelli et al., 2018 and
600 references therein), were reached ~46 Ma ago (46 ± 3 Ma; Monié and Philippot,
601 1989; Cliff et al., 1998; Rubatto and Hermann, 2003; Rubatto and Angiboust, 2015),
602 with indications for prograde growth around 49 Ma (Duchêne et al., 1997). A gap of
603 ~4-5 GPa and 70°C exists between the Lago Superiore and the overlying Monviso
604 unit (Angiboust et al., 2012a,b; Angiboust and Glodny, 2020). P-T conditions for the
605 latter unit (2.1 GPa, 480°C) resemble those of the lower and middle S units (Fig. 7e).

606

607 — Several general characteristics of the MUM units can be outlined:

608 (i) They show significant lateral variations in internal structure or in the amount
609 and type of crustal components, e.g. more metabasalts near Zermatt-Saas and more
610 Mg-rich metagabbros in Rocciavre and Monviso. However, nearly all MUM fragments
611 experienced strikingly similar P-T conditions, at 2.6 ± 0.2 GPa and $560^\circ\text{C} \pm 20^\circ\text{C}$ (Fig.

612 9b), except for the thin slice of the Cignana UHP unit. Another exception is the
613 Monviso sub-unit, which is transitional between blueschist and eclogite facies. These
614 P-T conditions align along the same P/T gradient as the Schistes Lustrés complex,
615 and that for mature subduction zones (Fig. 10; Agard et al., 2018).

616 (ii) Detailed tectonic mapping shows evidence for hm- to km-thick tectonic slices
617 with lithological continuities along several km (e.g., Zermatt-Saas Antrona, Avic;
618 Tartarotti et al., 2011) and km-thick bodies (in Monviso, Rocciavre, Lanzo). Some of
619 the pristine architecture of the top of the slab is still preserved, together with oceanic
620 structures (see also Beltrando et al., 2014; Fig. 8gd). This rules out the possibility
621 that the MUM units correspond to a large-scale mélange of rocks mixed up in a
622 subduction channel (as in early numerical models; Cloos, 1982; Gerya et al., 2002).
623 Local mélanges, at the m- to hm-scale, are inherited from sedimentary and/or
624 magmatic processes and reworked during subduction and exhumation (Fig. 8g;
625 Balestro et al., 2015; Tartarotti et al., 2017; Locatelli et al., 2018).

626 Observations nevertheless advocate for intense deformation, with duplications,
627 tectonic intercalations and shearing along the plate interface. This is shown by the
628 juxtaposition of km-long sub-units such as the Lago Superiore and Monviso units
629 (slab fragments with reverse polarity and contrasting P-T; Fig. 6a; Locatelli et al.,
630 2018) or the Bardonney and Broillot units (Ellero and Loprieno, 2017),
631 notwithstanding later complications during final exhumation and later Alpine
632 tectonics.

633 (iii) The age of HP (and UHP for Cignana) metamorphism of the MUM fragments
634 appears to be very restricted, with most ages falling in the range $\sim 45 \pm 3$ Ma (see the
635 compilation in Rebay et al., 2018; Fig. 9b). A more conservative value around 45 ± 5
636 Ma probably accounts for methodological uncertainties (e.g., Lu/Hf garnet ages of 40
637 or 46-52 Ma for the same type of samples near Zermatt-Saas; Amato et al., 1999;
638 Lapen et al., 2003; Skora et al., 2015). Lanzo might have reached peak burial slightly
639 before but ages overlap (52-46 Ma). Ages around 41-38 Ma are only found for
640 fragments located in the immediate vicinity of the Internal Basement complexes.

641 The Ligurian Alps evidence a similar tectonic organization (Messiga et al., 1995;
642 Federico et al., 2004; Vignaroli et al., 2009, 2010), with lithologies, tectonic units and
643 P-T conditions either resembling those of the Schistes Lustrés (e.g., Voltri group) or
644 Zermatt-Saas and Monviso units (Beiga and Erro-Tobio units). Mafic/ultramafic

645 bodies are smaller on average than for the Zermatt-Saas and Monviso units, and
646 large mafic fragments tens of km long and more than km thick are not found.

647

648

649 *3.3. Exhumation and juxtaposition of S and MUM units from the Liguro-Piemont* 650 *ocean and relationship to continental HP-LT units (Western Alps)*

651

652 Radiochronological constraints indicate that both S and MUM units were largely
653 exhumed by 35 Ma (Fig. 9a; Agard et al., 2002; Meffan-Main et al., 2004). This is
654 consistent with zircon fission-track thermochronological data indicating cooling below
655 $\sim 200^{\circ}\text{C}$ at 32 ± 2 Ma (Malusà et al., 2005; for apatite see Perrone et al., 2011) and
656 with the presence of blueschist/eclogite facies minerals in Oligocene sediments (de
657 Graciansky, 1972; Schwartz et al., 2012; Mark et al., 2016), at a time when the
658 altitude of the internal Alps was already high (Fauquette et al., 2015). Significant
659 differences in stacking history and exhumation patterns exist between the S and
660 MUM units of the Western Alps (Fig. 9b):

661 — Successive underplating is evidenced in the S units from ~ 60 to $\sim 50\text{-}45$ Ma
662 at least in the Cottian Alps and over $40\text{-}36$ Ma in the Combin. It takes place at
663 different depths, from ~ 30 to $55\text{-}60$ km. Exhumation velocities are on the order of $1\text{-}2$
664 mm/yr (Fig. 9b; Agard et al., 2002).

665 — The detachment of MUM units from the downgoing slab occurs at almost
666 constant depths (corresponding to ~ 2.6 GPa ± 0.2 , hence ~ 80 km) and is followed
667 by internal deformation and slicing along the plate interface (Figs. 8c,g). Their limited
668 imbrication with the S units (e.g., Entrelor, Grivola-Urtier; Ellero and Loprieno, 2017)
669 shows that the exhumation of S and MUM units occurred largely independently. More
670 generally, the absence of large-scale mixing of units, either in the S or in the MUM
671 units, suggests that subducted fragments were mostly returned as coherent tectonic
672 slices and nappes along the subduction interface (i.e., not as 'subduction mélange' in
673 the sense of Festa et al., 2019).

674 — The MUM units correspond to fragments metamorphosed and exhumed late
675 during the oceanic subduction history (Fig. 9b). The many age constraints for the
676 blueschist to greenschist facies exhumation of the MUM units (particularly in the
677 Zermatt-Saas area) reveal syn-convergence exhumation between ~ 40 and 36 Ma,
678 prior to collision, through large-scale shear zones: $45\text{-}36$ Ma (Reddy et al., 2003),

679 and 42-36 Ma (Angiboust et al., 2014a) near the Aosta valley and Dent Blanche; 40-
680 36 Ma (Amato et al., 1999) and 41-37 Ma (Gouzu et al., 2016) for Val Tournanche;
681 38-36 Ma (Angiboust and Glodny, 2020) for Monviso. Considering an average age
682 for peak burial at ~45 Ma for the MUM units (at 2.6 GPa or ~80 km) and shear zone
683 activity at ~350-400°C (i.e., at ~0.5 GPa, ~15 km depth), exhumation velocities are
684 on the order of 1 cm/yr (Fig. 9b).

685 — Contrary to the S units, MUM units are always tectonically underlain by the
686 Internal Basement Complexes (IBC: Monte Rosa, Grand Paradiso and Dora Maira).
687 They spatially (cartographically) coincide with the presence of these IBC and share
688 similar NS to NNW-SSE lineations (Philippot, 1990; Schmid et al., 2017). Several
689 authors have therefore suggested that the exhumation of MUM units could be
690 assisted by the buoyancy of continent material (Agard et al 2002, 2009; Lapen et al.,
691 2007; Angiboust and Agard, 2010; Skora et al., 2015), although this was recently
692 questioned (Angiboust and Glodny, 2020). Peak burial for the IBC are 42-43 Ma for
693 the Gran Paradiso (Meffan-Main et al., 2004; Manzotti et al., 2018) and 42.6 for
694 Monte Rosa (Lapen et al., 2007). Ages seem somewhat younger for Dora Maira (40-
695 35 Ma: Tilton et al, 1991; Gebauer et al., 1997; Vaggelli et al., 2006; Rubatto and
696 Hermann, 2001). Very young ages (e.g., 32.7 Ma; Duchêne et al., 1997; Rubatto and
697 Hermann, 2001) are probably geologically meaningless since collision had started by
698 ~34-32 Ma (Rosenbaum and Lister, 2005; Simon-Labric et al., 2009). For the above
699 reasons, exhumation of the MUM and/or their detachment from the slab seems at
700 least in part related to the subduction of the continental margin (see also Vitale-
701 Brovarone et al., 2014a and further discussion below).

702 Some other continental fragments were subducted earlier, as mentioned in
703 chapter 2, in particular the large Sesia body (\pm Ivrea ; Manzotti et al., 2014; Giuntoli
704 et al., 2018), whose peak burial clusters at ~70-65 Ma (Duchêne et al., 1997; Rubatto
705 et al., 1999, 2011; see Berger and Bousquet, 2008). Recently, a Lu/Hf garnet of 57
706 Ma was obtained for a small hm-thick continental fragment from the Zermatt-Saas
707 region, subducted at 1.7 GPa and 520 °C and interpreted as a former extensional
708 allochthon (Theodul Glacier; Bucher et al., 2020).

709

710

711 *3.4. The specific record of the Valais domain (Valaisan)*

712

713 Small subducted oceanic fragments associated with the closure of the Valais
714 domain are found further west, in the Petit Saint Bernard and Versoyen units
715 (Antoine, 1972; Cannic et al., 1996; Fügenschuh et al., 1999; Bousquet et al., 2002;
716 Loprieno et al., 2011). A similar tectonic differentiation between metasedimentary
717 dominated (Petit Saint Bernard) and more mafic tectonic units (Versoyen) can be
718 observed, but they show no gap in P-T conditions. Both units are characterized by
719 peak burial under blueschist facies conditions, as shown by the presence of
720 lawsonite, Fe-Mg carpholite and chloritoid, at 1.5–1.7 GPa and 350–400 °C
721 (Bousquet et al., 2002). Low pressure 'eclogites' formed through heating on
722 exhumation (~1.5 GPa, 500°C). Closure of the Valais domain is less well-constrained
723 than for Liguro-Piemont, but exhumation-related ages suggest a timing between 40
724 and 35 Ma in the Petit Saint-Bernard area (Markley et al., 1998; Villa et al., 2014).

725

726

727 **4. Subduction dynamics through space and time in the Alps**

728

729 Before examining the subduction record for the entire Alps, the tectonic insights
730 gained from the Western Alps are set back in the general tectonic evolution from the
731 subduction of oceanic lithosphere to subduction of the continental margin and then
732 final collision (Fig. 9c, after Agard et al., 2002; see also: Polino et al., 1990; Dal Piaz
733 et al., 2001; Jolivet et al., 2003; Bucher et al., 2003; Lapen et al., 2007; Berger and
734 Bousquet, 2008; Manzotti et al., 2014). This schematic reconstruction is used here as
735 a template to evaluate along-strike changes in the Alpine belt (§ 4.2). It outlines the
736 progressive shortening and accretion during the subduction of oceanic lithosphere
737 (step 1, bottom sketch in Fig. 9c), continental subduction (steps 2-3) and collision
738 with the External Massifs along the Pennine Frontal thrust (step 4).

739

740 *4.1. Geodynamics of the Western Alps as a template*

741

742 P-T-t-lithostratigraphic data for the Western Alps reveal a marked structural and
743 metamorphic contrast between the S and MUM units (Fig. 9). Underplating and
744 partial exhumation of the Schistes Lustrés complex along the plate interface occurred
745 during convergence after 65 Ma (Fig. 9b), when sediments from the slab were
746 scraped off from the underlying mafic and ultramafic MUM units.

747 MUM units show higher P-T values, larger coherent tracts of mafic units,
748 lithostratigraphic features ascribable to OCT in several locations and were buried
749 (and exhumed) during the final stages of the subduction process (Figs. 9b,c; see
750 Agard et al., 2009), i.e. a few Ma at most before the Internal Basement Complexes
751 went into subduction.

752 Several important observations can be underlined:

753 — (1): The S- and MUM units share the same P/T regime, consistent with rocks
754 formed in the same subduction zone (Fig. 10). This P/T consistency also rules out
755 significant overpressure, which would not allow for such consistency in P and T and
756 would scatter P/T estimates. The same cut-off in maximum pressure is observed at
757 ~2.8-3 GPa as for other localities worldwide (Fig. 10; Agard et al., 2018). Beyond this
758 cut-off, corresponding to a depth of some 90 km, mafic rocks (\pm serpentinites)
759 become negatively buoyant (Agard et al., 2009. Angiboust and Agard, 2010) and
760 recoupled to mantle counterflow (van Keken et al., 2011; Agard et al., 2020).
761 Noticeably, no deep fragment of the overlying plate/mantle is recovered in the
762 Western Alps, as is the case for many subduction-driven orogenies worldwide (Agard
763 et al., 2018).

764 —(2): P-T conditions for the Western Alps align along the typical gradient for
765 mature subduction (8-10°C/km; Agard et al., 2018; Fig. 7e). No remnants of early
766 subduction are found in the Western Alps: none of them testifies to warmer P/T
767 gradients accompanying subduction initiation (Fig. 10); all subducted fragments from
768 the Liguro-Piemont (and Valais) oceans were metamorphosed after ~60-65 Ma (Fig.
769 9b), i.e. postdate the subduction of the Sesia Zone. No slices were recovered from
770 depth between the start of subduction at 100-95 (chapter 2.3) and 65 Ma. The
771 contrasting rock recovery between S and MUM units through space and time also
772 testifies to different mechanical coupling states between the subducting slab and the
773 thinner HP/LT slices rising towards the surface. Strain localization steps down deeper
774 into the subducting slab, to reach the slab mantle and scrape off the MUM units (see
775 § 5), only near the end of oceanic subduction.

776 —(3): A more detailed restoration of the subduction configuration for the Western
777 Alps is proposed at ~60 Ma (Fig. 11a), after subduction and partial exhumation of the
778 Sesia micro-continental sliver. This idealized section is composite since the Sesia
779 Zone is projected here onto the southern Western Alps traverse. Assuming
780 convergence velocities around 1-2cm/a, burial of the MUM eclogitic units to 80 km

781 depth required ≥ 4 Ma. If the average estimate for their peak burial is 45 Ma (Fig. 6b),
782 then these units started to subduct near 50 Ma. The Lanzo massif, regarded by many
783 as closer to Sesia, may have reached its peak slightly before if an older age is
784 confirmed (52-46 Ma; Rubatto et al., 2008).

785 Assuming the same 1-2cm/a convergence velocity, the ~ 5 Ma difference
786 between the MUM and Internal Basement Complexes (these reached their peak
787 depth on average by 38-42 Ma: Fig. 9b) suggests that they were located $\leq \sim 50$ -100
788 km apart and places the MUM not far outboard of the continent (Figs. 3a,11a). With
789 this velocity, the entrance of the (thinned) continental margin must have taken place
790 ~ 5 Ma before, hence precisely when the MUM were at peak pressure conditions (45
791 Ma). This supports a causal link between the detachment of MUM units from the
792 sinking slab and the entrance of the continental margin. The faster exhumation
793 velocities, tighter P-T loops (Fig. 9a) and spatial association of the MUM units with
794 the HP-UHP continental IBC is therefore not fortuitous. Data suggest that (i) the
795 entrance of the continental margin at ~ 45 Ma (Fig. 9c) triggered the detachment of
796 MUM units from the slab, possibly facilitated by their discontinuous and/or OCT
797 nature, and that (ii) the detachment and exhumation of HP-UHP continental rocks
798 from the sinking plate dragged back the MUM units along the plate interface during
799 part (or all) of their return path (Fig. 11 steps 2-3, Fig. 9c).

800 — (4): Final exhumation of the deep-seated MUM units took place through major
801 extensional shear zones such as those separating the blueschist from eclogitic units
802 in the Queyras and Cottian Alps (Figs. 5a-b,7b; e.g., Kienast, 1983; Ballèvre et al.,
803 1990; Ballèvre and Merle, 1993; Reddy et al., 1999). Most of the exhumation took
804 place prior to the onset of collision of the Briançonnais and Liguro-Piemont oceanic
805 units with the External Massifs (c. 34-32 Ma; Fig. 6b). In a broader orogenic
806 perspective, the Alpine belt can be seen as the result of the imbrication of three
807 successive, different scale accretionary/decoupling systems (A-B-C, Fig. 9c): oceanic
808 (between the S and MUM units), crustal (between continental sediments of the
809 Briançonnais and the deeper subducted crust making the Internal Basement
810 Complexes), and finally lithospheric (with the Ivrea indenter during collision).

811

812

813 *4.2. Lateral variations of subducted oceanic fragments along the Alps*

814

815 The Alpine subduction record of the Central and Eastern Alps (Figs. 1,12)
816 appears far less abundant and lacks the many spectacular eclogites of the W Alps.
817 But those oceanic remnants are similar in that:

818 (i) No subducted fragment is recovered from the first part of the subduction
819 history (Fig. 9b; i.e., ~100-95 to 70 Ma in the Western Alps, ~100-65 Ma in the
820 Central Alps).

821 (ii) They align along the same subduction P-T gradient as for the Western Alps
822 (Fig. 10). Maximum pressures differ significantly: no deeply buried rocks are
823 recovered east of the Simplon/Leontine Central Alps (Berger and Bousquet, 2008;
824 Fig. 10). Before proceeding further with the comparison between the different Alpine
825 transects, a brief overview of the key information on the Central and Eastern Alps is
826 provided here (Fig. 12; see references for details).

827

828

829 *4.2.1. Complementary information from the Central and Eastern Alps*

830 — *Lepontine dome:*

831 Along the western Central Alps, near the Lepontine dome (Fig. 1), both the
832 Liguro-Piemont and Valais subducted oceanic fragments have been largely
833 overprinted by later collisional metamorphism (Bousquet et al., 2004; Engi et al.,
834 2004; Wiederkehr et al. 2008, 2009, 2011). This is for example the case in the
835 Centovalli area (Northern Steep Belt; Colombi and Pfeifer, 1986; Engi et al., 2004).
836 Some metasediments from the Valais domain located close to the Simplon line
837 nevertheless preserved P-T conditions around 1.3 GPa and 400°C (Visp, Fig. 12a;
838 Bousquet et al., 2008).

839

840 — *Central Alps (eastern part):*

841 - The Valais domain is largely exposed in the Grisons, with a ~10 km thick pile
842 of strongly deformed, blueschist facies metasediments (i.e., the Valais
843 Bündnerschiefer; Frey and Ferreiro, 1999). Two large scale units are recognized, the
844 Grava and Töimul nappes (Weh and Froitzheim, 2001 and references therein).
845 Metasediments host Fe-Mg-carpholite and chloritoid, and P-T conditions were
846 estimated at 1.2-1.4, GPa, 350-400 °C (Bousquet et al., 1998, 2002; Wiederkehr et
847 al., 2008, 2011). Peak burial occurred at 42-40 Ma (Wiederkehr et al., 2009). The

848 collisional overprint significantly increases from east to west and towards the Misox
849 root zone (Figs. 12a,b; Wiederkehr et al., 2011).

850 - The Liguro-Piemont domain is represented by a composite stack of different
851 units (Fig. 12b; e.g., Froitzheim et al., 1994, 1996). From bottom to top, it comprises
852 (i) the metasedimentary Avers Bündnerschiefer unit (locally with blue amphibole or
853 garnet-chloritoid; Oberhänsli, 1978; Ring, 1992); (ii) the Malenco and Platta units,
854 mostly made of mafic and ultramafic bodies, which are found at the bottom and top,
855 respectively, of the Margna-Sella micro-continental block subducted to blueschist
856 facies conditions (and considered an equivalent of Sesia); (iii) a ~ km-thick Arosa
857 zone characterized by mixed lithologies, with both oceanic and continental fragments
858 (Ring et al., 1990). The Arosa zone has been interpreted as marking the fossil plate
859 interface of the Alpine subduction zone (Ring et al., 1990; Bachmann et al., 2009b),
860 with P-T conditions increasing north to south from Davos (almost non-metamorphic)
861 to St Moritz (~0.6 300°C).

862 The Avers Bündnerschiefer were subducted to 1.1-1.3 GPa, 350-400°C (Fig.
863 12c; Ring, 1992). The Malenco ultramafic massif is a piece of exhumed sub-
864 continental mantle (Fig. 12d; Trommsdorff et al., 1993; Münterner and Hermann,
865 1996) later subducted to depths approximately comparable to those reached by the
866 Margna-Sella former extensional allochthon (Manatschal and Froitzheim, 1997), i.e.,
867 ~0.9 GPa 360°C (Fig. 12c; Ioannidi et al., 2020). Below the Malenco ultramafic
868 massif, the km² Lanzada tectonic window exposes a fragment of eclogitized
869 metagabbro (~2 GPa, 525°C). Its paleogeographic origin is uncertain, but thought to
870 represent the southernmost extension of the Avers unit (Droop and Chavrit, 2014).
871 Subduction of the Malenco massif is bracketed between 63 and 55 Ma (Picazo et al.,
872 2019). The Platta OCT (Fig. 12d; Manatschal and Müntener, 2009; Mohn et al.,
873 2011) experienced only HP greenschist-facies metamorphism (Handy et al., 1996).

874 These observations can set back in a schematic restoration of the subduction
875 configuration for the Central Alps at ~60-55 Ma (Fig. 12e) Above the Arosa zone, a
876 long-lived record of syn-subduction deformation is documented in the upper plate
877 (e.g., Bernina AustroAlpine units; Figs. 12a,b; Bachmann et al., 2009a, their figure 3),
878 mostly between ~80 and 60 Ma. In contrast, (de)formation of the Arosa zone is
879 thought to date back to the very last stages of oceanic subduction, between 58 and
880 47 Ma (Bachmann et al., 2009a), immediately prior to continental subduction of the
881 Briançonnais domain (around 50 Ma).

882 These observations are interpreted as marking a switch to short-lived subduction
883 accretion, following ~20 Ma of subduction erosion reflected by the reworking of the
884 base of the AustroAlpine upper plate, the relatively small amounts of flysch-type
885 sediments or the mode of deposition of the Coniacian-early Eocene Gosau basins
886 (Wagreich, 1995; Wagreich and Decker, 2001). Age constraints are lacking,
887 however, to assess when the underplating of the Avers Bündnerschiefer took place.
888 Closure of the Liguro-Piemont domain could be slightly diachronous, from ~50-45 Ma
889 in the Grisons (Bachmann et al., 2009a) to ~40 Ma in the Western Alps (see § 3.3
890 and 4.1).

891

892 — *Engadine window*

893 This tectonic window exposes the Valais and Liguro-Piemont domains separated
894 by the easternmost units of Briançonnais affinity (Fig. 12a). Both units comprise
895 mostly metasediments, with subordinate ophiolitic material restricted to metabasalts.
896 Diagnostic mineralogy includes Fe-Mg-carpholite and rare lawsonite or glaucophane
897 (Bousquet et al., 1998). P-T estimates for the Valais domain are close to those for
898 the Grisons (and Avers), i.e. 1.1-1.3 GPa, 350-375°C (Fig., 12c; Bousquet et al.,
899 1998) and show a similar age (42-40 Ma; Wiederkehr et al., 2009).

900

901 — *Eastern Alps, Tauern window*

902 Some blueschist facies ocean-derived metasediments crop out in the Tauern
903 window and were attributed to the Valais (Glockner nappe) and Liguro-Piemont units
904 (Reckner ophiolitic Complex and Matreier zone, respectively in the northwest and
905 south-central part of the window; Fig. 1a; Zimmermann et al., 1994; Berger and
906 Bousquet, 2008; Rosenberg et al., 2018). In the absence of a Briançonnais domain,
907 the distinction between the Valais and Liguro-Piemont units is difficult (Schmid et al.,
908 2013). These oceanic fragments, particularly the Glockner nappe, experienced
909 significant heating on exhumation and are commonly strongly retrogressed, with
910 lawsonite pseudomorphs at most (Hoinkes et al., 1999). P-T estimates for peak burial
911 lie around 0.9 and 370°C for the oceanic Matreier Zone (Koller and Pestal, 2003).
912 The Bündnerschiefer and mafic/ultramafic units from the Upper Schieferhülle
913 (Glockner nappe) are generally considered to have reached pressures ≤ 1 GPa
914 (Berger and Bousquet, 2008), showing a large pressure gap with the continent-
915 derived Eclogite zone below. However, some eclogitic units with P-T conditions

916 around ~1.7 GPa at 570 °C have been attributed by some authors an oceanic origin,
917 thus raising some doubts on the exact maximum pressure (Dachs and Proyer, 2001;
918 Gross et al., 2020). These deeper buried slices of oceanic metasediments (~2 GPa,
919 500°C; lower Glockner unit; Groß et al., 2020) represent fragments entrained and
920 deformed during continental subduction and exhumation of the distal European
921 margin. As for the eastern Central Alps, some lower Austro-Alpine units, together
922 with the Reckner ophiolitic Complex (Schmid et al., 2013), were entrained in
923 subduction between 0.8 and 1-1.1 GPa at 350-400°C around 50 Ma (Dingeldey, et
924 al., 1997), well before the 35-30 Ma continental subduction (Christensen et al., 1994).

925

926 — *Rechnitz window*

927 The Rechnitz window provides the easternmost outcrops of Liguro-Piemont
928 subducted fragments, with modest P-T conditions of 0.9-1.0 GPa 370°C (Koller,
929 2003). These were reached at 57 ± 3 Ma (Ratschbacher et al., 2004).

930

931

932 *4.2.2. Along strike changes*

933 Marked contrasts regarding S and MUM type units exist along the strike of the
934 orogen:

935 — Underplating of metasedimentary-dominated units, in the Bündnerschiefer
936 (mostly Valais) and the Schistes Lustrés (Liguro-Piemont) units is observed all along
937 the belt. Most units experienced P-T conditions around 1-1.3 GPa and ~ 350-380°C
938 (Fig. 9b; from east to west: Tauern, Engadine, Grisons, Valaisan, Combin, and the
939 upper S units of the Maurienne/Cottian/Queyras) corresponding to the worldwide
940 peak of recovery at ~30-40 km for sedimentary piles (i.e., depths with changes in
941 mechanical coupling; Agard et al., 2018). More unique is the underplating of several
942 units at different depths in the Western Alps, south of Gran Paradiso (§ 3.1).

943 All these units were accreted between ~60 and 35 Ma (Fig. 9b), with evidence for
944 underplating near 60 Ma in the eastern (~57 Ma; Rechnitz window; Ratsbacher et al.,
945 2004) or the south-western Alps (60-55 Ma; Cottian Alps; Agard et al., 2002). The
946 amount of underplated material varies along strike: from up to 10 km in the NE Valais
947 (e.g. in the Grisons; Frey and Ferreiro, 1999; Weh and Froitzheim, 2001) to a few hm
948 in the SW (Valaisan units; Bousquet et al., 2002), and from the km-scale in the

949 Liguro-Piemont Central Alps (Avers) and north-western Alps (Combin) to several km
950 in the south-western Alps (Maurienne to Queyras).

951 — Mafic/ultramafic-dominated units are found all along the belt, but differ
952 significantly between the Western Alps and further east. While extensive eclogite
953 facies bodies are exposed in the Western Alps, MUMs are volumetrically
954 insignificant, blueschist facies and reaching ~1 GPa at most in the Central and
955 Eastern Alps (save possibly for the small Lanzada window, Figs. 12a,c). MUMs of the
956 Western Alps tend to cluster around similar eclogitic conditions and are only
957 recovered late in the oceanic subduction history (peak burial ~45 Ma; Fig. 9b),
958 immediately prior to continental subduction. In contrast, P-T conditions vary in the
959 eastern Central Alps (Platta, Malenco) and subduction ages are somewhat older (60-
960 50 Ma). The unmetamorphosed, isolated and small Chenaillet massif (Fig. 7b;
961 Manatschal et al., 2011) is somewhat of an outlier, similar only to the northern extent
962 of Platta, accreted in the subduction forearc or obducted. Metamorphic soles typifying
963 obduction (Spray, 1984; Wakabayashi and Dilek, 2003) are nowhere found in the
964 Alps, but this may not be diagnostic since they are not expected to form in slow-
965 spreading oceans (Agard et al, 2016). In all zones MUM correspond to portions of
966 discontinuous oceanic lithosphere, OCT and/or exhumed subcontinental mantle.
967 These characteristics favor later recovery, as reflected by the subducted rock record
968 (see Agard et al., 2018).

969 These observations, when superimposed with maps of metamorphic facies for
970 the subducted oceanic fragments (Fig. 13a-c), reveal zones with contrasting
971 histories:

972 — areas where MUM are preferentially recovered, and the only ones where
973 eclogitic MUMs are found, coincide with the spatial extent of the subducted micro-
974 continental Briançonnais and Sesia domains (see also § 4.2.3). Subduction of Sesia
975 (~75-65 Ma) furthermore represents a major divide in the ~100-40 Ma period of
976 oceanic subduction, with no recovery of subducted oceanic rocks before (Fig. 9b).
977 These observations suggest a strong influence of both margin segmentation and
978 continental subduction.

979 — The relationship between the amount of oceanic MUM and continental
980 subduction can be scrutinized further: more MUM units are recovered in the vicinity
981 of the Gran Paradiso-Monte Rosa Internal Basement Complexes (and the Sesia
982 Zone) than around Dora Maira. Dora Maira is the only Internal Basement Complex

983 for which (i) one unit shows UHP conditions (the Brossasco-Isasca unit), with peak
984 pressure larger than that of adjacent MUMs and (ii) five to six distinct hm- to km-thick
985 slices were recognized (Henry et al., 1993; Compagnoni and Rolfo, 2003). The
986 thinner Dora Maira slices, hinting to a more extended portion of the European
987 basement (forming the Briançonnais), may have been more readily and deeply
988 subducted (hence in part UHP) yet not buoyant enough to help return dense MUM
989 units.

990 — On the other hand, continental subduction in the Western Alps was not greater
991 than in the Central Alps: the Briançonnais-derived nappes (Tambo, Suretta) and
992 even the more external European margin-derived units (Adula) reached the greatest
993 depths in the Alps (~4-5 GPa in Alpe Arami or Gagnone; Frey et al., 1999; Figs.
994 12a,b), and not much later (peak burial of the Adula nappe by ~38-35 Ma; Herwartz
995 et al., 2011; Sandmann et al., 2014). While the Central Alps oceanic fragments are
996 strongly overprinted by collisional (Leptontine, barrovian) metamorphism into
997 variegated facies (Engi et al., 2004), there is no indication that these rare MUM
998 slivers were buried to pressures as high as in the Western Alps. The initial lithological
999 nature of the oceanic rocks (e.g., OCT with variable proportions of mafic crust) and/or
1000 the geometrical configuration of the margin (e.g., presence of Sesia) therefore
1001 probably play a primary role in promoting chances of rock recovery.

1002

1003

1004 *4.3. Four distinct sectors: paleogeographic contrasts in subduction dynamics*

1005

1006 Based on first-order contrasts in subducted-related history, and with some
1007 reservations due to inevitable P-T-t-d-cartographic-paleogeographic uncertainties, it
1008 is possible to identify several distinct sector along the Alpine belt (Fig. 13):

1009 — *Sector A, south of Gran Paradiso* (along CIFALPS and south of the ECORS
1010 geophysical profiles; Fig. 1a), encompasses the Queyras, Cottian, Maurienne,
1011 Rocciavre, Monviso and Dora Maira sectors of the internal Alps. This sector is
1012 characterized by S units subducted across a range of depths and recovered across a
1013 relatively long period (~60-40 Ma), by the presence of pluri-km large gabbroic bodies
1014 (Rocciavre, Monviso) and, compared to the other sectors, a lesser influence of
1015 collision. It shows, at least from present exposures, the longest (mid-Penninic)
1016 Briançonnais margin subducted between high-grade blueschists and eclogites, with

1017 Ambin, Acceglio and Dora Maira (see the detailed reconstruction by Michard et al.,
1018 2004). The Dora Maira IBC is the only Briançonnais-derived continental UHP massif
1019 and the most composite one, with five or six slices including one UHP slice. There is
1020 almost no Valais domain along this sector (Fig. 8a-c).

1021 — *Transect B, Gran Paradiso and NE Monte Rosa* (and possibly into the western
1022 Central Alps; along the NFP20-W profile), encompasses the most voluminous MUM
1023 massifs (Zermatt-Saas, Antrona, Avic, Lanzo), which also show the largest individual
1024 mantle-dominated bodies (Lanzo, Avic). The S units are less abundant than in sector
1025 A and maximum pressures far less variable. No ages older than ~45 Ma were found
1026 for these metasedimentary units. The Gran Paradiso and Monte Rosa Internal
1027 Basement Complexes record P-T conditions similar to or slightly lower than the MUM
1028 units. Neither of them is UHP nor shows a complex stack of units (two only in Gran
1029 Paradiso; Manzotti et al., 2015). This sector is characterized by the presence of the
1030 subducted continental Sesia Zone (\pm Ivrea-Canavese), which is located in a more
1031 internal position (hinterland) than ocean-derived units. This sector is also where very
1032 low-grade nappes stacked in the Préalpes preserve a record of accretionary wedge
1033 formation; and where the Ivrea body, interpreted as a shallow piece of upper plate
1034 mantle, is also found (Fig. 13c).

1035 — *Transect C, (eastern) Central Alps and Engadine window* (along the NFP20-E
1036 profile), is overall metasedimentary-dominated and oceanic fragments reached
1037 maximum pressures around 1.2-1.3 GPa. The S units can be several km thick but
1038 are not subdivided as much (yet?) as in sectors A or B. The MUM remnants are
1039 made of recognizable and well-characterized OCT and subcontinental mantle which
1040 were not deeply subducted. Subducted oceanic remnants are younger than 65 Ma
1041 (although subduction initiated ~100 Ma; Bachmann et al., 2009a). A continental
1042 sliver, Margna-Sella, smaller than the Sesia Zone, is present in the same structural
1043 position. Contrary to sectors A and B the Briançonnais massifs are fairly restricted
1044 (Tambo, Suretta; absence of Internal Basement Complex). On the other hand, the
1045 very distal European margin experienced locally UHP conditions (e.g., 4-5 GPa in
1046 Alpe Arami).

1047 — *Transect D, east of the Engadine window* (i.e., along the TRANSALP profile), only
1048 preserves volumetrically small subducted fragments of the Alpine ocean (e.g., Matrei,
1049 Rechnitz) with maximum pressures around 1.2-1.3 GPa. There is no Briançonnais
1050 domain. The European margin was subducted as along sector C but far less deep

1051 (e.g., 1.8 GPa in the Eclogite zone). This sector also coincides with the area affected
1052 by the former Eoalpine (Cretaceous) metamorphism in the Austro-Alpine nappes

1053 For sectors A and B, the eclogitic facies MUM units are closely related to the
1054 Internal Basement Complexes. UHP conditions in Penninic domains (oceanic:
1055 Cignana; continental: Dora Maira) are only found in these two sectors. There is
1056 evidence for subduction erosion of the upper plate basement in sectors B-C-D,
1057 marked by prolonged deformation and recovery of subducted micro-continental
1058 slivers at 55-50 Ma at the base of the Austro-Alpine domain (B: Dent Blanche,
1059 Angiboust et al., 2014a; C: Bernina, Bachmann et al., 2009a; D: Tauern, Dingeldey,
1060 1997; see also Polino et al., 1990).

1061 These lateral contrasts in subduction dynamics along the Alpine belt are depicted
1062 in a snapshot of the Alpine oceanic subduction at ~40 Ma, towards the end of
1063 oceanic subduction (Fig. 14, to be compared with Fig. 3a). Further work could help
1064 determine whether this segmentation of the former Alpine subduction zone chiefly
1065 results from (i) margin segmentation inherited from the Variscan orogeny (Pfeifer et
1066 al., 1989; von Raumer et al., 1999, 2002; Manzotti et al., 2016; Balleve et al., 2018),
1067 (ii) rifting processes and/ or magmatic production (Mohn et al., 2011), (iii) differential
1068 response during material subduction, i.e. mechanical (rheology) or chemical (via
1069 fluid liberation), (iv) differential kinematics and/or (v) sedimentary inputs.

1070

1071

1072 **5. Alpine insights into subduction interface processes**

1073

1074 The good preservation of subducted fragments and of at least some of the Alpine
1075 subduction architecture allows tracking processes occurring along the plate boundary
1076 during active subduction, e.g. strain localization and fluid transfer (Fig. 15a). The
1077 section below provides a provisional overview of such investigations on S and MUM
1078 units, and sets them back into the tectonic frame described above (Fig. 15b) and
1079 against other fossil subduction zones (e.g., Bebout and Penniston-Dorland, 2016;
1080 Scambelluri et al., 2019).

1081

1082

1083 *5.1 Insights onto plate interface dynamics*

1084

1085 Changes in mechanical coupling between the sinking slab and the overlying
1086 mantle wedge have a strong impact on strain partitioning across the plate interface
1087 (Agard et al., 2018): when the interface is perfectly decoupled strain is localized on
1088 the subduction fault; when it gets locked, strain becomes distributed across some
1089 distance and develops either (1) downward into the slab, promoting off-scraping,
1090 underplating and potential rock recovery via subsequent exhumation or (2) into the
1091 upper plate base, removing material entrained at depth by subduction 'erosion' (or
1092 basal erosion; Fig. 15a).

1093 The Alpine example provides evidence for both:

1094 - Stacking of the S units demonstrates significant underplating at depths >20-40
1095 km in the Alps (Fig. 11a; Bousquet et al., 1998, 2002; Agard et al., 2001a; Seno et
1096 al., 2003, 2005; Plunder et al., 2012; Angiboust et al., 2014a). This implies tectonic
1097 decoupling between sediments and mafic/ultramafic protoliths, as in other fossil
1098 subduction complexes (e.g., Sanbagawa-Shimanto, Japan; Franciscan complex,
1099 California; Kimura and Ludden, 1995). Similar decoupling between the rising MUM
1100 units and the downgoing slab mantle took place near 80 km depth (Figs. 8c, 15b).
1101 Both suggest activation of deep décollement horizons, analogous to their shallow
1102 counterparts in present-day or fossil shallow accretionary wedges (e.g.; Nankai,
1103 Japan; Makran, Iran; Helminthoid flysch, Western Alps).

1104 - On the contrary, long-lived reworking of the base of the AustroAlpine nappes
1105 argues for subduction erosion for some period of time (e.g., Bachmann et al., 2009a)
1106 for three of the Alpine sectors (B-D; Fig. 14). This is consistent with the relative lack
1107 of rock recovery in the eastern Central Alps before ~60-55 Ma.

1108 Whether strain (re)localization operates through seismic activity or rather via
1109 distributed shear, and what role fluids play in the process is not well known yet (see
1110 Agard et al., 2018; Menant et al., 2019). Pseudotachylites produced by past
1111 earthquakes during oceanic subduction were documented in the Alps both at shallow
1112 depth in the upper plate (Austro-Alpine: Bachmann et al., 2009a; for cataclastic
1113 deformation: Angiboust et al., 2015) and in dry protoliths from the downgoing slab at
1114 eclogite facies conditions in Lanzo (~80 km depth; Scambelluri et al., 2017). In
1115 Monviso, eclogite breccia formed at ~80 km depth during subduction testify to the
1116 existence of discrete brittle and possibly seismic events along newly formed shear
1117 zones near the top of the slab (Angiboust et al., 2012a). This brecciation operates
1118 though several discrete steps/events and preludes to the detachment of the large

1119 tectonic slice of the Lago Superiore from the slab (Figs. 8,15b; Locatelli et al.,
1120 2019b). Diffusion modelling suggests that the whole brecciation process lasted \leq
1121 ~ 2 Ma and that healing of the fractures may be on the order of 100 ka at most
1122 (Broadwell et al., 2019).

1123

1124

1125 *5.2 Insights onto element budgets in subduction zones*

1126

1127 Alpine sedimentary, mafic and ultramafic protoliths were used to assess
1128 systematic element changes across depths, estimate element budgets or fingerprint
1129 exchanges between lithologies through trace element concentrations of large
1130 lithophile and fluid-mobile elements (LILE and FMEs) or isotopic signatures (H, Li, B,
1131 C, N, O, Cl, S, Fe and Zn). The assessment of element/fluid budgets across the plate
1132 interface is however limited by the absence of mantle wedge fragments in the Alps
1133 (as for most subducted complexes worldwide).

1134 The relatively continuous suite of P-T conditions of the Cottian metasedimentary
1135 units (Fig. 7e) has been used to monitor chemical changes with depth. They
1136 evidence significant element retention, with strong preservation of LILE (K, Rb, Ba
1137 and Cs), N, Li and Sr (but loss of As and Sb; Busigny et al., 2003; Bebout et al.,
1138 2013; Barnes et al., 2019), at odds with trends observed for the Franciscan
1139 subduction complex marked by intense devolatilization (Bebout et al., 1999; Bebout,
1140 2007). This high element retention (Bebout et al., 2013) may reflect the contrast
1141 between the cold and steady Alpine subduction gradient ($\sim 8^\circ\text{C}/\text{km}$; Figs. 7e,10) and
1142 the warmer and transient gradient of the Franciscan. Efficient carbon sequestration
1143 was also documented, both in blueschist facies metasediments (>80 - 90% ; Cook-
1144 Kollars et al., 2014; Lefeuvre et al., 2020) and in basalts and ophiicarbonates across
1145 grade (Collins et al., 2015), suggesting that any significant decarbonation (e.g.,
1146 Kelemen and Manning, 2015) must take place deeper, at sub-arc depths.

1147 Evolution of fluid chemistry with depth documented by fluid inclusions suggests
1148 the existence of moderately saline fluids in metasedimentary blueschists and
1149 hypersaline fluids in mafic eclogites (Scambelluri et al., 1997; Philippot et al., 1998;
1150 Agard et al., 2000; Scambelluri and Philippot, 2001). Fluid inclusions also provide
1151 evidence for carbon dissolution at UHP conditions (Frezzotti et al., 2011). The
1152 release of hypersaline and/or sulfate-rich fluids during prograde metamorphism of

1153 serpentinites (Monviso-Queyras traverse; Schwartz et al., 2013) may in addition
1154 oxydize the mantle wedge (Debret et al., 2016).

1155

1156

1157 *5.3 Insights onto scales of fluid mobility*

1158

1159 The wealth of HP-LT metamorphic veins at seismogenic zone depths, i.e. ~ 30-
1160 35 km in the S units (e.g., Lefeuvre et al., 2020) or intermediate depth near ~80 km in
1161 the MUM units (omphacite veins; e.g., Monviso; Philippot and Kienast, 1989;
1162 Spandler et al., 2011), attests to considerable fluid mobility within oceanic subducted
1163 fragments. In the S units, the lack of significant isotopic shift in volatiles (C, O, H)
1164 nevertheless suggests limited external fluid infiltration (for the Cottian, Maurienne
1165 and/or Combin: Henry et al., 1996; Cook-Kollars et al., 2014; Epstein et al. 2019),
1166 except along major tectonic contacts (Jaeckel et al., 2018). Similarly, mafic rocks
1167 from Monviso or Zermatt-Saas MUM units show local, mm-cm-scale fluid derivation,
1168 and even strong preservation of primary hydrothermal alteration signatures (Nadeau
1169 et al., 1993; Selverstone and Sharp, 2013). Most fluids percolating through these
1170 oceanic fragments appear internally-derived and/or derived from similar lithologies, in
1171 support of closed-system behavior at the meter scale and possibly up to the 100 m-
1172 scale (Fig. 15b), at least for components other than H₂O.

1173 Many observations nevertheless point to a more complex interaction between
1174 sedimentary, mafic and ultramafic lithologies (Fig. 15b). In serpentinitized peridotites
1175 from the Queyras, a trap-and-release mechanism was proposed to account for the
1176 enrichment of serpentinites in B, Li, Cs, As, Sb (at T<~360-390°C) by fluids derived
1177 from nearby metasediments, and their progressive loss at higher temperature with
1178 crystallization of antigorite (Lafay et al., 2013). Specific enrichments in Ba, Rb, U, Cs,
1179 and Pb in serpentinites from the Combin and Lanzo areas were also interpreted as
1180 reflecting the influx of sedimentary-derived fluids (Barnes et al., 2014). Differential
1181 release of fluids from metasediments or serpentinites with temperature could
1182 moreover exert a complex control on decarbonation (Queyras: Debret et al., 2018).

1183 Contrasting ultramafic/sedimentary contributions are documented when
1184 comparing Monviso, Lanzo and Zermatt-Saas (Gilio et al., 2020). In Monviso, km-
1185 scale shear zones cross-cutting metagabbros evidence a major influx of serpentinite-
1186 derived fluids (Spandler et al 2011; Angiboust et al., 2011) with additional

1187 contribution from metasediments (Rubatto and Angiboust, 2015). The influx of
1188 external-derived fluid appears transient and episodic in both metagabbros and
1189 eclogite breccia, and partly achieved via brittle fractures: incremental brecciation
1190 forms successive matrices recording internally- and then externally-derived fluids
1191 (Locatelli et al., 2018, 2019b), whose formation may short-lived (i.e., a few 100 ka;
1192 Broadwell et al., 2019). Ingression of externally-derived fluids occurs once sufficient
1193 brecciation has enabled full-scale connectivity across the shear zones (i.e.,
1194 permeability, fluid ingression and strain localization; after formation of the M2 matrix
1195 in Fig. 8b; Locatelli et al., 2019b).

1196

1197

1198 **6. What did we learn?**

1199

1200 *6.1. A faithful and useful subduction record*

1201

1202 *6.1.1. A reliable proxy for the subduction of oceanic lithosphere*

1203 The present study confirms that HP-LT oceanic fragments from the Alps provide
1204 a reliable P-T record diagnostic of cold subduction zones worldwide, one of the most
1205 extensive fossil examples so far. Several reasons allow to rule out significant tectonic
1206 overpressure in subducted Alpine fragments (see also Froitzheim, 2020):

1207 (i) Subducted remnants consistently align along the same P/T gradient (Fig. 10).
1208 Any significant overpressure would engender variable P/T ratios in the oceanic rock
1209 record (and in the Internal Basement Complexes, which align along the same P/T
1210 gradient). This P/T gradient is also typical of mature subduction worldwide (Agard et
1211 al., 2018).

1212 (ii) Maximum recorded pressures for mafic eclogites (~2.8-3 GPa) correspond to
1213 the threshold beyond which slab crust becomes negatively buoyant with respect to
1214 the surrounding mantle (Agard et al., 2009; Angiboust and Agard, 2010) and fully
1215 coupled to the upper plate (Wada et al., 2008; Agard et al., 2020). The match
1216 between the depth inferred from thermodynamic pressure and the depth of viscous
1217 coupling, at 80-90 km, strengthens the conclusion that overpressure is limited.

1218 (iii) Mineral parageneses found either in rheologically weak (sediments) or
1219 strong material (mafics and ultramafics) yield the same pressure estimates. The

1220 spatial distribution of pressures is also non random, as shown by the clear W-E
1221 gradient in the Western Alps or within a given unit (e.g., upper S unit: Figs. 2b, 7c-e).

1222 All this, however, does not preclude local but minor overpressure. The hm-thick
1223 Cignana UHP sub-unit could reflect overpressure of at most ~10% (3.2 vs. 2.8 GPa;
1224 Fig. 9a; or represent a deeper thin strip of slab).

1225

1226 *6.1.2. A direct access to subduction interface processes*

1227 Structural relationships and P-T-time-lithostratigraphic-petrological data preserve
1228 a good access to the subduction history: the collision-related metamorphic overprint
1229 is moderate or insignificant in many places (e.g., Berger and Bousquet, 2008); the
1230 distribution of tectonic units and deformation shows that subduction structures are
1231 not completely messed up. The organization of Alpine fragments does not result from
1232 some large-scale 'mélange' process in a subduction channel (unlike Cuba or Sistan:
1233 Garcia-Casco et al., 2002; Bonnet et al., 2018) but corresponds to tectonic
1234 slices/imbrications formed along the plate interface which were later variably
1235 disrupted by deformation (Angiboust and Agard, 2010; Tartarotti et al 2017, 2019;
1236 Agard et al., 2018; Locatelli et al., 2018; see models by Ruh et al., 2015). These
1237 features allow studying:

1238 (i) the former geometry of the plate interface, in some places at the hm-km
1239 scale, such as the down dip geometries of metasedimentary-dominated units south
1240 of Gran Paradiso, the geometry of OCT domains and/or specific horizons, or the
1241 shallow accretion of the Préalpes and Helminthoid flyschs.

1242 (ii) dynamic processes such as underplating, strain localization or subduction
1243 rheology. Dominant underplating at ~30-40 km (1 GPa), for example, could either be
1244 coupling-dependent (i.e., driven by some upper plate Moho barrier and/or fluid-
1245 related process) and/or buoyancy-controlled (e.g., assisted by joint subduction with
1246 lower density extensional allochthons). Rheological contrasts between specific
1247 sedimentary horizons may explain preferential localization of décollements in
1248 metapelite- or carbonate-dominated sequences (e.g., Vannucchi et al., 2017), hence
1249 the successive accretion of the upper (more pelitic) and middle (more carbonate-rich)
1250 S units. Alternatively, strain localization could be chiefly controlled by fluids (Kimura
1251 and Ludden, 1995. Menant et al., 2019) or mineral reactions, as suspected from fluid
1252 redistribution associated with the growth of lawsonite veins, lawsonite breakdown or

1253 garnet formation (Dragovic et al., 2012; Vitale-Brovarone and Agard, 2013; Vitale-
1254 Brovarone et al., 2014b; Lefeuvre et al., 2020).

1255

1256 *6.1.3. A window onto fluid-rock interactions along subduction zones*

1257 The Alpine archive can contribute to refining the picture of element/fluid transfer
1258 along the slab in cold subduction environments (Fig. 15b; Spandler and Pirard, 2013;
1259 Bebout and Penniston-Dorland, 2016; Scambelluri et al., 2017, 2019):

1260 (i) The frequent preservation of chemical and isotopic signatures advocates for
1261 relatively closed system behaviour except along some shear zones in both S units
1262 (Henry et al., 1996; Lafay et al., 2013; Barnes et al., 2019) and MUM units (Spandler
1263 et al., 2011; Locatelli et al., 2019b). Rock hybridization appears limited except at
1264 primary sedimentary/mafic/ultramafic lithological contacts and heterogeneities, as
1265 shown by syn-subduction Ca \square metasomatism of metagabbros in former sedimentary
1266 mélanges (Avic: Tartarotti et al., 2019; Corsica: Vitale-Brovarone et al., 2014b;
1267 Piccoli et al., 2018) or in metasomatic rinds formed along shear zones (Angiboust et
1268 al., 2014b). Mass-balance calculations are probably fraught with large uncertainties,
1269 however, given the variations in bulk composition of slow-spreading oceans (e.g.,
1270 serpentinite to sediment ratio).

1271 (ii) Fluid flow appears to be episodic (Spandler et al., 2011; Angiboust et al.,
1272 2012a; Locatelli et al., 2018). External fluid ingression accompanies progressive
1273 strain localization across shear zones (Locatelli et al., 2019b). Fluid (re)distribution
1274 amongst the various protoliths is probably complex, however, since hydration of
1275 relatively dry protoliths (e.g., Allalin gabbro, Zermatt-Saas unit; Bucher and Grapes,
1276 2009) may coincide with dehydration from nearby rocks (e.g., metapillows; Angiboust
1277 and Agard, 2010).

1278

1279 *6.1.4. An access to along-strike segmentation*

1280 The along-strike contrasts in subduction dynamics of sectors A-D can help refine
1281 the initial setting/paleogeography of the Alpine subduction (Fig. 13; see § 4.3): the
1282 Briançonnais continental margin was likely more stretched along sector A during
1283 rifting (i.e., Dora Maira); the presence of the Sesia Zone resulted in specific
1284 subduction dynamics along sector B; its subduction triggered a change in boundary
1285 conditions which initiated the recovery of oceanic rocks (~60-40 Ma). Figure 13c
1286 shows, in addition, that these lateral contrasts largely persisted during continental

1287 subduction and collision (as shown, for example, by the Préalpes and Ivrea body
1288 located along sector B).

1289 From ~65-60 to ~50 Ma, subduction appears to have been erosive along sectors
1290 B-D (particularly in the eastern Central Alps) but accretionary along sector A. During
1291 the first period (pre-Sesia subduction), the Alpine subduction was either (entirely?) in
1292 erosive mode, sediment starved and/or efficiently lubricated so that underplating was
1293 impeded at depth.

1294 These lateral contrasts could be ascribed to inherited structures (Variscan- or
1295 rifting-related), differences in incoming material impacting subduction (nature,
1296 proportions; e.g., sediment input, magmatic production) or differential kinematics.
1297 The present-day Chilean example shows such lateral contrasts in
1298 accretionary/erosive mode and sediment input along one single subduction zone
1299 (Maksymowicz, 2015). The four A-D sectors recognized here may be further tied to
1300 geophysical slab imaging to read through tomographic images and assess some of
1301 the later, Oligocene to Present evolution of the Alpine slab (Handy et al., 2010;
1302 Hétenyi et al., 2018).

1303 Worthy of note, the Alpine example shows that slab retreat, which may assist
1304 exhumation (Brun and Faccenna, 2008), did not trigger the offscraping from the slab
1305 (see also Agard et al., 2018): the detachment of the MUM units, shortly followed by
1306 exhumation, occurs only when subduction dies out. And there was no S unit returned
1307 during the first 30 Ma, a long enough period for the slab to retreat (nor is there any
1308 exhumation of HP-LT rocks in retreating subduction zones from south-east Asia).

1309

1310

1311 *6.2. Why such a profuse subducted record? How (a)typical is the Alpine example?*

1312

1313 *6.2.1. Why are so many HP-LT oceanic fragments returned and is this abnormal?*

1314 It should first be stressed that subducted fragments are abundant only in the
1315 Western Alps (Fig. 13a) and that no oceanic rocks were recovered between the
1316 onset of subduction (~100 Ma) and ~60 Ma. It only started after subduction of the
1317 Sesia Zone (Fig. 9b). Subduction may have been more 'classical' before 70-65 Ma,
1318 i.e. not returning anything, as many large-scale subduction zones today (e.g., Chile
1319 or Japan). The 165-150 Ma cluster of Liguro-Piemont magmatic ages (Fig. 3d) shows
1320 that the oceanic lithosphere formed between ~150 and 120 Ma (even possibly with

1321 thicker crust) was entirely subducted, over roughly the same amount of time (~30
1322 Ma, from ~100 to 70 Ma).

1323 The local abundance of subducted oceanic fragments most likely results from the
1324 slow-spreading character of the ocean and the presence of OCT domains. This
1325 configuration provides many primary discontinuities/weaknesses facilitating later
1326 strain localization and offscraping along the subduction interface (Ruh et al, 2015),
1327 together with relatively buoyant material. The separation between sediments and
1328 crustal fragments, on the one hand, and between mafic/strongly serpentinized
1329 ultramafic and a drier mantle, on the other hand, appears most effective. The Alpine
1330 record is indeed characterized by (i) a marked contrast between units that are
1331 metasedimentary-dominated (S units) and others representing km-thick portions of
1332 slab lithosphere (MUM units); (ii) a contrast in their relative timing of burial and
1333 exhumation; (iii) the role of continental margin subduction on initiating detachment
1334 from the slab (and partly exhumation; Fig. 11); (iv) the preferential recovery of OCT
1335 domains (as for Corsica; Vitale-Brovarone et al., 2013, 2014a).

1336 The Alpine situation stands in contrast with large-scale subduction zones from
1337 fast-spreading oceans characterized by a more regular ocean-plate stratigraphy
1338 (Kusky et al., 2014; Wakabayashi, 2015, 2017). For these, underplating (and/or
1339 shallow accretion) is commonly restricted to slivers of metagraywackes with
1340 interleaved horizons of metabasalts (Kimura and Ludden, 1995) and to depths of
1341 ~30-40 km. This is the case in subduction complexes from the Sanbagawa-Shimanto
1342 belt (Japan; Yamaguchi et al., 2012), Kodiak-Alaska (Sample and Fisher, 1986;
1343 Fisher and Byrne, 1987) or New Zealand (Fagereng, 2011). The Alpine example
1344 supports the view that there is a recovery/exhumation filter in the rock record, which
1345 preferentially returns eclogitic fragments from slow-spreading oceans or thinned
1346 margins (Agard et al., 2018).

1347

1348

1349 *6.2.2. Are Alpine subducted fragments informative about subduction processes or*
1350 *rather inherited from earlier stages?*

1351 The question, then, is the extent to which the intermittent rock recovery
1352 accompanying the subduction of oceanic lithosphere is controlled by plate interface
1353 rheology and kinematics or rather by structures inherited from the former (passive)
1354 margin, seafloor structure and/or sediment type. The answer probably lies

1355 somewhere in between. While the Alpine record shows that discontinuous oceanic
1356 structure, margin segmentation and heterogeneous stretching exert an important
1357 control, not every tectonic feature is inherited. New structures (i.e. further damage)
1358 form during subduction lifetime as shown, for example, by intermediate depth
1359 earthquakes, strain localization along freshly nucleated shear zones, overturned km-
1360 scale folds or eclogite breccias genuinely formed along the plate interface (§ 5; Fig.
1361 5; Scambelluri et al., 2017; Locatelli et al., 2018).

1362 The extent to which recovery (i.e., detachment and exhumation) relates to the
1363 impingement of the continental margin could be quantified. While increased coupling
1364 via continental micro-slivers induces downstepping of the subduction interface
1365 (Angiboust et al., 2014a), this process is most likely size dependent: e.g., the 100m-
1366 thick and 2 km-long Theodul Glacier sliver (Bucher et al., 2020) did not trigger the
1367 recovery of the large-scale Zermatt-Saas units. Determining the size threshold would
1368 inform on effective rheological properties. The step down of the décollement deeper
1369 into the slab at the end of oceanic subduction shows, in any case, that the plate
1370 interface widens and advocates for greater interplate coupling (Fig. 15a).

1371

1372 *6.2.3. Some remaining unknowns*

1373 The lack of a magmatic arc atop the subduction zone is a long-standing enigma.
1374 It was recently associated to the slow-spreading nature of the ocean (McCarthy et al.,
1375 2018, 2020). These authors suggested that serpentinization of the upper portion of
1376 the sinking lithospheric mantle and efficient decoupling from the dry mantle below
1377 had caused its shallow accretion, thereby preventing enough water transfer at depth.
1378 Evidence for significant underplating of serpentinized mantle or shallow serpentinite
1379 diapirs (such as in the Izu-Bonin subduction zone; Tamblyn et al., 2019) is lacking in
1380 the Alpine record. Two alternative explanations may be put forward: (i) 200-300 km of
1381 oceanic subduction may not be sufficient to hydrate the mantle wedge at sub-arc
1382 depths, depending on the fertility of the sub-continental mantle, and/or (ii) the Alpine
1383 slab may have been too short (Fig. 14) to trigger sufficient counter-flow and mantle
1384 upwelling, thereby hindering the formation of a magmatic arc (in the Izu-Bonin, the
1385 time-lag between subduction initiation and mature arc magmatism corresponds to the
1386 time needed for the slab to reach the 660 mantle discontinuity; Ishizuka et al., 2020;
1387 see also Agard et al., 2020).

1388 The initiation process of Alpine subduction is unknown, as for (nearly) all
1389 subduction zones. Subduction initiation was likely intra-oceanic since initiation next to
1390 a continent has not been documented yet (e.g., Leng and Gurnis, 2015). The Alpine
1391 subduction archive and paleogeographic record suggest that subduction initiated
1392 next to the Adria margin (which also explains subduction of exhumed mantle pieces
1393 from Adria; i.e. Lanzo, Malenco). Although intra-oceanic subduction initiation appears
1394 most likely, there was either no obduction in the Alpine domain or a different one
1395 from that of large-scale ophiolites (as noted by Auzende et al., 1983). Conceivably, it
1396 would also be difficult to detect: no diagnostic metamorphic sole is expected to form
1397 along a relatively cold subcontinental mantle (Agard et al., 2016) and low rigidity of
1398 slow-spreading ophiolite would probably favor short-lived overthrusting.

1399

1400

1401 **7. Conclusions**

1402

1403 Two hundred years of thorough studies have made the Alps a uniquely detailed and
1404 informative orogen. The relatively modest collisional-related thermal imprint across
1405 most of the Alps, its simple organization and the 3D nature of the Alpine belt enable
1406 restoring a significant part of the history and dynamics of oceanic subduction.
1407 Realizing the importance of seafloor (and margin) inheritance has enabled to access
1408 even further details of subduction processes. The Alpine record of subducted oceanic
1409 lithosphere appears overall quite good and representative:

1410

1411 *(1) The Alpine P-T record is representative of subduction processes.*

1412 The consistent P/T gradient of oceanic fragments, similar to mature subduction, their
1413 recovery below a maximum pressure threshold (2.8-3 GPa), their consistent
1414 distribution along spatial gradients and within units, all indicate that the oceanic
1415 subduction record can be trusted and used as a reliable proxy of the pressure and
1416 temperature regime of subduction (one of the best we have at least), and that
1417 tectonic overpressure is limited (<~10%). For example, the Alpine record can inform
1418 on how underplating, fluid transfer or subduction earthquakes took place during ~60
1419 Ma of slow-spreading ocean subduction.

1420

1421 *(2) Spatiotemporal variations allow reconstructing subduction dynamics.*

1422 Significant contrasts exist between (i) underplating of metasediments, locally long-
1423 lived and across variable depths (e.g., south-west of Gran Paradiso; Liguro-Piemont
1424 ocean) or volumetrically large (e.g., Grisons; Valais ocean), (ii) spikes of rock
1425 recovery, as for the large mafic/ultramafic (MUM) eclogitic bodies or (iii) the greater
1426 recovery next to micro-continental slivers (Briançonnais, Sesia Zone), which
1427 demonstrates a strong influence of margin segmentation and continental subduction.
1428 Along-strike contrasts allow recognizing four main sectors, respectively south of Gran
1429 Paradiso (A), between Gran Paradiso and NE Monte Rosa (B), between the
1430 (eastern) Central Alps and the Engadine window (C), and east of the Engadine
1431 window (D).

1432 During the first half of the subduction period, between the onset of subduction (~100-
1433 95 Ma) and ~70-65 Ma, no subducted oceanic fragment was recovered; this only
1434 started after subduction of the Sesia Zone. Subduction to ~80 km depth of the MUM
1435 units of the Western Alps (which represent fragments of oceanic crust formed early at
1436 ~165-150 Ma), a few Ma before continental subduction, shows that only oceanic
1437 domains next to the continental margin and/or OCT domains are recovered. All other
1438 fragments formed between ~150 and 120 Ma have disappeared over a similar
1439 amount of time, during the first 30 Ma of subduction. Between ~65 and 50 Ma,
1440 subduction erosion is documented along sectors B-D (particularly in the eastern
1441 Central Alps) whereas subduction accretion prevailed along sector A. Before that
1442 time, the Alpine subduction was therefore either erosive, sediment starved and/or
1443 efficiently lubricated (thereby impeding rock recovery).

1444

1445 *(3) Preservation of the Alpine subduction record is remarkable but not atypical.*

1446 The Alpine subduction record is only exceptional in that it exposes many subducted
1447 fragments, particularly in the Western Alps, and documents the closure of a short-
1448 lived (60 Ma), slow-spreading, slowly closing ocean. Past seafloor essentially
1449 comprised variably refertilized exhumed mantle, irregularly distributed magmatic
1450 rocks and pelagic sediments, together with OCT domains and extensional allochtons.
1451 Nothing such as the incoming ocean plate stratigraphy observed off Chile or Japan
1452 today. In addition to plate kinematics, syn-subduction sedimentation and plate
1453 interface rheology, the Alpine record shows that inherited features (i.e., former
1454 Variscan- or rifting-related structures, distribution of magmatic bodies/provinces

1455 and/or sediments) largely impacted the subduction dynamics of the oceanic
1456 lithosphere.

1457 What the Alpine record exemplifies is the preferential recovery of eclogitic fragments
1458 from slow-spreading oceans. This conclusion is strengthened by the spectacular
1459 subduction-related rock record of the Cyclades/Pindos 'ocean', recently reappraised
1460 as a former stretched continental margin (Schmid et al., 2020). In contrast with the
1461 Cyclades, however, at least ~200-300 km of real Atlantic-type seafloor disappeared
1462 in the Alps. With such a short slab the Alpine subduction likely never reached the 660
1463 km discontinuity, another significant difference with large-scale subduction zones
1464 associated with wholesale mantle convection.

1465

1466

1467
1468
1469
1470
1471
1472
1473
1474
1475
1476
1477
1478
1479
1480
1481
1482
1483
1484
1485
1486
1487

ACKNOWLEDGMENTS

This contribution is dedicated to Marcel Lemoine, a man of energy, vision and wisdom. Twenty years after a short field excursion together, the systematic combination of lithostratigraphy and detailed metamorphic petrology still appears very promising. Very warm thanks are due to B. Goffé and L. Jolivet for their initial enthusiasm, and to C. Rosenberg for pushing me to do this. S. Schmid and L. Jolivet are greatly thanked for their many suggestions. This contribution would not have been possible without the students with whom I have shared so many good moments in the Alpine trails, i.e. S. Angiboust, M. Locatelli, B. Lefeuvre, C. Herviou. As well as with P. Yamato and H. Raimbourg, and with R. Bousquet and M. Patriat in the good old days. Special thanks go to P. Monié, G. Bebout and A. Verlaquet. Many colleagues, too many to name here, are thanked for inspiration. Special thoughts go to my ZIP and EFIRE colleagues and friends. Finally, please bear with the author: I have tried to acknowledge the merits of as many studies as possible and be representative. I sincerely apologize to those either not cited or insufficiently acknowledged here.

1488 **References**

1489

1490 Agard, P., 1999. Evolution métamorphique et structurale des métapelites océaniques dans l'orogène
1491 Alpin: l'exemple des Schistes Lustrés des Alpes occidentales (Alpes Cottiennes). PhD
1492 dissertation, 324 p.

1493 Agard, P., Goffé, B., Touret, J.L., Vidal, O., 2000. Retrograde mineral and fluid evolution in high-
1494 pressure metapelites (Schistes lustrés unit, Western Alps). *Contributions to Mineralogy and*
1495 *Petrology* 140, 296–315.

1496 Agard, P., Jolivet, L., Goffe, B., 2001a. Tectonometamorphic evolution of the Schistes Lustre's
1497 complex: implications for the exhumation of HP and UHP rocks in the western Alps. *Bull. Soc.*
1498 *Geol. Fr.* 172, 617–636. <https://doi.org/10.2113/172.5.617>

1499 Agard P., Vidal O., Goffé B., 2001b. Interlayer and Si content of phengite in HP-LT carpholite-bearing
1500 metapelites. *Journal of metamorphic geology*, 19, 477-493.

1501 Agard, P., Monie, P., Jolivet, L., Goffe, B., 2002. Exhumation of the Schistes Lustres complex: in situ
1502 laser probe Ar-40/Ar-39 constraints and implications for the Western Alps. *J. Metamorph.*
1503 *Geol.* 20, 599–618. <https://doi.org/10.1046/j.1525-1314.2002.00391.x>

1504 Agard, P., Yamato, P., Jolivet, L., Burov, E., 2009. Exhumation of oceanic blueschists and eclogites in
1505 subduction zones: Timing and mechanisms. *Earth-Science Reviews* 92, 53–79.
1506 <https://doi.org/10.1016/j.earscirev.2008.11.002>

1507 Agard, P., Yamato, P., Soret, M., Prigent, C., Guillot, S., Plunder, A., Dubacq, B., Chauvet, A., Monie,
1508 P., 2016. Plate interface rheological switches during subduction infancy: Control on slab
1509 penetration and metamorphic sole formation. *Earth Planet. Sci. Lett.* 451, 208–220.
1510 <https://doi.org/10.1016/j.epsl.2016.06.054>

1511 Agard, P., Plunder, A., Angiboust, S., Bonnet, G., Ruh, J., 2018. The subduction plate interface: rock
1512 record and mechanical coupling (from long to short timescales). *Lithos* 320–321, 537–566.
1513 <https://doi.org/10.1016/j.lithos.2018.09.029>

1514 Agard, P., Prigent, C., Soret, M., Dubacq, B., Guillot, S., Deldicque D., 2020. Slabitzation:
1515 mechanisms controlling subduction development and viscous coupling. *Earth-Science*
1516 *Reviews* 103259

1517 Amato, J.M., Johnson, C.M., Baumgartner, L.P., Beard, B.L., 1999. Rapid exhumation of the Zermatt-
1518 Saas ophiolite deduced from high-precision Sm-Nd and Rb-Sr geochronology. *Earth and*
1519 *Planetary Science Letters* 171, 425–438.

1520 Ampferer, O., Hammer, W., 1911. Geologischer Querschnitt durch die Ostalpen vom Allgäu zum
1521 Gardasee. *Jahrbuch der Kaiserlich-Königlichen Geologischen Reichsanstalt* 61, 532–710.

1522 Amstutz, A., 1951. Sur l'évolution des structures alpines. *Arch. Sci* 4, 323–329.

1523 Angiboust, S., Agard, P., 2010. Initial water budget The key to detaching large volumes of eclogitized
1524 oceanic crust along the subduction channel? *Lithos* 120, 453–474.
1525 <https://doi.org/10.1016/j.lithos.2010.09.007>

1526 Angiboust, S., Glodny, J., 2020. Exhumation of eclogitic ophiolitic nappes in the W. Alps: New age
1527 data and implications for crustal wedge dynamics. *Lithos* 105374.

- 1528 Angiboust, S., Agard, P., Jolivet, L., Beyssac, O., 2009. The Zermatt-Saas ophiolite: the largest (60-
1529 km wide) and deepest (c. 70-80 km) continuous slice of oceanic lithosphere detached from a
1530 subduction zone? *Terr. Nova* 21, 171–180. <https://doi.org/10.1111/j.1365-3121.2009.00870.x>
- 1531 Angiboust, S., Agard, P., Raimbourg, H., Yamato, P., Huet, B., 2011. Subduction interface processes
1532 recorded by eclogite-facies shear zones (Monviso, W. Alps). *Lithos* 127, 222–238.
1533 <https://doi.org/10.1016/j.lithos.2011.09.004>
- 1534 Angiboust, S., Agard, P., Yamato, P., Raimbourg, H., 2012a. Eclogite breccias in a subducted
1535 ophiolite: A record of intermediate-depth earthquakes? *Geology* 40, 707–710.
1536 <https://doi.org/10.1130/G32925.1>
- 1537 Angiboust, S., Langdon, R., Agard, P., Waters, D., Chopin, C., 2012b. Eclogitization of the Monviso
1538 ophiolite (W. Alps) and implications on subduction dynamics. *J. Metamorph. Geol.* 30, 37–61.
1539 <https://doi.org/10.1111/j.1525-1314.2011.00951.x>
- 1540 Angiboust, S., Wolf, S., Burov, E., Agard, P., Yamato, P., 2012c. Effect of fluid circulation on
1541 subduction interface tectonic processes: Insights from thermo-mechanical numerical
1542 modelling. *Earth Planet. Sci. Lett.* 357, 238–248. <https://doi.org/10.1016/j.epsl.2012.09.012>
- 1543 Angiboust, S., Glodny, J., Oncken, O., Chopin, C., 2014a. In search of transient subduction interfaces
1544 in the Dent Blanche-Sesia Tectonic System (W. Alps). *Lithos* 205, 298–321.
1545 <https://doi.org/10.1016/j.lithos.2014.07.001>
- 1546 Angiboust, S., Pettke, T., De Hoog, J.C.M., Caron, B., Oncken, O., 2014b. Channelized Fluid Flow
1547 and Eclogite-facies Metasomatism along the Subduction Shear Zone. *J. Petrol.* 55, 883–916.
1548 <https://doi.org/10.1093/petrology/egu010>
- 1549 Angiboust, S., Kirsch, J., Oncken, O., Glodny, J., Monie, P., Rybacki, E., 2015. Probing the transition
1550 between seismically coupled and decoupled segments along an ancient subduction interface.
1551 *Geochem. Geophys. Geosyst.* 16, 1905–1922. <https://doi.org/10.1002/2015GC005776>
- 1552 Anonymous, 1972. Penrose field conference on ophiolites. *Geotimes* 17, 24–25.
- 1553 Antoine, P., 1972. Le domaine pennique externe entre Bourg-Saint-Maurice (Savoie) et la frontière
1554 italo-suisse. *Géol. Alpine* 48, 5–40.
- 1555 Argand, E., 1924. *Des Alpes et de l’Afrique*.
- 1556 Audet, P., Bürgmann, R., 2014. Possible control of subduction zone slow-earthquake periodicity by
1557 silica enrichment. *Nature* 510, 389.
- 1558 Auzende, J.-M., Polino, R., Lagabrielle, Y., Olivet, J.-L., 1983. Considérations sur l’origine et la mise
1559 en place des ophiolites des Alpes occidentales: apport de la connaissance des structures
1560 océaniques. *Comptes Rendus de l’Academie des Sciences Serie II* 296.
- 1561 Bachmann, R., Glodny, J., Oncken, O., Seifert, W., 2009a. Abandonment of the South Penninic–
1562 Austroalpine palaeosubduction zone, Central Alps, and shift from subduction erosion to
1563 accretion: constraints from Rb/Sr geochronology. *Journal of the Geological Society* 166, 217–
1564 231.
- 1565 Bachmann, R., Oncken, O., Glodny, J., Seifert, W., Georgieva, V., Sudo, M., 2009b. Exposed plate
1566 interface in the European Alps reveals fabric styles and gradients related to an ancient

1567 seismogenic coupling zone. *Journal of Geophysical Research: Solid Earth* 114.
1568 <https://doi.org/10.1029/2008JB005927>

1569 Balestro, G., Festa, A., Dilek, Y., Tartarotti, P., 2015. Pre-Alpine extensional tectonics of a peridotite-
1570 localized oceanic core complex in the late Jurassic, high-pressure Monviso ophiolite (Western
1571 Alps). *Episodes* 38, 266–282.

1572 Balestro, G., Lombardo, B., Vaggelli, G., Borghi, A., Festa, A., Gattiglio, M., 2014. Tectonostratigraphy
1573 of the northern Monviso meta-ophiolite complex (Western Alps). *Italian Journal of
1574 Geosciences* 133, 409–426.

1575 Ballèvre, M., Merle, O., 1993. The Combin fault: compressional reactivation of a Late Cretaceous-
1576 Early Tertiary detachment fault in the Western Alps. *Schweizerische Mineralogische und
1577 Petrographische Mitteilungen* 73, 205–227.

1578 Balleve, M., Lagabrielle, Y., Merle, O., 1990. Tertiary ductile normal faulting as a consequence of
1579 lithospheric stacking in the western Alps. *Mémoires de la Société géologique de France
1580 (1833)* 156, 227–236.

1581 Balleve, M., Manzotti, P., Dal Piaz, G.V., 2018. Pre-Alpine (Variscan) Inheritance: A Key for the
1582 Location of the Future Valais Basin (Western Alps). *Tectonics* 37, 786–817.

1583 Barfety, J.-C., Polino, R., Mercier, D., Caby, R., Fourneaux, J., 2006. Notice de la carte géologique
1584 Névache-Bardonecchia-Modane, 799, Bureau des Recherches Géologiques et Minières.

1585 Barnes, J.D., Beltrando, M., Lee, C.-T.A., Cisneros, M., Loewy, S., Chin, E., 2014. Geochemistry of
1586 Alpine serpentinites from rifting to subduction: A view across paleogeographic domains and
1587 metamorphic grade. *Chemical Geology* 389, 29–47.

1588 Barnes, J.D., Penniston-Dorland, S.C., Bebout, G.E., Hoover, W., Beaudoin, G.M., Agard, P., 2019.
1589 Chlorine and lithium behavior in metasedimentary rocks during prograde metamorphism: A
1590 comparative study of exhumed subduction complexes (Catalina Schist and Schistes Lustrés).
1591 *Lithos* 336, 40–53.

1592 Barnicoat, A., Rex, D., Guise, P., Cliff, R., 1995. The timing of and nature of greenschist facies
1593 deformation and metamorphism in the upper Pennine Alps. *Tectonics* 14, 279–293.

1594 Bebout, G.E., 2007. Metamorphic chemical geodynamics of subduction zones. *Earth and Planetary
1595 Science Letters* 260, 373–393. <https://doi.org/10.1016/j.epsl.2007.05.050>

1596 Bebout, G.E., Penniston-Dorland, S.C., 2016. Fluid and mass transfer at subduction interfaces—The
1597 field metamorphic record. *Lithos* 240–243, 228–258.
1598 <https://doi.org/10.1016/j.lithos.2015.10.007>

1599 Bebout, G.E., Ryan, J.G., Leeman, W.P., Bebout, A.E., 1999. Fractionation of trace elements by
1600 subduction-zone metamorphism—effect of convergent-margin thermal evolution. *Earth and
1601 Planetary Science Letters* 171, 63–81.

1602 Bebout, G.E., Agard, P., Kobayashi, K., Moriguti, T., Nakamura, E., 2013. Devolatilization history and
1603 trace element mobility in deeply subducted sedimentary rocks: Evidence from Western Alps
1604 HP/UHP suites. *Chemical Geology* 342, 1–20.

1605 Bechennec, F., Le Metour, J., Rabu, D., Beurrier, M., Bourdillon-Jeudy-de-Grissac, C., De Wever, P.,
1606 Tegye, M., Villey, M., 1989. Geologie d'une chaine issue de la Tethys; les montagnes
1607 d'Oman. *Bulletin de la Société géologique de France* 167–188.

1608 Bedford, J., Moreno, M., Baez, J.C., Lange, D., Tilmann, F., Rosenau, M., Heidbach, O., Oncken, O.,
1609 Bartsch, M., Rietbrock, A., 2013. A high-resolution, time-variable afterslip model for the 2010
1610 Maule Mw= 8.8, Chile megathrust earthquake. *Earth and Planetary Science Letters* 383, 26–
1611 36.

1612 Beltrando, M., Compagnoni, R., Lombardo, B., 2010. (Ultra-) High-pressure metamorphism and
1613 orogenesis: an Alpine perspective. *Gondwana Research* 18, 147–166.

1614 Beltrando, M., Lister, G.S., Forster, M., Dunlap, W.J., Fraser, G., Hermann, J., 2009. Dating
1615 microstructures by the ⁴⁰Ar/³⁹Ar step-heating technique: deformation–pressure–
1616 temperature–time history of the Penninic Units of the Western Alps. *Lithos* 113, 801–819.

1617 Beltrando, M., Manatschal, G., Mohn, G., Dal Piaz, G.V., Brovarone, A.V., Masini, E., 2014.
1618 Recognizing remnants of magma-poor rifted margins in high-pressure orogenic belts: The
1619 Alpine case study. *Earth-Science Reviews* 131, 88–115.

1620 Berger, A., Bousquet, R., 2008. Subduction-related metamorphism in the Alps: review of isotopic ages
1621 based on petrology and their geodynamic consequences. *Geological Society, London, Special
1622 Publications* 298, 117–144.

1623 Berger, A., Mercolli, I., Engi, M., 2005. The central Lepontine Alps: Notes accompanying the tectonic
1624 and petrographic map sheet Sopra Ceneri (1: 100'000). *Schweizerische Mineralogische und
1625 Petrographische Mitteilungen* 85, 109–146.

1626 Beyssac, O., Goffé, B., Chopin, C., Rouzaud, J., 2002. Raman spectra of carbonaceous material in
1627 metasediments: a new geothermometer. *Journal of metamorphic Geology* 20, 859–871.

1628 Bonnet, G., Agard, P., Angiboust, S., Monié, P., Jentzer, M., Omrani, J., Whitechurch, H., Fournier,
1629 M., 2018. Tectonic slicing and mixing processes along the subduction interface: The Sistan
1630 example (Eastern Iran). *Lithos* 310–311, 269–287. <https://doi.org/10.1016/j.lithos.2018.04.016>

1631 Bortolotti, V., Principi, G., 2005. Tethyan ophiolites and Pangea break-up. *Island Arc* 14, 442–470.

1632 Bouffette, J., Caron, J.-M., 1991. Trajets métamorphiques prograde et rétrograde dans des éclogites
1633 piémontaises (Ouest du massif du Rocciavrè, Alpes cottiennes). *Comptes rendus de
1634 l'Académie des sciences. Série 2, Mécanique, Physique, Chimie, Sciences de l'univers,
1635 Sciences de la Terre* 312, 1459–1465.

1636 Bousquet, R., 2008. Metamorphic heterogeneities within a single HP unit: overprint effect or
1637 metamorphic mix? *Lithos* 103, 46–69.

1638 Bousquet, R., Engi, M., Gosso, G., Berger, A., Spalla, M.I., Zucali, M., Goffè, B., 2004. Explanatory
1639 notes to the map: Metamorphic structure of the Alps. Presented at the Central Alps. *Mitt.
1640 Österr. Miner. Ges, Citeseer*.

1641 Bousquet, R., Goffe, B., Vidal, O., Oberhänsli, R., Patriat, M., 2002. The tectono-metamorphic history
1642 of the Valaisan domain from the Western to the Central Alps: New constraints on the evolution
1643 of the Alps. *Geol. Soc. Am. Bull.* 114, 207–225. [https://doi.org/10.1130/0016-
1644 7606\(2002\)114<0207:TTMHOT>2.0.CO;2](https://doi.org/10.1130/0016-7606(2002)114<0207:TTMHOT>2.0.CO;2)

- 1645 Bousquet, R., Oberhänsli, R., Goffe, B., Jolivet, L., Vidal, O., 1998. High-pressure-low-temperature
1646 metamorphism and deformation in the Bündnerschiefer of the Engadine window: implications
1647 for the regional evolution of the eastern Central Alps. *J. Metamorph. Geol.* 16, 657–674.
1648 <https://doi.org/10.1111/j.1525-1314.1998.00161.x>
- 1649 Bousquet, R., Oberhänsli, R., Goffé, B., Wiederkehr, M., Koller, F., Schmid, S.M., Schuster, R., Engi,
1650 M., Berger, A., Martinotti, G., 2008. Metamorphism of metasediments at the scale of an
1651 orogen: a key to the Tertiary geodynamic evolution of the Alps. Geological Society, London,
1652 Special Publications 298, 393–411.
- 1653 Bousquet, R.; Oberhänsli, R.; Schmid, S.M.; Berger, A.; Wiederkehr, M.; Robert, Ch.; Möller, A.;
1654 Rosenberg, C.; Zeilinger, G.; Molli, G.; Koller, F., 2012: Metamorphic Framework of the Alps.
1655 Map 1 : 1 000 000. CCGM/CGMW (Commission for the Geological Map of the World, Paris).
1656 <http://www.geodynamps.org>
- 1657 Bowtell, S., Cliff, R., Barnicoat, A., 1994. Sm–Nd isotopic evidence on the age of eclogitization in the
1658 Zermatt–Saas ophiolite. *Journal of Metamorphic Geology* 12, 187–196.
- 1659 Broadwell, K.S., Locatelli, M., Verlaguet, A., Agard, P., Caddick, M.J., 2019. Transient and periodic
1660 brittle deformation of eclogites during intermediate-depth subduction. *Earth and Planetary
1661 Science Letters* 521, 91–102.
- 1662 Brun, J.-P., Faccenna, C., 2008. Exhumation of high-pressure rocks driven by slab rollback. *Earth and
1663 Planetary Science Letters* 272, 1–7. <https://doi.org/10.1016/j.epsl.2008.02.038>
- 1664 Bucher, K., Fazis, Y., De Capitani, C., Grapes, R., 2005. Blueschists, eclogites, and decompression
1665 assemblages of the Zermatt–Saas ophiolite: High-pressure metamorphism of subducted
1666 Tethys lithosphere. *Am. Miner.* 90, 821–835. <https://doi.org/10.2138/am.2005.1718>
- 1667 Bucher, K., Grapes, R., 2009. The eclogite-facies Allalin Gabbro of the Zermatt–Saas ophiolite,
1668 Western Alps: A record of subduction zone hydration. *Journal of Petrology* 50, 1405–1442.
- 1669 Bucher, K., Weisenberger, T.B., Weber, S., Klemm, O., Corfu, F., 2020. The Theodul Glacier Unit, a
1670 slab of pre-Alpine rocks in the Alpine meta-ophiolite of Zermatt–Saas, Western Alps. *Swiss
1671 Journal of Geosciences* 113, 1–22.
- 1672 Bucher, S., Schmid, S.M., Bousquet, R., Fügenschuh, B., 2003. Late-stage deformation in a
1673 collisional orogen (Western Alps): nappe refolding, back-thrusting or normal faulting? *Terra
1674 Nova* 15, 109–117.
- 1675 Burrioni, A., Levi, N., Marroni, M., Pandolfi, L., 2003. Lithostratigraphy and structure of the Lago Nero
1676 unit (Chenaillet massif, western Alps): comparison with internal liguride units of northern
1677 Apennines. *Ofioliti* 28, 1–11.
- 1678 Busigny, V., Cartigny, P., Philippot, P., Javoy, M., 2003. Ammonium quantification in muscovite by
1679 infrared spectroscopy. *Chemical Geology* 198, 21–31.
- 1680 Caby, R., 1973. Les plis transversaux dans les Alpes occidentales; implications pour la genèse de la
1681 chaîne alpine. *Bulletin de la Société géologique de France* 7, 624–634.
- 1682 Calahorrano, A., Sallarès, V., Collot, J.-Y., Sage, F., Ranero, C.R., 2008. Nonlinear variations of the
1683 physical properties along the southern Ecuador subduction channel: Results from depth-
1684 migrated seismic data. *Earth and Planetary Science Letters* 267, 453–467.

- 1685 Cannat, M., Lagabriele, Y., Bougault, H., Casey, J., de Coutures, N., Dmitriev, L., Fouquet, Y., 1997.
 1686 Ultramafic and gabbroic exposures at the Mid-Atlantic Ridge: Geological mapping in the 15 N
 1687 region. *Tectonophysics* 279, 193–213.
- 1688 Cannat, M., Manatschal, G., Sauter, D., Peron-Pinvidic, G., 2009. Assessing the conditions of
 1689 continental breakup at magma-poor rifted margins: what can we learn from slow spreading
 1690 mid-ocean ridges? *Comptes Rendus Geoscience* 341, 406–427.
- 1691 Cannat, M., Mevel, C., Maia, M., Deplus, C., Durand, C., Gente, P., Agrinier, P., Belarouchi, A.,
 1692 Dubuisson, G., Humler, E., 1995. Thin crust, ultramafic exposures, and rugged faulting
 1693 patterns at the Mid-Atlantic Ridge (22–24 N). *Geology* 23, 49–52.
- 1694 Cannic, S., Lardeaux, J., Mugnier, J., Hernandez, J., 1996. Tectono-metamorphic evolution of the
 1695 Roignais-Versoyen Unit (Valaisan domain, France). *Eclogae Geologicae Helvetiae* 89, 321–
 1696 343.
- 1697 Caron, J.-M., 1977. Lithostratigraphie et tectonique des Schistes lustrés dans les Alpes cottiennes
 1698 septentrionales et en Corse orientale. *Persée-Portail des revues scientifiques en SHS*.
- 1699 Castelli, D., Rostagno, C., Lombardo, B., 2002. JD-QTZ-bearing metaplagiogranite from the Monviso
 1700 meta-ophiolite (Western Alps). *Ofioliti* 27, 81–90.
- 1701 Castelli, Daniele, Rostagno, C., Lombardo, B., 2002. Jd-Qtz-bearing metaplagiogranite from the
 1702 Monviso meta-ophiolite (Western Alps). *Ofioliti* 27, 81–90.
- 1703 Chalot-Prat, F., Ganne, J., Lombard, A., 2003. No significant element transfer from the oceanic plate
 1704 to the mantle wedge during subduction and exhumation of the Tethys lithosphere (Western
 1705 Alps). *Lithos* 69, 69–103.
- 1706 Chlieh, M., Perfettini, H., Tavera, H., Avouac, J., Remy, D., Nocquet, J., Rolandone, F., Bondoux, F.,
 1707 Gabalda, G., Bonvalot, S., 2011. Interseismic coupling and seismic potential along the Central
 1708 Andes subduction zone. *Journal of Geophysical Research: Solid Earth* 116.
- 1709 Chopin, C., 1981. Mise en évidence d'une discontinuité du métamorphisme alpin entre le massif du
 1710 Grand Paradis et sa couverture allochtone (Alpes occidentales françaises). *Bulletin de la*
 1711 *Société Géologique de France* 7, 297–301.
- 1712 Chopin, C., 1984. Coesite and pure pyrope in high-grade blueschists of the Western Alps: a first
 1713 record and some consequences. *Contributions to Mineralogy and Petrology* 86, 107–118.
- 1714 Chopin, C., 2003. Ultrahigh-pressure metamorphism: tracing continental crust into the mantle. *Earth*
 1715 *and Planetary Science Letters* 212, 1–14.
- 1716 Chopin, C., Schertl, H.-P., 1999. The UHP unit in the Dora-Maira massif, western Alps. *International*
 1717 *geology review* 41, 765–780.
- 1718 Christensen, J.N., Selverstone, J., Rosenfeld, J.L., DePaolo, D.J., 1994. Correlation by Rb-Sr
 1719 geochronology of garnet growth histories from different structural levels within the Tauern
 1720 Window, Eastern Alps. *Contributions to Mineralogy and Petrology* 118, 1–12.
- 1721 Cliff, R., Barnicoat, A., Inger, S., 1998. Early Tertiary eclogite facies metamorphism in the Monviso
 1722 Ophiolite. *Journal of Metamorphic Geology* 16, 447–455.

- 1723 Cloos, M., 1982. Flow Melanges - Numerical Modeling and Geologic Constraints on Their Origin in the
1724 Franciscan Subduction Complex, California. *Geol. Soc. Am. Bull.* 93, 330–345.
1725 [https://doi.org/10.1130/0016-7606\(1982\)93<330:FMNMAG>2.0.CO;2](https://doi.org/10.1130/0016-7606(1982)93<330:FMNMAG>2.0.CO;2)
- 1726 Collins, N.C., Bebout, G.E., Angiboust, S., Agard, P., Scambelluri, M., Crispini, L., John, T., 2015.
1727 Subduction zone metamorphic pathway for deep carbon cycling: II. Evidence from HP/UHP
1728 metabasaltic rocks and ophicarbonates. *Chemical Geology* 412, 132–150.
- 1729 Colombi, A., Pfeifer, H.-R., 1986. Ferrogabbroic and basaltic meta-eclogites from the Antrona mafic-
1730 ultramafic complex and the Centovalli-Locarno region (Italy and Southern Switzerland)-first
1731 results. *Schweizerische Mineralogische und Petrographische Mitteilungen* 66, 99–110.
- 1732 Coltice, N., Husson, L., Faccenna, C., Arnould, M., 2019. What drives tectonic plates? *Science*
1733 *advances* 5, eaax4295.
- 1734 Compagnoni, R., Rolfo, F., 2003. UHPM units in the Western Alps. *Ultrahigh pressure metamorphism*
1735 5, 13–49.
- 1736 Conrad, C.P., Lithgow-Bertelloni, C., 2002. How mantle slabs drive plate tectonics. *Science* 298, 207–
1737 209.
- 1738 Cook-Kollars, J., Bebout, G.E., Collins, N.C., Angiboust, S., Agard, P., 2014b. Subduction zone
1739 metamorphic pathway for deep carbon cycling: I. Evidence from HP/UHP metasedimentary
1740 rocks, Italian Alps. *Chem. Geol.* 386, 31–48. <https://doi.org/10.1016/j.chemgeo.2014.07.013>
- 1741 Corno, A., Mosca, P., Borghi, A., Gatteggio, M., 2019. Lithostratigraphy and petrography of the Monte
1742 Banchetta-Punta Rognosa oceanic succession (Troncea and Chisonetto Valleys, Western
1743 Alps). *Ofioliti* 44, 83–95.
- 1744 Costa, S., Caby, R., 2001. Evolution of the Ligurian Tethys in the Western Alps: Sm/Nd and U/Pb
1745 geochronology and rare-earth element geochemistry of the Montgenèvre ophiolite (France).
1746 *Chemical Geology* 175, 449–466.
- 1747 Dachs, E., Proyer, A., 2001. Relics of high-pressure metamorphism from the Grossglockner region,
1748 Hohe Tauern, Austria: Paragenetic evolution and PT-paths of retrogressed eclogites.
1749 *European Journal of Mineralogy* 13, 67–86.
- 1750 Dal Piaz, G.V., 2001. History of tectonic interpretations of the Alps. *Journal of geodynamics* 32, 99–
1751 114.
- 1752 Dal Piaz, G., Ernst, W., 1978. Areal geology and petrology of eclogites and associated metabasites of
1753 the Piemonte ophiolite nappe, breuil—st. Jacques area, Italian Western Alps. *Tectonophysics*
1754 51, 99–126.
- 1755 Dal Piaz G.V., Hunziker J.C., Martinotti G., 1972. La zona Sesia-Lanzo e l'evoluzione tettonico-
1756 metamorfica delle Alpi nord-occidentali interne. *Memorie della Società Geologica Italiana*, 11,
1757 433-466.
- 1758 Dal Piaz, G., Cortiana, G., Del Moro, A., Martin, S., Pennacchioni, G., Tartarotti, P., 2001. Tertiary age
1759 and paleostructural inferences of the eclogitic imprint in the Austroalpine outliers and Zermatt–
1760 Saas ophiolite, western Alps. *International Journal of Earth Sciences* 90, 668–684.

- 1761 de Graciansky, P., 1972. Le bassin tertiaire de Barrême (Alpes de Haute-Provence): Relations entre
1762 déformation et sédimentation; chronologie des plissements. *Comptes Rendus de l'Académie*
1763 *des Sciences, Paris* 275, 2825–2828.
- 1764 De Wever, P., Caby, R., 1981. Datation de la base des schistes lustrés postophiolitiques par des
1765 radiolaires (Oxfordien-Kimmeridgien moyen) dans les Alpes Cottiennes (Saint Véran, France).
1766 *Compte rendu de l'académie des Sciences de Paris* 292, 467–472.
- 1767 Debelmas, J., Lemoine, M., 1970. The western Alps: palaeogeography and structure. *Earth-Science*
1768 *Reviews* 6, 221–256.
- 1769 Debret, B., Bouilhol, P., Pons, M.L., Williams, H., 2018. Carbonate transfer during the onset of slab
1770 devolatilization: new insights from Fe and Zn stable isotopes. *Journal of Petrology* 59, 1145–
1771 1166.
- 1772 Debret, B., Millet, M.-A., Pons, M.-L., Bouilhol, P., Inglis, E., Williams, H., 2016. Isotopic evidence for
1773 iron mobility during subduction. *Geology* 44, 215–218.
- 1774 Debret, B., Nicollet, C., Andreani, M., Schwartz, S., Godard, M., 2013. Three steps of serpentinization
1775 in an eclogitized oceanic serpentinization front (Lanzo Massif–Western Alps). *Journal of*
1776 *Metamorphic Geology* 31, 165–186.
- 1777 Dercourt, J., Zonenshain, L., Ricou, L.-E., Kazmin, V., Le Pichon, X., Knipper, A., Grandjacquet, C.,
1778 Sbortshikov, I., Geysant, J., Lepvrier, C., 1986. Geological evolution of the Tethys belt from
1779 the Atlantic to the Pamirs since the Lias. *Tectonophysics* 123, 241–315.
- 1780 Deschamps, F., Godard, M., Guillot, S., Hattori, K., 2013. Geochemistry of subduction zone
1781 serpentinites: A review. *Lithos* 178, 96–127.
- 1782 Deville, E., Fudral, S., Lagabrielle, Y., Marthaler, M., Sartori, M., 1992. From oceanic closure to
1783 continental collision: A synthesis of the " Schistes lustrés" metamorphic complex of the
1784 Western Alps. *Geological Society of America Bulletin* 104, 127–139.
- 1785 Dewey, J., Helman, M., Knott, S., Turco, E., Hutton, D., 1989. Kinematics of the western
1786 Mediterranean. *Geological Society, London, Special Publications* 45, 265–283.
- 1787 Dingeldey, C., Dallmeyer, R.D., Koller, F., Massonne, H.-J., 1997. P-T-t history of the Lower
1788 Austroalpine Nappe Complex in the "Tarntaler Berge" NW of the Tauern Window: implications
1789 for the geotectonic evolution of the central Eastern Alps. *Contributions to Mineralogy and*
1790 *Petrology* 129, 1–19.
- 1791 Dragovic, B., Samanta, L.M., Baxter, E.F., Selverstone, J., 2012. Using garnet to constrain the
1792 duration and rate of water-releasing metamorphic reactions during subduction: An example
1793 from Sifnos, Greece. *Chem. Geol.* 314, 9–22. <https://doi.org/10.1016/j.chemgeo.2012.04.016>
- 1794 Dragovic, B., Angiboust, S., Tappa, M.J., 2020. Petrochronological close-up on the thermal structure
1795 of a paleo-subduction zone (W. Alps). *Earth and Planetary Science Letters* 547, 116446.
- 1796 Droop, G.T., Chavrit, D., 2014. Eclogitic metagabbro from the Lanzada Window, eastern Central Alps:
1797 confirmation of subduction beneath the Malenco Unit. *Swiss Journal of Geosciences* 107,
1798 113–128.

- 1799 Duchêne, S., Blichert-Toft, J., Luais, B., Télouk, P., Lardeaux, J.-M., Albaredo, F., 1997. The Lu–Hf
1800 dating of garnets and the ages of the Alpine high-pressure metamorphism. *Nature* 387, 586–
1801 589.
- 1802 Dumitru, T.A., Wakabayashi, J., Wright, J.E., Wooden, J.L., 2010. Early Cretaceous transition from
1803 nonaccretionary behavior to strongly accretionary behavior within the Franciscan subduction
1804 complex. *Tectonics* 29, TC5001. <https://doi.org/10.1029/2009TC002542>
- 1805 Dumont, T., Lemoine, M., Tricart, P., 1984. Tectonique synsédimentaire triasico-jurassique et rifting
1806 téthysien dans l'unité prépiémontaise de Rochebrune au Sud-Est de Briançon. *Bulletin de la*
1807 *Société géologique de France* 7, 921–933.
- 1808 Ellero, A., Loprieno, A., 2017. Nappe stack of Piemontese–Ligurian units south of Aosta Valley: New
1809 evidence from Urtier Valley (Western Alps). *Geological Journal* 53, 1665–1684.
- 1810 Elter, G., 1971. Schistes lustrés et ophiolites de la zone piémontaise entre Orco et Doire Baltée (Alpes
1811 Graies). Hypothèses sur l'origine des ophiolites. *Géologie Alpine* 47, 147–169.
- 1812 Engi, M., Bousquet, R., Berger, A., 2004. Explanatory notes to the map: metamorphic structure of the
1813 Alps. Presented at the Central Alps. *Mitt. Österr. Miner. Ges.*, Citeseer.
- 1814 Epstein, G.S., Bebout, G.E., Angiboust, S., Agard, P., 2020. Scales of fluid-rock interaction and
1815 carbon mobility in the deeply underplated and HP-Metamorphosed Schistes Lustrés, Western
1816 Alps. *Lithos* 354, 105229.
- 1817 Ernst, W., 1975. Systematics of large-scale tectonics and age progressions in Alpine and Circum-
1818 Pacific blueschist belts. *Tectonophysics* 26, 229–246.
- 1819 Ernst, W., 1971. Metamorphic zonations on presumably subducted lithospheric plates from Japan,
1820 California and the Alps. *Contributions to Mineralogy and Petrology* 34, 43–59.
- 1821 Ernst, W.G., 2001. Subduction, ultrahigh-pressure metamorphism, and regurgitation of buoyant crustal
1822 slices—implications for arcs and continental growth. *Physics of the Earth and Planetary*
1823 *Interiors* 127, 253–275.
- 1824 Faccenda, M., 2014. Water in the slab: A trilogy. *Tectonophysics* 614, 1–30.
1825 <https://doi.org/10.1016/j.tecto.2013.12.020>
- 1826 Fagereng, A., 2011. Geology of the seismogenic subduction thrust interface, in: Fagereng, A., Toy,
1827 V.G., Rowland, J.V. (Eds.), *Geology of the Earthquake Source: A Volume in Honour of Rick*
1828 *Sibson*. Geological Soc Publishing House, Bath, pp. 55–76.
- 1829 Faryad, S., Hoinkes, G., 2003. P–T gradient of Eo-Alpine metamorphism within the Austroalpine
1830 basement units east of the Tauern Window (Austria). *Mineralogy and Petrology* 77, 129–159.
- 1831 Fauquette, S., Bernet, M., Suc, J.-P., Grosjean, A.-S., Guillot, S., Van Der Beek, P., Jourdan, S.,
1832 Popescu, S.-M., Jiménez-Moreno, G., Bertini, A., 2015. Quantifying the Eocene to Pleistocene
1833 topographic evolution of the southwestern Alps, France and Italy. *Earth and Planetary Science*
1834 *Letters* 412, 220–234.
- 1835 Festa, A., Pini, G.A., Ogata, K., Dilek, Y., 2019. Diagnostic features and field-criteria in recognition of
1836 tectonic, sedimentary and diapiric mélanges in orogenic belts and exhumed subduction-
1837 accretion complexes. *Gondwana Research*.

- 1838 Fisher, D., Byrne, T., 1987. Structural evolution of underthrust sediments, Kodiak Islands, Alaska.
1839 Tectonics 6, 775–793.
- 1840 Forsyth D., Uyeda S., 1975. On the relative importance of the driving forces of plate motion. Geophys.
1841 J. R. astr. Soc., 43, 163-200.
- 1842 Frey, M., Desmons, J., Neubauer, F., 1999. The new metamorphic maps of the Alps: Introduction.
1843 Schweizerische Mineralogische und Petrographische Mitteilungen 1–4.
- 1844 Frey, M., Ferreiro Mählmann, R., 1999. Alpine metamorphism of the Central Alps. Schweizerische
1845 Mineralogische und Petrographische Mitteilungen 79, 135–154.
- 1846 Frezzotti, M.L., Selverstone, J., Sharp, Z.D., Compagnoni, R., 2011. Carbonate dissolution during
1847 subduction revealed by diamond-bearing rocks from the Alps. Nat. Geosci. 4, 703–706.
1848 <https://doi.org/10.1038/NGEO1246>
- 1849 Froitzheim, N., Schmid, S.M. and Conti, P., 1994. Repeated change from crustal shortening to orogen-
1850 parallel extension in the Austroalpine units of Graubünden. Eclogae geol. Helv., 87, 559-612.
- 1851 Froitzheim, N., Manatschal, G., 1996. Kinematics of Jurassic rifting, mantle exhumation, and passive-
1852 margin formation in the Austroalpine and Penninic nappes (eastern Switzerland). Geological
1853 society of America bulletin 108, 1120–1133.
- 1854 Froitzheim, N., Schmid, S.M., Frey, M., 1996. Mesozoic paleogeography and the timing of eclogite-
1855 facies metamorphism in the Alps: a working hypothesis. Eclogae Geologicae Helvetiae 89, 81.
- 1856 Froitzheim, N. 2020. Deep subduction and exhumation of continental crust in the Alps, EGU General
1857 Assembly 2020, Online, 4–8 May 2020, EGU2020-8378, <https://doi.org/10.5194/egusphere-egu2020-8378>.
- 1859 Fudral, S., 1996. Etude géologique de la suture tethysienne dans les Alpes franco-italiennes Nord-
1860 Occidentales de la Doire Ripaire (Italie) à la région de Bourg Saint-Maurice.(France).
- 1861 Fudral, S., Deville, E., Marthaler, M., 1987. Distinction de trois ensembles d'unités dans les «Schistes
1862 lustrés» compris entre la Vanoise et le Val de Suse (Alpes franco-italiennes septentrionales):
1863 aspects lithostratigraphiques, paléogéographiques et géodynamiques. Comptes rendus de
1864 l'Académie des sciences. Série 2, Mécanique, Physique, Chimie, Sciences de l'univers,
1865 Sciences de la Terre 305, 467–472.
- 1866 Fügenschuh, B., Loprieno, A., Ceriani, S., Schmid, S., 1999. Structural analysis of the
1867 Subbriançonnais and Valais units in the area of Moûtiers (Savoy, Western Alps):
1868 paleogeographic and tectonic consequences. International Journal of Earth Sciences 88, 201–
1869 218.
- 1870 Gabalda, S., Beyssac, O., Jolivet, L., Agard, P., Chopin, C., 2009. Thermal structure of a fossil
1871 subduction wedge in the Western Alps. Terra Nova 21, 28–34.
- 1872 Garcia-Casco, A., Torres-Roldan, R.L., Millan, G., Monie, P., Schneider, J., 2002. Oscillatory zoning in
1873 eclogitic garnet and amphibole, Northern Serpentinite Melange, Cuba: a record of tectonic
1874 instability during subduction? J. Metamorph. Geol. 20, 581–598.
1875 <https://doi.org/10.1046/j.1525-1314.2002.00390.x>

1876 Gebauer, D., Schertl, H.-P., Brix, M., Schreyer, W., 1997. 35 Ma old ultrahigh-pressure metamorphism
1877 and evidence for very rapid exhumation in the Dora Maira Massif, Western Alps. *Lithos* 41, 5–
1878 24.

1879 Gerya, T.V., Stöckhert, B., Perchuk, A.L., 2002. Exhumation of high-pressure metamorphic rocks in a
1880 subduction channel: A numerical simulation. *Tectonics* 21, 6-1-6–19.
1881 <https://doi.org/10.1029/2002TC001406>

1882 Ghignone, Stefano, Balestro, G., Gattiglio, M., Borghi, A., 2020. Structural evolution along the Susa
1883 Shear Zone: the role of a first-order shear zone in the exhumation of meta-ophiolite units
1884 (Western Alps). *Swiss Journal of Geosciences* 113, 1–16.

1885 Gilio, M., Scambelluri, M., Agostini, S., Godard, M., Pettke, T., Agard, P., Locatelli, M., Angiboust, S.,
1886 2020. Fingerprinting and relocating tectonic slices along the plate interface: Evidence from the
1887 Lago Superiore unit at Monviso (Western Alps). *Lithos* 352, 105308.

1888 Giuntoli, F., Lanari, P., Engi, M., 2018. Deeply subducted continental fragments—Part 1: Fracturing,
1889 dissolution–precipitation, and diffusion processes recorded by garnet textures of the central
1890 Sesia Zone (western Italian Alps). *Solid Earth* 9, 167.

1891 Godard, G., 2001. Eclogites and their geodynamic interpretation: a history. *Journal of Geodynamics*
1892 32, 165–203.

1893 Goffe, B., Chopin, C., 1986. High-pressure metamorphism in the Western Alps: zoneography of
1894 metapelites, chronology and consequences. *Schweizerische mineralogische und*
1895 *petrographische Mitteilungen* 66, 41–52.

1896 Goffé, B., Goffé-Urbano, G., Saliot, P., 1973. Sur la présence d'une variété magnésienne de la
1897 ferrocapholite en Vanoise (Alpes françaises): sa signification probable dans le
1898 métamorphisme alpin. *Comptes Rendus de l'Académie des Sciences Paris* 277, 1965–1968.

1899 Goffé, B., Schwartz, S., Lardeaux, J.-M., Bousquet, R., 2004. Metamorphic structure of the Western
1900 and Ligurian Alps.

1901 Gouzu, C., Itaya, T., Hyodo, H., Matsuda, T., 2006. Excess ⁴⁰Ar-free phengite in ultrahigh-pressure
1902 metamorphic rocks from the Lago di Cignana area, Western Alps. *Lithos* 92, 418–430.

1903 Gouzu, C., Yagi, K., Thanh, N.X., Itaya, T., Compagnoni, R., 2016. White mica K–Ar geochronology of
1904 HP–UHP units in the Lago di Cignana area, western Alps, Italy: tectonic implications for
1905 exhumation. *Lithos* 248, 109–118.

1906 Groppo, C., Beltrando, M., Compagnoni, R., 2009. The P–T path of the ultra-high pressure Lago di
1907 Cignana and adjoining high-pressure meta-ophiolitic units: insights into the evolution of the
1908 subducting Tethyan slab. *Journal of Metamorphic Geology* 27, 207–231.

1909 Groppo, C.T., Castelli, D.C.C., Rolfo, F., 2007. HT, Pre-Alpine relics in a spinel-bearing dolomite
1910 marble from the UHP Brossasco-Isasca Unit (Dora-Maira Massif, western Alps).

1911 Groppo, C., Castelli, D., 2010. Prograde P-T Evolution of a Lawsonite Eclogite from the Monviso
1912 Meta-ophiolite (Western Alps): Dehydration and Redox Reactions during Subduction of
1913 Oceanic FeTi-oxide Gabbro. *J. Petrol.* 51, 2489–2514.
1914 <https://doi.org/10.1093/petrology/egq065>

- 1915 Groß, P., Handy, M.R., John, T., Pestal, G., Pleuger, J., 2020. Crustal□Scale Sheath Folding at HP
 1916 Conditions in an Exhumed Alpine Subduction Zone (Tauern Window, Eastern Alps). *Tectonics*
 1917 39, e2019TC005942.
- 1918 Hacker, B.R., Peacock, S.M., Abers, G.A., Holloway, S.D., 2003. Subduction factory 2. Are
 1919 intermediate□depth earthquakes in subducting slabs linked to metamorphic dehydration
 1920 reactions? *Journal of Geophysical Research: Solid Earth* 108.
- 1921 Handy, M., Oberhänsli, R., 2004. Explanatory notes to the map: metamorphic structure of the Alps–
 1922 Age map of metamorphic structure of the Alps–Tectonic interpretation and outstanding
 1923 problems. *Mitt. Österr. Miner. Ges* 149, 201–225.
- 1924 Handy, M.R., Herwegh, M., Kamber, B.S., Tietz, R., Villa, I.M., 1996. Geochronologic, petrologic and
 1925 kinematic constraints on the evolution of the Err-Platta boundary, part of a fossil continent-
 1926 ocean suture in the Alps (eastern Switzerland). *Schweizerische Mineralogische und*
 1927 *Petrographische Mitteilungen* 76, 453–474.
- 1928 Handy, M.R., Schmid, S.M., Bousquet, R., Kissling, E., Bernoulli, D., 2010. Reconciling plate-tectonic
 1929 reconstructions of Alpine Tethys with the geological–geophysical record of spreading and
 1930 subduction in the Alps. *Earth-Science Reviews* 102, 121–158.
- 1931 Haüy, R.J., 1822. *Traite de cristallographie, suivi d’une application des principes de cette science a la*
 1932 *determination des especes minerales, et d’une nouvelle methode pour mettre les formes*
 1933 *cristallines en projection; par M. l’Abbe Hauy,... Tome premier [-second]: 1. Bachelier et*
 1934 *Huzard.*
- 1935 Henry, C., Burkhard, M., Goffe, B., 1996. Evolution of synmetamorphic veins and their wallrocks
 1936 through a Western Alps transect: no evidence for large-scale fluid flow. Stable isotope, major-
 1937 and trace-element systematics. *Chemical Geology* 127, 81–109.
- 1938 Henry, C., Michard, A., Chopin, C., 1993. Geometry and structural evolution of ultra-high-pressure and
 1939 high-pressure rocks from the Dora-Maira massif, Western Alps, Italy. *Journal of Structural*
 1940 *Geology* 15, 965–965.
- 1941 Herwartz, D., Nagel, T.J., Münker, C., Scherer, E.E., Froitzheim, N., 2011. Tracing two orogenic
 1942 cycles in one eclogite sample by Lu–Hf garnet chronometry. *Nature Geoscience* 4, 178–183.
- 1943 Hetényi, G., Molinari, I., Clinton, J., Bokelmann, G., Bondár, I., Crawford, W.C., Dessa, J.-X., Doubré,
 1944 C., Friederich, W., Fuchs, F., 2018. The AlpArray seismic network: a large-scale European
 1945 experiment to image the Alpine Orogen. *Surveys in geophysics* 39, 1009–1033.
- 1946 Hilairet, N., Reynard, B., Wang, Y., Daniel, I., Merkel, S., Nishiyama, N., Petitgirard, S., 2007. High-
 1947 Pressure Creep of Serpentine, Interseismic Deformation, and Initiation of Subduction. *Science*
 1948 318, 1910–1913. <https://doi.org/10.1126/science.1148494>
- 1949 Hoinkes, G., Koller, F., Rantitsch, G., Dachs, E., Höck, V., Neubauer, F., Schuster, R., 1999. Alpine
 1950 metamorphism of the Eastern Alps. *Schweizerische Mineralogische und Petrographische*
 1951 *Mitteilungen* 155–181.
- 1952 Ioannidi, P.I., Angiboust, S., Oncken, O., Agard, P., Glodny, J., Sudo, M., 2020. Deformation along the
 1953 roof of a fossil subduction interface in the transition zone below seismogenic coupling: The

- 1954 Austroalpine case and new insights from the Malenco Massif (Central Alps). *Geosphere* 16,
1955 510–532.
- 1956 Ishizuka, O., Tani, K., Reagan, M.K., 2014. Izu-Bonin-Mariana forearc crust as a modern ophiolite
1957 analogue. *Elements* 10, 115–120.
- 1958 Jolivet, L., Faccenna, C., Goffe, B., Burov, E., Agard, P., 2003. Subduction tectonics and exhumation
1959 of high-pressure metamorphic rocks in the Mediterranean orogens. *Am. J. Sci.* 303, 353–409.
1960 <https://doi.org/10.2475/ajs.303.5.353>
- 1961 Kästle, E.D., Rosenberg, C., Boschi, L., Bellahsen, N., Meier, T., El-Sharkawy, A., 2019. Slab break-
1962 offs in the Alpine subduction zone. *International Journal of Earth Sciences* 1–17.
- 1963 Kelemen, P.B., Manning, C.E., 2015. Reevaluating carbon fluxes in subduction zones, what goes
1964 down, mostly comes up. *Proceedings of the National Academy of Sciences* 112, E3997–
1965 E4006.
- 1966 Keller, L.M., Hess, M., Fügenschuh, B., Schmid, S.M., 2005. Structural and metamorphic evolution of
1967 the Camughera–Moncucco, Antrona and Monte Rosa units southwest of the Simplon line,
1968 Western Alps. *Eclogae Geologicae Helvetiae* 98, 19–49.
- 1969 Kienast, J.-R., 1983. Le métamorphisme de haute pression et basse température (éclogites et schistes
1970 bleus: données nouvelles sur la pétrologie des roches de la croûte océanique subductée et
1971 des sédiments associés.
- 1972 Kienast, J., Velde, B., 1970. Le métamorphisme alpin dans les Alpes franco-italiennes: mise en
1973 évidence d'un gradient de température et de pression. *CR Acad. Sci.* 271, 637–640.
- 1974 Kienast, J., Pognante, U., 1988. Chloritoid-bearing assemblages in eclogitised metagabbros of the
1975 Lanzo peridotite body (western Italian Alps). *Lithos* 21, 1–11.
- 1976 Kimura, G., Ludden, J., 1995. Peeling oceanic crust in subduction zones. *Geology* 23, 217–220.
1977 [https://doi.org/10.1130/0091-7613\(1995\)023<0217:POCISZ>2.3.CO;2](https://doi.org/10.1130/0091-7613(1995)023<0217:POCISZ>2.3.CO;2)
- 1978 Koller, F., 2003. 5th workshop of Alpine geological studies. Field trip guide E5. Low T—high P
1979 metamorphism in the Tarntal Mountains (Lower Austroalpine Unit). *Geologisch-
1980 Paläontologische Mitteilungen Innsbruck* 26, 47–59.
- 1981 Koller, F., Pestal, G., 2003. Die ligurischen Ophiolite der Tarntaler Berge und der Matreier
1982 Schuppenzone. *Arbeitstagung* 65–76.
- 1983 Kusky, T.M., Windley, B.F., Safonova, I., Wakita, K., Wakabayashi, J., Polat, A., Santosh, M., 2013.
1984 Recognition of ocean plate stratigraphy in accretionary orogens through Earth history: A
1985 record of 3.8 billion years of sea floor spreading, subduction, and accretion. *Gondwana
1986 Research* 24, 501–547. <https://doi.org/10.1016/j.gr.2013.01.004>
- 1987 Lafay, R., Deschamps, F., Schwartz, S., Guillot, S., Godard, M., Debret, B., Nicollet, C., 2013. High-
1988 pressure serpentinites, a trap-and-release system controlled by metamorphic conditions:
1989 Example from the Piedmont zone of the western Alps. *Chemical Geology* 343, 38–54.
- 1990 Lagabrielle, Y., 2009. Mantle exhumation and lithospheric spreading: An historical perspective from
1991 investigations in the Oceans and in the Alps-Appennines ophiolites. *Bollettino della Società
1992 Geologica Italiana* 128, 279–293.

- 1993 Lagabrielle, Y., 1987. Les ophiolites: marqueurs de l'histoire tectonique des domaines océaniques: le
 1994 cas des Alpes franco-italiennes (Queyras, Piémont).
- 1995 Lagabrielle, Y., Brovarone, A.V., Ildefonse, B., 2015. Fossil oceanic core complexes recognized in the
 1996 blueschist metaophiolites of Western Alps and Corsica. *Earth-Sci. Rev.* 141, 1–26.
- 1997 Lagabrielle, Y., Cannat, M., 1990. Alpine Jurassic ophiolites resemble the modern central Atlantic
 1998 basement. *Geology* 18, 319–322.
- 1999 Lagabrielle, Y., Fudral, S., Kienast, J.-R., 1990. La couverture océanique des ultrabasites de Lanzo
 2000 (Alpes occidentales): arguments lithostratigraphiques et pétrologiques. *Geodinamica Acta* 4,
 2001 43–55.
- 2002 Lagabrielle, Y., Lemoine, M., 1997. Alpine, Corsican and Apennine ophiolites: the slow-spreading
 2003 ridge model. *Comptes Rendus de l'Académie des Sciences-Series IIA-Earth and Planetary
 2004 Science* 325, 909–920.
- 2005 Lagabrielle, Y., Lemoine, M., Tricart, P., 1985. Paléotectonique océanique et déformations alpines
 2006 dans le massif ophiolitique du Pelvas d'Abriès (Alpes Occidentales-Queyras-France). *Bulletin
 2007 de la Société Géologique de France* 1, 473–480.
- 2008 Lapen, T.J., Johnson, C.M., Baumgartner, L.P., Dal Piaz, G.V., Skora, S., Beard, B.L., 2007. Coupling
 2009 of oceanic and continental crust during Eocene eclogite-facies metamorphism: evidence from
 2010 the Monte Rosa nappe, western Alps. *Contributions to Mineralogy and Petrology* 153, 139–
 2011 157.
- 2012 Lapen, T.J., Johnson, C.M., Baumgartner, L.P., Mahlen, N.J., Beard, B.L., Amato, J.M., 2003. Burial
 2013 rates during prograde metamorphism of an ultra-high-pressure terrane: an example from Lago
 2014 di Cignana, western Alps, Italy. *Earth and Planetary Science Letters* 215, 57–72.
- 2015 Lardeaux, J.-M., Schwartz, S., Tricart, P., Paul, A., Guillot, S., Béthoux, N., Masson, F., 2006. A
 2016 crustal-scale cross-section of the south-western Alps combining geophysical and geological
 2017 imagery. *Terra Nova* 18, 412–422.
- 2018 Le Bayon, B., Pitra, P., Balleve, M., Bohn, M., 2006. Reconstructing P–T paths during continental
 2019 collision using multi-stage garnet (Gran Paradiso nappe, Western Alps). *Journal of
 2020 Metamorphic Geology* 24, 477–496.
- 2021 Le Mer, O., Lagabrielle, Y., Polino, R., 1986. Une série sédimentaire détritico liée aux ophiolites
 2022 piémontaises: analyses lithostratigraphiques, texturales et géochimiques dans le massif de la
 2023 Crete Mouloun (Haut Queyras, Alpes sud-occidentales, France). *Géol. Alpine* 62, 63–86.
- 2024 Lefeuvre, B., Agard, P., Verlaquet, A., Dubacq, B., Plunder, A., 2020. Massive lawsonite formation in
 2025 carbonate-rich subducted metasediments: implications for mass transfer, decarbonation and
 2026 fluid-mediated processes (Schistes Lustrés, W. Alps), *Lithos* (accepted pending minor
 2027 revisions).
- 2028 Lemoine, M., Bas, T., Arnaud-Vanneau, A., Arnaud, H., Dumont, T., Gidon, M., Bourbon, M., de
 2029 Graciansky, P.-C., Rudkiewicz, J.-L., Megard-Galli, J., 1986. The continental margin of the
 2030 Mesozoic Tethys in the Western Alps. *Marine and petroleum geology* 3, 179–199.
- 2031 Lemoine, M., Marthaler, M., Caron, M., Sartori, M., Amaudric du Chaffaut, S., 1984. Découverte de
 2032 foraminifères planctoniques du Crétacé supérieur dans les schistes lustrés du Queyras (Alpes

occidentales). Conséquences paléogéographiques et tectoniques. Comptes-rendus des
séances de l'Académie des sciences. Série 2, Mécanique-physique, chimie, sciences de
l'univers, sciences de la terre 299, 727–732.

Lemoine, M., Steen, D., Vuagnat, M., 1970. Sur le problème stratigraphique des ophiolites
piémontaises et de roches sédimentaires associées: observations dans le massif de Chabrière
en Haute-Ubaye (Basses-Alpes, France), CR Sot. Sci. Nat. GenGve 5, 44–59.

Lemoine, M., Tricart, P., 1986. Les Schistes lustrés piémontais des Alpes occidentales: approche
stratigraphique, structurale et sédimentologique. *Eclogae Geologicae Helvetiae* 79, 271–294.

Lemoine, M., Tricart, P., Boillot, G., 1987. Ultramafic and gabbroic ocean floor of the Ligurian Tethys
(Alps, Corsica, Apennines): In search of a genetic model. *Geology* 15, 622–625.

Leng, W., Gurnis, M., 2015. Subduction initiation at relic arcs. *Geophysical Research Letters* 42,
7014–7021.

Lippitsch, R., Kissling, E., Ansorge, J., 2003. Upper mantle structure beneath the Alpine orogen from
high-resolution teleseismic tomography. *Journal of Geophysical Research: Solid Earth* 108.

Locatelli, M., Federico, L., Agard, P., Verlaquet, A., 2019a. Geology of the southern Monviso
metaophiolite complex (W-Alps, Italy). *Journal of Maps* 15, 283–297.

Locatelli, M., Verlaquet, A., Agard, P., Federico, L., Angiboust, S., 2018. Intermediate-depth
brecciation along the subduction plate interface (Monviso eclogite, W. Alps). *Lithos* 320, 378–
402.

Locatelli, M., Verlaquet, A., Agard, P., Pettke, T., Federico, L., 2019b. Fluid pulses during stepwise
brecciation at intermediate subduction depths (Monviso eclogites, W. Alps): first internally then
externally sourced. *Geochemistry, geophysics, geosystems* 20, 5285–5318.

Lombardo, B., 1978. Osservazioni preliminari sulle ophioliti metamorfiche del Monviso (Alpi Occidentali).

Loprieno, A., Bousquet, R., Bucher, S., Ceriani, S., Dalla Torre, F.H., Fügenschuh, B., Schmid, S.M.,
2011. The Valais units in Savoy (France): a key area for understanding the palaeogeography
and the tectonic evolution of the Western Alps. *International Journal of Earth Sciences* 100,
963–992.

Luisier, C., Baumgartner, L., Schmalholz, S.M., Siron, G., Vennemann, T., 2019. Metamorphic
pressure variation in a coherent Alpine nappe challenges lithostatic pressure paradigm.
Nature communications 10, 1–11.

Luoni, P., Rebay, G., Spalla, M.I., Zanoni, D., 2018. UHP Ti-chondrodite in the Zermatt-Saas
serpentinite: Constraints on a new tectonic scenario.

Maksymowicz, A., 2015. The geometry of the Chilean continental wedge: Tectonic segmentation of
subduction processes off Chile. *Tectonophysics* 659, 183–196.

Malusà, M.G., Polino, R., Zattin, M., Bigazzi, G., Martin, S., Piana, F., 2005. Miocene to Present
differential exhumation in the Western Alps: Insights from fission track thermochronology.
Tectonics 24.

Manatschal, G., Müntener, O., 2009. A type sequence across an ancient magma-poor ocean–
continent transition: the example of the western Alpine Tethys ophiolites. *Tectonophysics* 473,
4–19.

- 2073 Manatschal, G., Sauter, D., Karpoff, A.M., Masini, E., Mohn, G., Lagabrielle, Y., 2011. The Chenaillet
2074 Ophiolite in the French/Italian Alps: An ancient analogue for an oceanic core complex? *Lithos*
2075 124, 169–184.
- 2076 Manatschal, G., Nievergelt, P., 1997. A continent-ocean transition recorded in the Err and Platta
2077 nappes (Eastern Switzerland). *Eclogae Geologicae Helveticae* 90, 3–28.
- 2078 Manzotti, P., Ballèvre, M., Poujol, M., 2016. Detrital zircon geochronology in the Dora-Maira and
2079 Zone Houillère: a record of sediment travel paths in the Carboniferous. *Terra Nova* 28, 279–
2080 288.
- 2081 Manzotti, P., Balleve, M., Zucali, M., Robyr, M., Engi, M., 2014. The tectonometamorphic evolution of
2082 the Sesia–Dent Blanche nappes (internal Western Alps): review and synthesis. *Swiss Journal*
2083 *of Geosciences* 107, 309–336.
- 2084 Manzotti, P., Bosse, V., Pitra, P., Robyr, M., Schiavi, F., Balleve, M., 2018. Exhumation rates in the
2085 Gran Paradiso Massif (Western Alps) constrained by in situ U–Th–Pb dating of accessory
2086 phases (monazite, allanite and xenotime). *Contributions to Mineralogy and Petrology* 173, 24.
- 2087 Manzotti, P., Poujol, M., Ballèvre, M., 2015. Detrital zircon geochronology in blueschist-facies meta-
2088 conglomerates from the Western Alps: implications for the late Carboniferous to early Permian
2089 palaeogeography. *International Journal of Earth Sciences* 104, 703–731.
- 2090 Mark, C., Cogné, N., Chew, D., 2016. Tracking exhumation and drainage divide migration of the
2091 Western Alps: A test of the apatite U-Pb thermochronometer as a detrital provenance tool.
2092 *Bulletin* 128, 1439–1460.
- 2093 Markley, M.J., Teyssier, C., Cosca, M.A., Caby, R., Hunziker, J.C., Sartori, M., 1998. Alpine
2094 deformation and ⁴⁰Ar/³⁹Ar geochronology of synkinematic white mica in the Siviez-
2095 Mischabel Nappe, western Pennine Alps, Switzerland. *Tectonics* 17, 407–425.
- 2096 Marthaler, M., Stampfli, G., 1989. Les Schistes lustrés à ophiolites de la nappe du Tsaté: un ancien
2097 prisme d'accrétion issu de la marge active apulienne? *Schweizerische Mineralogische und*
2098 *Petrographische Mitteilungen* 69, 211–216.
- 2099 Martin, S., Polino, R., 1984. Le metaradiolariti a ferro di Cesana (Valle di Susa-Alpi occidentali). *Mem.*
2100 *Soc. Geol. It* 29, 107–125.
- 2101 Maruyama, S., Liou, J., Terabayashi, M., 1996. Blueschists and eclogites of the world and their
2102 exhumation. *International geology review* 38, 485–594.
- 2103 McCarthy, A., Müntener, O., 2015. Ancient depletion and mantle heterogeneity: Revisiting the
2104 Permian-Jurassic paradox of Alpine peridotites. *Geology* 43, 255–258.
- 2105 McCarthy, A., Chelle-Michou, C., Müntener, O., Arculus, R., Blundy, J., 2018. Subduction initiation
2106 without magmatism: The case of the missing Alpine magmatic arc. *Geology* 46, 1059–1062.
- 2107 McCarthy, A., Tugend, J., Mohn, G., Candiotti, L., Chelle-Michou, C., Arculus, R., Schmalholz, S.M.,
2108 Müntener, O., 2020. A case of Ampferer-type subduction and consequences for the Alps and
2109 the Pyrenees. *American Journal of Science* 320, 313–372.
- 2110 Meffan-Main, S., Cliff, R., Barnicoat, A., Lombardo, B., Compagnoni, R., 2004. A Tertiary age for
2111 Alpine high-pressure metamorphism in the Gran Paradiso massif, Western Alps: A Rb–Sr
2112 microsampling study. *Journal of Metamorphic Geology* 22, 267–281.

- 2113 Menant, A., Angiboust, S., Gerya, T., Lacassin, R., Simoes, M., Grandin, R., 2020. Transient stripping
2114 of subducting slabs controls periodic forearc uplift. *Nature communications* 11, 1–10.
- 2115 Merle, O., 1982. Mise en place séquentielle de la Nappe du Parpaillon en Embrunais-Ubaye (Flysch à
2116 Helminthoïdes, Alpes occidentales).
- 2117 Merle, O., Brun, J., 1984. The curved translation path of the Parpaillon Nappe (French Alps). *Journal*
2118 *of structural Geology* 6, 711–719.
- 2119 Messiga, B., Scambelluri, M., Piccardo, G.B., 1995. Chloritoid-bearing assemblages in mafic systems
2120 and eclogite-facies hydration of alpine Mg-Al metagabbros (Erro-Tobbio Unit, Ligurian western
2121 Alps). *European Journal of mineralogy* 1149–1168.
- 2122 Mevel, C., Caby, R., Kienast, J.-R., 1978. Amphibolite facies conditions in the oceanic crust: Example
2123 of amphibolitized fiaser-gabbro and amphibolites from the Chenaillet ophiolite massif (Hautes
2124 Alpes, France). *Earth and Planetary Science Letters* 39, 98–108.
- 2125 Michard, A., 1977. Charriages et métamorphisme haute pression dans les Alpes cottiennes
2126 meridionales; a propos des schistes a jadeite de la bande d'Acceglio. *Bulletin de la Société*
2127 *Géologique de France* 7, 883–892.
- 2128 Michard, A., Avigad, D., Goffé, B., Chopin, C., 2004. The high-pressure metamorphic front of the south
2129 Western Alps (Ubaye-Maira transect, France, Italy). *Schweiz. Mineral. Petrogr. Mitt* 84, 215–
2130 235.
- 2131 Michard, A., Goffé, B., Chopin, C., Henry, C., 1996. Did the Western Alps develop through an Oman-
2132 type stage? The geotectonic setting of high-pressure metamorphism in two contrasting
2133 Tethyan transects. *Eclogae Geologicae Helvetiae* 89, 43–80.
- 2134 Miller, C., Thöni, M., 1997. Eo-Alpine eclogitisation of Permian MORB-type gabbros in the Koralpe
2135 (Eastern Alps, Austria): new geochronological, geochemical and petrological data. *Chemical*
2136 *Geology* 137, 283–310.
- 2137 Mohn, G., Manatschal, G., Masini, E., Müntener, O., 2011. Rift-related inheritance in orogens: a case
2138 study from the Austroalpine nappes in Central Alps (SE-Switzerland and N-Italy). *International*
2139 *Journal of Earth Sciences* 100, 937–961.
- 2140 Mohn, G., Manatschal, G., Beltrando, M., Masini, E., Kuszniir, N., 2012. Necking of continental crust in
2141 magma-poor rifted margins: Evidence from the fossil Alpine Tethys margins. *Tectonics* 31.
- 2142 Monié, P., Philippot, P., 1989. Mise en évidence de l'âge éocène moyen du métamorphisme de haute-
2143 pression dans la nappe ophiolitique du Monviso (Alpes occidentales) par la méthode ^{39}Ar -
2144 ^{40}Ar . *Comptes rendus de l'Académie des sciences. Série 2, Mécanique, Physique, Chimie,*
2145 *Sciences de l'univers, Sciences de la Terre* 309, 245–251.
- 2146 Moulas, E., Schmalholz, S.M., Podladchikov, Y., Tajčmanová, L., Kostopoulos, D., Baumgartner, L.,
2147 2019. Relation between mean stress, thermodynamic, and lithostatic pressure. *Journal of*
2148 *metamorphic geology* 37, 1–14.
- 2149 Mueller, P., Maino, M., Seno, S., 2020. Progressive Deformation Patterns from an Accretionary Prism
2150 (Helminthoid Flysch, Ligurian Alps, Italy). *Geosciences* 10, 26.

- 2151 Müller, W., Dallmeyer, R.D., Neubauer, F., Thöni, M., 1999. Deformation-induced resetting of Rb/Sr
2152 and ⁴⁰Ar/³⁹Ar mineral systems in a low-grade, polymetamorphic terrane (Eastern Alps,
2153 Austria). *Journal of the Geological Society* 156, 261–278.
- 2154 Müntener, O., Hermann, J., 1996. The Val Malenco lower crust–upper mantle complex and its field
2155 relations (Italian Alps). *Schweizerische Mineralogische und Petrographische Mitteilungen* 76,
2156 475–500.
- 2157 Nábělek, J., Hetényi, G., Vergne, J., Sapkota, S., Kafle, B., Jiang, M., Su, H., Chen, J., Huang, B.-S.,
2158 2009. Underplating in the Himalaya-Tibet collision zone revealed by the Hi-CLIMB experiment.
2159 *Science* 325, 1371–1374.
- 2160 Nadeau, S., Philippot, P., Pineau, F., 1993. Fluid inclusion and mineral isotopic compositions (HCO) in
2161 eclogitic rocks as tracers of local fluid migration during high-pressure metamorphism. *Earth
2162 and Planetary Science Letters* 114, 431–448.
- 2163 Nagel, T.J., 2008. Tertiary subduction, collision and exhumation recorded in the Adula nappe, central
2164 Alps. *Geological Society, London, Special Publications* 298, 365–392.
- 2165 Negro, F., Bousquet, R., Vils, F., Pellet, C.-M., Hänggi-Schaub, J., 2013. Thermal structure and
2166 metamorphic evolution of the Piemonte-Ligurian metasediments in the northern Western Alps.
2167 *Swiss Journal of Geosciences* 106, 63–78.
- 2168 Nicolas, A., 1989. Structures of ophiolites and dynamics of oceanic lithosphere. *Structures of
2169 ophiolites and dynamics of oceanic lithosphere*.
- 2170 Oberhänsli, R., 1978. *Chemische Untersuchungen an Glaukophan-führenden basischen Gesteinen
2171 aus den Bündnerschiefern Graubündens*.
- 2172 Oberhänsli, R., Bousquet, R., Engi, M., Goffé, B., Gosso, G., Handy, M., Höck, V., Koller, F.,
2173 Lardeaux, J., Polino, R., 2004. *Metamorphic Structure of the Alps*. CCGM (Commission of the
2174 Geological Maps of the World), Paris.
- 2175 Oberhänsli, R., Goffé, B., 2004. Explonatory notes to the Map: Metamorphic structure of the Alps
2176 introduction. *Mitteilungen der Österreichischen Mineralogischen Gesellschaft* 149, 115–123.
- 2177 Pelletier, L., Müntener, O., 2006. High-pressure metamorphism of the Lanzo peridotite and its oceanic
2178 cover, and some consequences for the Sesia–Lanzo zone (northwestern Italian Alps). *Lithos*
2179 90, 111–130.
- 2180 Perrone, G., Cadoppi, P., Tallone, S., Balestro, G., 2011. Post-collisional tectonics in the Northern
2181 Cottian Alps (Italian Western Alps). *International Journal of Earth Sciences* 100, 1349–1373.
- 2182 Pfeifer, H., Colombi, A., Ganguin, J., 1989. Zermatt-Saas and Antrona zone: A petrographic and
2183 geochemical comparison of polyphase metamorphic ophiolites of the West-Central Alps.
2184 *Schweizerische Mineralogische und Petrographische Mitteilungen* 69, 217–236.
- 2185 Philippot, P., 1990. Opposite vergence of nappes and crustal extension in the French–Italian Western
2186 Alps. *Tectonics* 9, 1143–1164.
- 2187 Philippot, P., Agrinier, P., Scambelluri, M., 1998. Chlorine cycling during subduction of altered oceanic
2188 crust. *Earth and Planetary Science Letters* 161, 33–44.

- 2189 Philippot, P., Kienast, J.-R., 1989. Chemical-microstructural changes in eclogite-facies shear zones
2190 (Monviso, Western Alps, north Italy) as indicators of strain history and the mechanism and
2191 scale of mass transfer. *Lithos* 23, 179–200.
- 2192 Picazo, S., Müntener, O., Manatschal, G., Bauville, A., Karner, G., Johnson, C., 2016. Mapping the
2193 nature of mantle domains in Western and Central Europe based on clinopyroxene and spinel
2194 chemistry: Evidence for mantle modification during an extensional cycle. *Lithos* 266, 233–263.
- 2195 Picazo, S.M., Ewing, T.A., Müntener, O., 2019. Paleocene metamorphism along the Pennine–
2196 Austroalpine suture constrained by U–Pb dating of titanite and rutile (Malenco, Alps). *Swiss
2197 Journal of Geosciences* 112, 517–542.
- 2198 Piccardo, G.B., Ranalli, G., Guarnieri, L., 2010. Seismogenic shear zones in the lithospheric mantle:
2199 ultramafic pseudotachylytes in the Lanzo Peridotite (Western Alps, NW Italy). *Journal of
2200 Petrology* 51, 81–100.
- 2201 Piccoli, F., Brovarone, A.V., Ague, J.J., 2018. Field and petrological study of metasomatism and high-
2202 pressure carbonation from lawsonite eclogite-facies terrains, Alpine Corsica. *Lithos* 304, 16–
2203 37.
- 2204 Platt, J., 1986. Dynamics of orogenic wedges and the uplift of high-pressure metamorphic rocks.
2205 *Geological society of America bulletin* 97, 1037–1053.
- 2206 Platt, J., Behrmann, J., Cunningham, P., Dewey, J., Helman, M., Parish, M., Shepley, M., Wallis, S.,
2207 Western, P., 1989. Kinematics of the Alpine arc and the motion history of Adria. *Nature* 337,
2208 158–161.
- 2209 Plunder, A., Agard, P., Dubacq, B., Chopin, C., Bellanger, M., 2012. How continuous and precise is
2210 the record of P-T paths? Insights from combined thermobarometry and thermodynamic
2211 modelling into subduction dynamics (Schistes Lustrés, W. Alps). *J. Metamorph. Geol.* 30,
2212 323–346. <https://doi.org/10.1111/j.1525-1314.2011.00969.x>
- 2213 Pognante, U., 1991. Petrological constraints on the eclogite and blueschist facies metamorphism and
2214 P–T paths in the western Alps. *Journal of Metamorphic Geology* 9, 5–17.
- 2215 Pognante, U., Kienast, J.-R., 1987. Blueschist and eclogite transformations in Fe-Ti gabbros: a case
2216 from the Western Alps ophiolites. *Journal of Petrology* 28, 271–292.
- 2217 Polino, R., Lemoine, M., 1984. Détritisme mixte d'origine continentale et océanique dans les
2218 sédiments jurassico-crétacés supra-ophiolitiques de la Téthys ligurienne: la série du Lago Nero
2219 (Alpes Occidentales franco-italiennes). *Comptes-rendus des séances de l'Académie des
2220 sciences. Série 2, Mécanique-physique, chimie, sciences de l'univers, sciences de la terre*
2221 298, 359–364.
- 2222 Polino, R., Dal Piaz, G., Gosso, G., 1990. Tectonic erosion at the Adria Margin and accretionary
2223 processes for the Cretaceous orogeny of the Alps.
- 2224 Polino, R., Borghi, A., Carraro, F., Dela Pierre, F., Fioraso, G., Giardino, M., 2002. Note Illustrative
2225 Della Carta Geologica D'italia Alla Scala 1: 50.000–FOGLIO 132-152-153
2226 “BARDONECCHIA”.

- 2227 Ratschbacher, L., Dingeldey, C., Miller, C., Hacker, B.R., McWilliams, M.O., 2004. Formation,
2228 subduction, and exhumation of Penninic oceanic crust in the Eastern Alps: time constraints
2229 from $^{40}\text{Ar}/^{39}\text{Ar}$ geochronology. *Tectonophysics* 394, 155–170.
- 2230 Rebay, G., Zanoni, D., Langone, A., Luoni, P., Tiepolo, M., Spalla, M.I., 2018. Dating of ultramafic
2231 rocks from the Western Alps ophiolites discloses Late Cretaceous subduction ages in the
2232 Zermatt-Saas Zone. *Geological Magazine* 155, 298–315.
- 2233 Reddy, S., Wheeler, J., Cliff, R., 1999. The geometry and timing of orogenic extension: an example
2234 from the Western Italian Alps. *Journal of Metamorphic Geology* 17, 573–590.
- 2235 Reddy, S.M., Wheeler, J., Butler, R.W.H., Cliff, R.A., Freeman, S., Inger, S., Pickles, C., Kelley, S.P.,
2236 2003. Kinematic reworking and exhumation within the convergent Alpine Orogen.
2237 *Tectonophysics* 365, 77–102.
- 2238 Reinecke, T., 1998. Prograde high-to ultrahigh-pressure metamorphism and exhumation of oceanic
2239 sediments at Lago di Cignana, Zermatt-Saas Zone, western Alps. *Lithos* 42, 147–189.
- 2240 Reinecke, T., 1991. Very-high-pressure metamorphism and uplift of coesite-bearing metasediments
2241 from the Zermatt-Saas zone, Western Alps. *European Journal of Mineralogy* 7–18.
- 2242 Reynard, B., 2013. Serpentine in active subduction zones. *Lithos, Serpentinites from mid-oceanic*
2243 *ridges to subduction* 178, 171–185. <https://doi.org/10.1016/j.lithos.2012.10.012>
- 2244 Ricard Y., Richards M., Lithgow-Bertelloni C., Le Stunff Y. 1993. A geodynamic model of mantle
2245 density heterogeneity. *Journal of Geophysical Research*, 98, 21895-21909.
- 2246 Ricou, L., Siddans, A., 1986. Collision tectonics in the western Alps. Geological Society, London,
2247 Special Publications 19, 229–244.
- 2248 Ring, U., 1992. The Alpine geodynamic evolution of Penninic nappes in the eastern Central Alps:
2249 geothermobarometric and kinematic data. *Journal of Metamorphic Geology* 10, 33–53.
- 2250 Ring, U., Ratschbacher, L., Frisch, W., Durr, S., Borchert, S., 1991. Late-stage east-directed
2251 deformation in the Platta, Arosa, and lowermost Austroalpine nappes (eastern Swiss Alps).
2252 *Neues Jahrbuch für Geologie und Paläontologie-Monatshefte* 357–363.
- 2253 Rosenbaum, G., Lister, G.S., 2005. The Western Alps from the Jurassic to Oligocene: spatio-temporal
2254 constraints and evolutionary reconstructions. *Earth-Science Reviews* 69, 281–306.
- 2255 Rosenbaum, G., Lister, G.S., Duboz, C., 2002. Relative motions of Africa, Iberia and Europe during
2256 Alpine orogeny. *Tectonophysics* 359, 117–129.
- 2257 Rosenberg, C.L., Schneider, S., Scharf, A., Bertrand, A., Hammerschmidt, K., Rabaute, A., Brun, J.-
2258 P., 2018. Relating collisional kinematics to exhumation processes in the Eastern Alps. *Earth-*
2259 *Science Reviews* 176, 311–344.
- 2260 Royden, L., Faccenna, C., 2018. Subduction orogeny and the Late Cenozoic evolution of the
2261 mediterranean arcs. *Annual Review of Earth and Planetary Sciences* 46, 261–289.
- 2262 Rubatto, D., Hermann, J., 2003. Zircon formation during fluid circulation in eclogites (Monviso,
2263 Western Alps): implications for Zr and Hf budget in subduction zones. *Geochimica et*
2264 *Cosmochimica Acta* 67, 2173–2187.

- 2265 Rubatto, D., Angiboust, S., 2015. Oxygen isotope record of oceanic and high-pressure metasomatism:
 2266 a P–T–time–fluid path for the Monviso eclogites (Italy). *Contributions to mineralogy and*
 2267 *petrology* 170, 44.
- 2268 Rubatto, D., Gebauer, D., Fanning, M., 1998. Jurassic formation and Eocene subduction of the
 2269 Zermatt–Saas-Fee ophiolites: implications for the geodynamic evolution of the Central and
 2270 Western Alps. *Contributions to Mineralogy and Petrology* 132, 269–287.
- 2271 Rubatto, D., Gebauer, D., Compagnoni, R., 1999. Dating of eclogite-facies zircons: the age of Alpine
 2272 metamorphism in the Sesia–Lanzo Zone (Western Alps). *Earth and Planetary Science Letters*
 2273 167, 141–158.
- 2274 Rubatto, D., Müntener, O., Barnhoorn, A., Gregory, C., 2008. Dissolution-reprecipitation of zircon at
 2275 low-temperature, high-pressure conditions (Lanzo Massif, Italy). *American Mineralogist* 93,
 2276 1519–1529.
- 2277 Ruh, J.B., Le Pourhiet, L., Agard, P., Burov, E., Gerya, T., 2015. Tectonic slicing of subducting
 2278 oceanic crust along plate interfaces: Numerical modeling. *Geochemistry, Geophysics,*
 2279 *Geosystems* 16, 3505–3531.
- 2280 Saliot, P., Dal Piaz, G., Frey, M., 1980. Métamorphisme de haute pression dans les Alpes franco-italo-
 2281 suisses. *Geologie alpine* 56, 203–235.
- 2282 Sample, J.C., Fisher, D.M., 1986. Duplex accretion and underplating in an ancient accretionary
 2283 complex, Kodiak Islands, Alaska. *Geology* 14, 160–163.
- 2284 Sandmann, S., Nagel, T.J., Herwartz, D., Fonseca, R.O., Kurzwaski, R.M., Münker, C., Froitzheim, N.,
 2285 2014. Lu–Hf garnet systematics of a polymetamorphic basement unit: new evidence for
 2286 coherent exhumation of the Adula Nappe (Central Alps) from eclogite-facies conditions.
 2287 *Contributions to Mineralogy and Petrology* 168, 1075.
- 2288 Scambelluri, M., Cannà, E., Gilio, M., 2019. The water and fluid-mobile element cycles during
 2289 serpentinite subduction. A review. *European Journal of Mineralogy* 31, 405–428.
- 2290 Scambelluri, M., Müntener, O., Hermann, J., Piccardo, G.B., Trommsdorff, V., 1995. Subduction of
 2291 water into the mantle: history of an Alpine peridotite. *Geology* 23, 459–462.
- 2292 Scambelluri, M., Pennacchioni, G., Gilio, M., Bestmann, M., Plumper, O., Nestola, F., 2017. Fossil
 2293 intermediate-depth earthquakes in subducting slabs linked to differential stress release. *Nat.*
 2294 *Geosci.* 10, 960-+. <https://doi.org/10.1038/s41561-017-0010-7>
- 2295 Scambelluri, M., Philippot, P., 2001. Deep fluids in subduction zones. *Lithos* 55, 213–227.
- 2296 Scambelluri, M., Piccardo, G.B., Philippot, P., Robbiano, A., Negretti, L., 1997. High salinity fluid
 2297 inclusions formed from recycled seawater in deeply subducted alpine serpentinite. *Earth and*
 2298 *Planetary Science Letters* 148, 485–499.
- 2299 Schmid, S., Kissling, E., 2000. The arc of the western Alps in the light of geophysical data on deep
 2300 crustal structure. *Tectonics* 19, 62–85.
- 2301 Schmid, S.M., Fügenschuh, B., Kissling, E., Schuster, R., 2004. Tectonic map and overall architecture
 2302 of the Alpine orogen. *Eclogae Geologicae Helvetiae* 97, 93–117.

- 2303 Schmid, S.M., Kissling, E., Diehl, T., van Hinsbergen, D.J., Molli, G., 2017. Ivrea mantle wedge, arc of
 2304 the Western Alps, and kinematic evolution of the Alps–Apennines orogenic system. *Swiss*
 2305 *Journal of Geosciences* 110, 581–612.
- 2306 Schmid, S.M., Pfiffner, O.-A., Froitzheim, N., Schönborn, G., Kissling, E., 1996. Geophysical
 2307 geological transect and tectonic evolution of the Swiss–Italian Alps. *Tectonics* 15, 1036–1064.
- 2308 Schmid, S.M., Scharf, A., Handy, M.R., Rosenberg, C.L., 2013. The Tauern Window (Eastern Alps,
 2309 Austria): a new tectonic map, with cross-sections and a tectonometamorphic synthesis. *Swiss*
 2310 *Journal of Geosciences* 106, 1–32.
- 2311 Schmid, S.M., Fügenschuh, B., Kounov, A., Matenco, L., Nievergelt, P., Oberhänsli, R., Pleuger, J.,
 2312 Schefer, S., Schuster, R., Tomljenovic, B., Ustaszewski, K., van Hinsbergen, D.J.J. 2020.
 2313 Tectonic units of the Alpine collision zone between Eastern Alps and western Turkey.
 2314 *Gondwana Research*, 78, 308-374. <https://doi.org/10.1016/j.gr.2019.07.005>
- 2315 Schwartz, S., 2000. La zone piémontaise des Alpes Occidentales: un paléocomplexe de subduction.
 2316 *Arguments métamorphiques, géochronologiques et structuraux.*
- 2317 Schwartz, S., Guillot, S., Reynard, B., Lafay, R., Debret, B., Nicollet, C., Lanari, P., Auzende, A.L.,
 2318 2013. Pressure–temperature estimates of the lizardite/antigorite transition in high pressure
 2319 serpentinites. *Lithos* 178, 197–210.
- 2320 Schwartz, S., Guillot, S., Tricart, P., Bernet, M., Jourdan, S., Dumont, T., Montagnac, G., 2012.
 2321 Source tracing of detrital serpentinite in the Oligocene molasse deposits from the western
 2322 Alps (Barrême basin): implications for relief formation in the internal zone. *Geological*
 2323 *Magazine* 149, 841–856.
- 2324 Schwartz, S., Lardeaux, J.-M., Guillot, S., Tricart, P., 2000. Diversité du métamorphisme écolitique
 2325 dans le massif ophiolitique du Monviso (Alpes occidentales, Italie). *Geodinamica Acta* 13,
 2326 169–188.
- 2327 Schwartz, S., Tricart, P., Lardeaux, J.-M., Guillot, S., Vidal, O., 2009. Late tectonic and metamorphic
 2328 evolution of the Piedmont accretionary wedge (Queyras Schistes lustrés, western Alps):
 2329 Evidences for tilting during Alpine collision. *Geological Society of America Bulletin* 121, 502–
 2330 518.
- 2331 Selverstone, J., Sharp, Z., 2013. Chlorine isotope constraints on fluid–rock interactions during
 2332 subduction and exhumation of the Zermatt–Saas ophiolite. *Geochemistry, Geophysics,*
 2333 *Geosystems* 14, 4370–4391.
- 2334 Seno, S., Dallagiovanna, G., Vanossi, M., 2005. A kinematic evolutionary model for the Penninic
 2335 sector of the central Ligurian Alps. *International Journal of Earth Sciences* 94, 114–129.
- 2336 Seno, S., Dallagiovanna, G., Vanossi, M., 2003. Palaeogeography and thrust development in the
 2337 Penninic domain of the Western Alpine chain: examples from the Ligurian Alps.
 2338 *BOLLETTINO-SOCIETA GEOLOGICA ITALIANA* 122, 223–232.
- 2339 Shillington, D.J., Bécel, A., Nedimović, M.R., Kuehn, H., Webb, S.C., Abers, G.A., Keranen, K.M., Li,
 2340 J., Delescluse, M., Mattei-Salicrup, G.A., 2015. Link between plate fabric, hydration and
 2341 subduction zone seismicity in Alaska. *Nature Geoscience* 8, 961–964.

2342 Simon-Labric, T., Rolland, Y., Dumont, T., Heymes, T., Authemayou, C., Corsini, M., Fornari, M.,
2343 2009. 40Ar/39Ar dating of Penninic Front tectonic displacement (W Alps) during the Lower
2344 Oligocene (31–34 Ma). *Terra Nova* 21, 127–136.

2345 Skora, S., Mahlen, N., Johnson, C.M., Baumgartner, L.P., Lapen, T., Beard, B.L., Szilvagy, E., 2015.
2346 Evidence for protracted prograde metamorphism followed by rapid exhumation of the
2347 Zermatt-Saas Fee ophiolite. *Journal of Metamorphic Geology* 33, 711–734.

2348 Spalla, M.I., Lardeaux, J.M., Vittorio Dal Piaz, G., Gosso, G., Messiga, B., 1996. Tectonic significance
2349 of Alpine eclogites. *Journal of geodynamics* 21, 257–285.

2350 Spandler, C., Pettke, T., Rubatto, D., 2011. Internal and external fluid sources for eclogite-facies veins
2351 in the Monviso meta-ophiolite, Western Alps: implications for fluid flow in subduction zones.
2352 *Journal of Petrology* 52, 1207–1236.

2353 Spandler, C., Pirard, C., 2013. Element recycling from subducting slabs to arc crust: A review. *Lithos*
2354 170, 208–223. <https://doi.org/10.1016/j.lithos.2013.02.016>

2355 Spray, J.G., 1984. Possible causes and consequences of upper mantle decoupling and ophiolite
2356 displacement. Geological Society, London, Special Publications 13, 255–268.

2357 Stampfli, G., Marchant, R., 1997. Geodynamic evolution of the Tethyan margins of the Western Alps.
2358 Deep structure of the Swiss Alps-Results from NRP 20 223–239.

2359 Stampfli, G., Mosar, J., Marquer, D., Marchant, R., Baudin, T., Borel, G., 1998. Subduction and
2360 obduction processes in the Swiss Alps. *Tectonophysics* 296, 159–204.

2361 Stampfli, G.M., Borel, G., 2002. A plate tectonic model for the Paleozoic and Mesozoic constrained by
2362 dynamic plate boundaries and restored synthetic oceanic isochrons. *Earth and Planetary*
2363 *Science Letters* 196, 17–33.

2364 Stern, R.J., 2002. Subduction zones. *Reviews of geophysics* 40, 3–1.

2365 Sternai, P., Sue, C., Husson, L., Serpelloni, E., Becker, T.W., Willett, S.D., Faccenna, C., Di Giulio, A.,
2366 Spada, G., Jolivet, L., 2019. Present-day uplift of the European Alps: Evaluating mechanisms
2367 and models of their relative contributions. *Earth-science reviews* 190, 589–604.

2368 Stüwe, Schuster, R. 2010. Initiation of subduction in the Alps: Continent or ocean? *Geology*, 38/2,
2369 175-178

2370 Tamblyn, R., Zack, T., Schmitt, A., Hand, M., Kelsey, D., Morrissey, L., Pabst, S., Savov, I., 2019.
2371 Blueschist from the Mariana forearc records long-lived residence of material in the subduction
2372 channel. *Earth and Planetary Science Letters* 519, 171–181.

2373 Tartarotti, P., Guerini, S., Rotondo, F., Festa, A., Balestro, G., Bebout, G.E., Cannà, E., Epstein,
2374 G.S., Scambelluri, M., 2019. Superposed sedimentary and tectonic block-in-matrix fabrics in a
2375 subducted serpentinite mélangé (High-pressure zermatt saas ophiolite, western alps).
2376 *Geosciences* 9, 358.

2377 Tartarotti, P., Zucali, M., Panseri, M., Lissandrelli, S., Capelli, S., Ouladdiaf, B., 2011. Mantle origin of
2378 the Antrona serpentinites (Antrona ophiolite, Pennine Alps) as inferred from microstructural,
2379 microchemical, and neutron diffraction quantitative texture analysis. *Ophioliti* 36, 167–189.

2380 Thöni, M., 1999. A review of geochronological data from the Eastern Alps. *Schweizerische*
2381 *Mineralogische und Petrographische Mitteilungen* 79, 209–230.

- 2382 Tilton, G., Schreyer, W., Schertl, H.-P., 1991. Pb– Sr– Nd isotopic behavior of deeply subducted
 2383 crustal rocks from the Dora Maira Massif, Western Alps, Italy-II: what is the age of the
 2384 ultrahigh-pressure metamorphism? *Contributions to Mineralogy and Petrology* 108, 22–33.
- 2385 Tricart, P., 1984. From passive margin to continental collision; a tectonic scenario for the Western
 2386 Alps. *American Journal of Science* 284, 97–120.
- 2387 Tricart, P., Bourbon, M., Lagabrielle, Y., 1982. Révision de la coupe Péouvou-Roche Noire (zone
 2388 piémontaise, Alpes franco-italiennes): bréchification synsédimentaire d'un fond océanique
 2389 ultrabasique. *Géol. alp. Grenoble* 58, 105–113.
- 2390 Tricart, P., Lemoine, M., 1991. The Queyras ophiolite West of Monte Viso (Western Alps): indicator of
 2391 a peculiar ocean floor in the Mesozoic Tethys. *Journal of Geodynamics* 13, 163–181.
- 2392 Tricart, P., Lemoine, M., 1986. From faulted blocks to megamullions and megaboudins: Tethyan
 2393 heritage in the structure of the Western Alps. *Tectonics* 5, 95–118.
- 2394 Trommsdorff, V., Piccardo, G., Montrasio, A., 1993. From magmatism through metamorphism to sea
 2395 floor emplacement of subcontinental Adria lithosphere during pre-Alpine rifting (Malenco,
 2396 Italy). *Schweizerische Mineralogische und Petrographische Mitteilungen* 73, 191–203.
- 2397 Trümpy, R., 1960. Paleotectonic evolution of the Central and Western Alps. *Geological Society of
 2398 America Bulletin* 71, 843–907.
- 2399 Trümpy, 2006. *Geologie der Iberger Klippen und ihrer Flysch-Unterlage*. *Eclogae geol. Helv.* 99, 79–
 2400 121. DOI 10.1007/s00015-006-1180-2
- 2401 Vaggelli, G., Borghi, A., Cossio, R., Fedi, M., Giuntini, L., Lombardo, B., Marino, A., Massi, M., Olmi,
 2402 F., Petrelli, M., 2006. Micro-PIXE analysis of monazite from the Dora Maira massif, western
 2403 Italian Alps. *Microchimica Acta* 155, 305–311.
- 2404 Van der Klauw, S., Reinecke, T., Stöckhert, B., 1997. Exhumation of ultrahigh-pressure metamorphic
 2405 oceanic crust from Lago di Cignana, Piemontese zone, western Alps: the structural record in
 2406 metabasites. *Lithos* 41, 79–102.
- 2407 Van Hinsbergen, D.J., Torsvik, T.H., Schmid, S.M., Mañenco, L.C., Maffione, M., Vissers, R.L., Gürer,
 2408 D., Spakman, W., 2020. Orogenic architecture of the Mediterranean region and kinematic
 2409 reconstruction of its tectonic evolution since the Triassic. *Gondwana Research* 81, 79–229.
- 2410 van Keken, P.E., Hacker, B.R., Syracuse, E.M., Abers, G.A., 2011. Subduction factory: 4. Depth-
 2411 dependent flux of H₂O from subducting slabs worldwide. *Journal of Geophysical Research:*
 2412 *Solid Earth* 116.
- 2413 Vannucchi, P., Spagnuolo, E., Aretusini, S., Di Toro, G., Ujiie, K., Tsutsumi, A., Nielsen, S., 2017. Past
 2414 seismic slip-to-the-trench recorded in Central America megathrust. *Nat. Geosci.* 10, 935–940.
 2415 <https://doi.org/10.1038/s41561-017-0013-4>
- 2416 Vignaroli, G., Faccenna, C., Rossetti, F., 2009. Retrogressive fabric development during exhumation
 2417 of the Voltri Massif (Ligurian Alps, Italy): arguments for an extensional origin and implications
 2418 for the Alps–Apennines linkage. *International Journal of Earth Sciences* 98, 1077–1093.
- 2419 Vignaroli, G., Rossetti, F., Rubatto, D., Theye, T., Lisker, F., Phillips, D., 2010. Pressure-
 2420 temperature-deformation-time (P-T-d-t) exhumation history of the Voltri Massif HP
 2421 complex, Ligurian Alps, Italy. *Tectonics* 29.

- 2422 Villa, I.M., Bucher, S., Bousquet, R., Kleinhanns, I.C., Schmid, S.M., 2014. Dating polygenetic
2423 metamorphic assemblages along a transect across the Western Alps. *Journal of Petrology* 55,
2424 803–830.
- 2425 Vissers, R.L., van Hinsbergen, D.J., Meijer, P.T., Piccardo, G.B., 2013. Kinematics of Jurassic ultra-
2426 slow spreading in the Piemonte Ligurian ocean. *Earth and Planetary Science Letters* 380,
2427 138–150.
- 2428 Vitale Brovarone, A., Agard, P., 2013. True metamorphic isograds or tectonically sliced metamorphic
2429 sequence? New high-spatial resolution petrological data for the New Caledonia case study.
2430 *Contrib. Mineral. Petrol.* 166, 451–469. <https://doi.org/10.1007/s00410-013-0885-2>
- 2431 Vitale Brovarone, A., Beyssac, O., Malavieille, J., Molli, G., Beltrando, M., Compagnoni, R., 2013.
2432 Stacking and metamorphism of continuous segments of subducted lithosphere in a high-
2433 pressure wedge: the example of Alpine Corsica (France). *Earth-Science Reviews* 116, 35–56.
- 2434 Vitale Brovarone, A., Picatto, M., Beyssac, O., Lagabrielle, Y., Castelli, D., 2014a. The blueschist-
2435 eclogite transition in the Alpine chain: P-T paths and the role of slow-spreading extensional
2436 structures in the evolution of HP-LT mountain belts. *Tectonophysics* 615, 96–121.
2437 <https://doi.org/10.1016/j.tecto.2014.01.001>
- 2438 Vitale Brovarone, A., Alard, O., Beyssac, O., Martin, L., Picatto, M., 2014b. Lawsonite metasomatism
2439 and trace element recycling in subduction zones. *Journal of Metamorphic Geology* 32, 489–
2440 514.
- 2441 Von Raumer, J., Abrecht, J., Bussy, F., Lombardo, B., Menot, R.-P., Schaltegger, U., 1999. The
2442 Paleozoic metamorphic evolution of the Alpine external massifs. *Schweizerische*
2443 *Mineralogische und Petrographische Mitteilungen* 79, 5–22.
- 2444 Wada, I., Wang, K., He, J., Hyndman, R.D., 2008. Weakening of the subduction interface and its
2445 effects on surface heat flow, slab dehydration, and mantle wedge serpentinization. *Journal of*
2446 *Geophysical Research: Solid Earth* 113.
- 2447 Wagreich, M., 2001. A 400 km long piggyback basin (Upper Aptian–Lower Cenomanian) in the
2448 Eastern Alps. *Terra Nova* 13, 401–406.
- 2449 Wagreich, M., 1995. Subduction tectonic erosion and Late Cretaceous subsidence along the northern
2450 Austroalpine margin (Eastern Alps, Austria). *Tectonophysics* 242, 63–78.
- 2451 Wagreich, M., Decker, K., 2001. Sedimentary tectonics and subsidence modelling of the type Upper
2452 Cretaceous Gosau basin (Northern Calcareous Alps, Austria). *International Journal of Earth*
2453 *Sciences* 90, 714–726.
- 2454 Wakabayashi, J., 2017. Structural context and variation of ocean plate stratigraphy, Franciscan
2455 Complex, California: insight into mélangé origins and subduction-accretion processes.
2456 *Progress in Earth and Planetary Science* 4, 18. <https://doi.org/10.1186/s40645-017-0132-y>
- 2457 Wakabayashi, J., 2015. Anatomy of a subduction complex: architecture of the Franciscan Complex,
2458 California, at multiple length and time scales. *International Geology Review* 57, 669–746.
2459 <https://doi.org/10.1080/00206814.2014.998728>
- 2460 Wakabayashi, J., Dilek, Y., 2003. Ophiolites in Earth history, Geological Society of London Special
2461 Publication 218.

- 2462 Wannamaker, P.E., Evans, R.L., Bedrosian, P.A., Unsworth, M.J., Maris, V., McGary, R.S., 2014.
2463 Segmentation of plate coupling, fate of subduction fluids, and modes of arc magmatism in C
2464 ascadia, inferred from magnetotelluric resistivity. *Geochemistry, Geophysics, Geosystems* 15,
2465 4230–4253.
- 2466 Weh, M., Froitzheim, N., 2001. Penninic cover nappes in the Prattigau half-window (Eastern
2467 Switzerland): Structure and tectonic evolution. *Eclogae Geologicae Helvetiae* 94, 237–252.
- 2468 White, D.A., Roeder, D.H., Nelson, T.H., Crowell, J.C., 1970. Subduction. *Geological Society of
2469 America Bulletin* 81, 3431–3432.
- 2470 Wiederkehr, M., Bousquet, R., Schmid, S.M. & Berger, A. 2008. From subduction to collision: thermal
2471 overprint of HP/LT meta-sediments in the north-eastern Lepontine Dome (Swiss Alps) and
2472 consequences regarding the tectono-metamorphic evolution of the Alpine orogenic wedge.
2473 *Swiss Journal of Geosciences* 101/Supplement 1, S127–S155. DOI 10.1007/s00015-008-1289-6
- 2474 Wiederkehr, M., Sudo, M., Bousquet, R., Berger, A., Schmid, S.M., 2009. Alpine orogenic evolution
2475 from subduction to collisional thermal overprint: The ⁴⁰Ar/³⁹Ar age constraints from the
2476 Valaisan Ocean, central Alps. *Tectonics* 28.
- 2477 Wiederkehr, M., Bousquet, R., Ziemann, M.A., Berger, A. & Schmid, S.M., 2011. 3-D assessment of
2478 peak-metamorphic conditions by Raman spectroscopy of carbonaceous material: an example
2479 from the margin of the Lepontine dome (Swiss Central Alps). *International Journal of Earth
2480 Sciences* 100,1029–1063. DOI 10.1007/s00531-010-0622-2
- 2481 Willner, A.P., 2005. Pressure–temperature evolution of a Late Palaeozoic paired metamorphic belt in
2482 North–Central Chile (34–35 30' S). *Journal of Petrology* 46, 1805–1833.
- 2483 Winkler, W., Wildi, W., Stuijvenberg, J.V., Caron, C., 1985. Wägital-Flysch et autres flyschs pénniques
2484 en Suisse Centrale: Stratigraphie, sédimentologie et comparaisons. *Eclogae Geologicae
2485 Helvetiae* 78, 1–22.
- 2486 Yamaguchi, A., Ujje, K., Nakai, S., Kimura, G., 2018. Sources and physicochemical characteristics of
2487 fluids along a subduction-zone megathrust: A geochemical approach using syn-tectonic
2488 mineral veins in the Mugi mélange, Shimanto accretionary complex. *Geochemistry,
2489 Geophysics, Geosystems* 13. <https://doi.org/10.1029/2012GC004137>
- 2490 Yamato, P., Brun, J.P., 2017. Metamorphic record of catastrophic pressure drops in subduction zones.
2491 *Nat. Geosci.* 10, 46–50. <https://doi.org/10.1038/NGEO2852>
- 2492 Zanoni, D., Rebay, G., Spalla, M., 2016. Ocean floor and subduction record in the Zermatt–Saas
2493 rodingites, Valtournanche, Western Alps. *Journal of Metamorphic Geology* 34, 941–961.
- 2494 Zhao, L., Paul, A., Guillot, S., Solarino, S., Malusà, M.G., Zheng, T., Aubert, C., Salimbeni, S.,
2495 Dumont, T., Schwartz, S., 2015. First seismic evidence for continental subduction beneath the
2496 Western Alps. *Geology* 43, 815–818.
- 2497 Zhao, L., Malusà, M.G., Yuan, H., Paul, A., Guillot, S., Lu, Y., Stehly, L., Solarino, S., Eva, E., Lu, G.,
2498 2020. Evidence for a serpentized plate interface favouring continental subduction. *Nature
2499 Communications* 11, 1–8.

2500 Zimmermann, R., Hammerschmidt, K., Franz, G., 1994. Eocene high pressure metamorphism in the
2501 Penninic units of the Tauern Window (Eastern Alps): evidence from ^{40}Ar - ^{39}Ar dating and
2502 petrological investigations. Contributions to Mineralogy and Petrology 117, 175–186.
2503

2504

2505

2506

Figure captions

2507

2508 **Fig. 1**

2509 a) General structural map of the Alpine belt (after Handy and Oberhänsli, 2004;
2510 Schmid et al., 2004). The two branches of the Alpine 'ocean', the Valais and Liguro-
2511 Piemont Penninic domains, are outlined in light and dark blue respectively.

2512 b) Highly schematic cross-section (along A-A', ; after Agard and Lemoine, 2005)
2513 illustrating the structural organization of the major paleogeographic domains
2514 recognized in the belt, from the Austro-Alpine units on top to the European units
2515 below. The sub-division into Western, Central and Eastern Alps corresponds to that
2516 adopted in the text. The location of the main geophysical profiles and cross-sections
2517 shown in later figures is indicated (B-B' and C-C'; Fig. 7; D-D': Fig. 12).
2518 Abbreviations: AM: Argentera-Mercantour; AG: Aar-Gotthard; BO: Belledonne-
2519 Oisans; DM: Dora Maira; GP: Gran Paradiso; MB: Mont Blanc; MR: Monte Rosa.

2520 c) Cartoon showing the simplified geodynamic subduction setting of the Alps, with
2521 emphasis on subduction interface processes. The respective location of the Valais
2522 and Liguro-Piemont oceans can be readily deduced from the structural relationships
2523 between the European, Penninic and Austro/Southalpine domains (to be compared
2524 with figure 1b).

2525

2526 **Fig. 2**

2527 a) Close-up view of figure 1a for the Western Alps for comparison with b) and c).
2528 Abbreviations as for Fig. 1.

2529 b) Distribution of metamorphic facies (as in Oberhänsli and Goffé, 2004) within the
2530 ocean-derived units across the same area.

2531 c) Distribution of lithologies across the oceanic units separating the sedimentary-
2532 dominated ('S') domains from those dominated by oceanic crust and serpentinitized
2533 peridotites (i.e., mafic and ultramafic: 'MUM'). See § 3.1, 3.2.

2534 Note the marked W-E zoning in b) and c). For the sake of convenience, the main
2535 sectors of the Western Alps are sub-divisioned into the Combin, Grivola, Maurienne,
2536 Cottian and Queyras (b). The main mafic- and ultramafic-dominated MUM massifs
2537 referred to in the text are shown in c).

2538

2539 **Fig. 3**

2540 a) Representative lithostratigraphic columns for metasedimentary domains of the
2541 Western Alps (after Lemoine et al., 1986; Tricart and Lemoine, 1991; Deville et al.,
2542 1992; Michard et al., 1996; compilation by Epstein et al., 2019). Inset: detailed
2543 section at the base of one of the Queyras units (Tricart et al., 1982).

2544 b) Paleogeography of the Alpine realm at ~120 Ma (Aptian) after Vissers et al.
2545 (2013), at its maximum extent (see § 2.3). Uncertainties are on the order of 100-200
2546 km at least.

2547 c) Schematic 3D view of the Alpine domain at ~120 Ma (compare with b)
2548 emphasizing the highly stretched nature of the continental margins, the presence of
2549 micro-continental blocks (e.g., Briançonnais, Sesia Zone) or extensional allochtons.
2550 The location of the main units discussed in the text is modified after Berger and
2551 Bousquet (2008), Manatschal and Müntener (2009) and Picazo et al. (2016). The
2552 Eoalpine subduction, whose orientation is still debated, is shown to the NE of the
2553 Alpine domain considered here (Froitzheim et al., 1996; Kästle et al., 2019). The
2554 exact location of subduction initiation within the Alpine domain is unknown, but
2555 probably to be looked for to the east, as shown here.

2556 Abbreviations (same as in the following figures, unless specified; Continental
2557 fragments are capitalized): A: Avers; Av: Avic; Bu: Bündnerschiefer; C: Cottian; Ch:
2558 Chenaillet; Co: Combin; DM: Dora Maira; E: Engadine; GP: Gran Paradiso; K:
2559 Koralpe; M: Maurienne; Ma: Malenco; MR: Monte Rosa; MS: Margna-Sella; PI:
2560 Platta; Pm: Piemonte units; Q: Queyras; R: Rechnitz; Ro: Rocciavre; Sa: Saualpe;
2561 SE: Sesia; T: Tauern; Ta: Tasna; Ve: Versoyen; Vi: Monviso; Z: Zermat-Saas.

2562 d) Chronological overview of the main Alpine geodynamic stages. See text for
2563 details.

2564

2565

2566 **Fig. 4**

2567 Typical former oceanic sediments deposited on ophiolitic seafloor (i.e., calcschists,
2568 pelagic limestones and shales, radiolarian cherts; locations in the Western Alps).

2569 a) Characteristic calcschist exposure of the Schistes Lustrés (E. of Aiguilles,
2570 Queyras).

2571 b)

2572 Direct sedimentary contact between serpentinitized and brecciated peridotite criss-
2573 crossed by calcite veins ('ophicalcite') and metasediments (Col d'Urine, Pelvas
2574 d'Abries; see Lagabrielle et al., 2015). The first horizon is a fine-grained mixture of
2575 ultramafic debris and pelagic sediments. The sequence is progressively richer in
2576 sedimentary fraction, then changes to carbonate-dominated. These rocks were
2577 affected by blueschist facies metamorphism.

2578 c-d) Regular alternations of pelitic- (white arrows) and carbonate-rich horizons (black
2579 arrows), overall more carbonate-rich (particularly in d).e) Boudinaged mafic horizon
2580 in impure marble (Zermatt-Saas area).

2581 f) Diagnostic late Jurassic marble horizon (Crête de la Taillante, north of Col
2582 Agnel, Queyras). These tend to be more abundant in the eastern (lower) S units.

2583 g) Carbonates directly overlapping onto a large mafic body (north of Rocca Bianca,
2584 Queyras; see also Lagabrielle et al., 2015).

2585 h)) Large km-scale extensional allochthon in the Haute Ubaye valley (Western
2586 Queyras). The well-stratified dolomitic Triassic limestone from the Peouvou, which
2587 dominates the scenery to the right/east of the picture, is wrapped up in organic-rich
2588 calcschists (left part of the picture). Dm-scale, very fresh blueschist facies carpholite
2589 crystals are found in the scree from landslides reworking the calcschists.

2590

2591

2592

2593 **Fig. 5**

2594 Characteristic features of the metasedimentary (S) units of the Western Alps
2595 (Schistes Lustrés).

2596 a) View across the three main units recognized in the Cottian Alps (near Sestriere),
2597 i.e. the upper, middle and lower S units. Compare with the map of Fig. 7d. Note the
2598 relatively smooth landscape, which partly results from the erodability of the
2599 calcschist-dominated units and the smoother slopes of the more pelitic Lago Nero
2600 unit.

2601 b) View across the main units recognized in the Queyras (following Lagabrielle et al.,
2602 2015; view from Bric froid), the middle, lower and Monviso units (see Fig. 6a for the
2603 extension to the east across MUM units). Note the larger mafic (gabbroic) masses
2604 embedded in the S units (Pelvas d'Abries, Crête des Lauzes).

- 2605 c) Alternation of pelitic- and carbonate-rich horizons. The pelitic fraction is littered
2606 with black lawsonite crystals.
- 2607 d) Microphotograph of fresh mm- to cm-scale lawsonite crystals hosting a significant
2608 fraction of dispersed organic matter (together with rutile) and showing evidence for
2609 growth zoning (Triplex, Fig. 5a; after Lefeuvre et al., 2020).
- 2610 e) Almost pure, very fresh ferro-magnesian carpholite-bearing veins in pelitic schist
2611 (Ubaye valley, Queyras; location in Fig. 4g).
- 2612 f) Lawsonite blueschist facies metabasalt embedded in the upper S unit, preserving
2613 fresh lawsonite and glaucophane (Queyras; courtesy M. Ballèvre).
- 2614 g) Typical chloritoid-bearing calcschist from the lower S unit (Val Clavalité, southern
2615 Aosta valley).
- 2616 h) Strongly deformed chloritoid-chlorite-bearing mica(calc)schist, with phengite
2617 composition attesting to high pressure conditions. Chloritoid is partly retrogressed
2618 here.

2619

2620

2621 **Fig. 6**

2622 Characteristic features of the mafic and ultramafic-dominated (MUM) units of the
2623 Western Alps.

2624 a) View onto one of the best-preserved 'slab' fragments in the world (Fig. 8): the 2-
2625 2.5 km-thick Lago Superiore unit (Monviso massif, Italy; see Fig. 5b for location).
2626 Note the tectonic contact with the overlying blueschist facies Monviso unit, whose
2627 lithostratigraphy is completely overturned. In the Lago Superiore unit, the pristine
2628 lithological succession of the downgoing lithosphere is preserved to a first
2629 approximation with, from bottom to top: ~500m thick serpentized basal peridotites,
2630 eclogitized Mg-rich metagabbros, sills, dykes and a discontinuous layer of Fe-Ti
2631 metagabbros hosting garnet, omphacite, abundant rutile and lawsonite
2632 pseudomorphs, partly retrogressed metabasalts and a few meters of metamorphosed
2633 calcschists at the very top, below the Monviso unit.

2634 b) Eclogite facies metapillows unveiled by glacial retreat (N of Pfulwe pass, Zermatt-
2635 Saas): note the abundance of lawsonite pseudomorphs, particularly around the
2636 former pillows (see close-up view in Fig. 6e; S. Angiboust for scale)

- 2637 c-d) Large, several km-thick metaperidotite bodies of the Avic massif (also noticeable
2638 from the sparse vegetation; location in Fig. 2). Some hm-scale gabbroic horizons are
2639 found here and there, as in c).
- 2640 e) Metapillows, pillow-breccias and surrounding hyaloclastites metamorphosed under
2641 eclogite facies conditions. Note the contrast between the lawsonite-rich rim of the
2642 elliptic former pillow, hydrated during seafloor hydrothermal alteration, and the dry
2643 garnet-omphacite-bearing core. Lawsonite pseudomorphs are ubiquitous across km-
2644 scale exposures between Zermatt and Täsch.
- 2645 f) Metagabbros boudins, with composition intermediate between magnesian and Fe-
2646 Ti rich, in strongly deformed basalts (Zermatt-Saas region).
- 2647 g) Garnet-chloritoid-glaucophane \pm omphacite-bearing metabasalt (Val Clavalité,
2648 Aosta valley).
- 2649 h) Garnet-glaucophane-bearing eclogite with large lawsonite pseudomorphs
2650 (Zermatt-Saas).
- 2651 i) Typical garnet-omphacite-rutile-bearing Fe-Ti-rich metagabbro from the Monviso
2652 massif (Lago Superiore unit, Fig. 6a).

2653
2654
2655

2656 **Fig. 7**

2657 Focus on the metasedimentary-dominated (S) units from the Maurienne to Northern
2658 Queyras, Western Alps. Abbreviations (all others as in Fig. 3c): Amb: Ambin; Br:
2659 Briançonnais; HF: Helminthoid flysch; PF: Penninic front.

2660 a) Schematic crustal-scale section across the Western Alps along profile B-B',
2661 approximately at the latitude of Briançon (see location on Fig. 1a; after Agard et al.,
2662 2009).

2663 b) Close-up, simplified section across the S units along profile C-C' (location in Fig.
2664 7d). Note the fairly regular increase of P-T conditions from west to east.

2665 c) Structural map of the area from the Maurienne to Northern Queyras, showing the
2666 sub-division into three major units (lower, middle and upper S units). In the Queyras-
2667 Cottian Alps, three or four units are recognized depending on latitude and authors
2668 (see § 3.1; the two upper S units are after Lagabrielle et al., 2015). Temperatures
2669 correspond to maximum temperature estimated using the irreversible transformation
2670 of organic matter in the rocks (data and calibration from Beyssac et al., 2002; data

2671 from Gabalda et al. 2009; Plunder et al., 2012; Schwartz et al., 2013). Figure
2672 modified after Vitale-Brovarone et al. (2014a).

2673 d) Simplified structural map of the area embraced by the landscape view of Fig. 5a,
2674 to the east of Sestriere, at the latitude between the Chenaillet and Rocciavre massifs.
2675 Mineral isograds outline the eastward increase in temperature. Phengite isopleths,
2676 which vary from 3.3 to 3.6 Si per formula unit, outline the eastward increase in
2677 pressure. Both are from Agard et al. (2001).

2678 e) Pressure-temperature estimates for the area shown in Fig. 7d (plain ellipses;
2679 updated from Agard et al., 2001, 2002). Dotted ellipses refer to studies further north
2680 in the Maurienne (PI12: Plunder et al., 2012) or further south in the Monviso area
2681 (Locatelli et al., 2018 and references therein; AG20: Angiboust and Glodny, 2020).

2682 f) Boxplots capturing the range of maximum temperatures for the lower, middle and
2683 upper units across the area shown in Fig. 7c.

2684

2685

2686 **Fig. 8**

2687 Strain localization and fluid migration in the MUM fragment of the Monviso massif
2688 (Lago Superiore unit).

2689 a) Eclogite breccia formed by angular fragments of eclogitized Fe-Ti-rich
2690 metagabbros dispersed in an eclogite-facies matrix/cement (Angiboust et al., 2012a;
2691 Locatelli et al., 2018). They reveal the existence of intermediate-depth brittle events,
2692 possibly seismic, during the subduction process. These breccia are found along ~15
2693 km in the Lago Superiore unit (see Locatelli et al., 2019a,b for detailed mapping and
2694 characterization). c) Relocation of the Lago Superiore unit within its past subduction
2695 environment, prior to detachment from the downgoing slab (and that of the Monviso
2696 unit; see Fig. 6a; after Locatelli et al., 2018). The km-scale internal shear zones (LSZ,
2697 ISZ) operated during eclogite facies metamorphism, prior to tectonic slicing along the
2698 basal shear zone now separating the oceanic unit from the continental Dora Maira
2699 massif below.

2700 d) Schematic sequence of events leading to the formation of eclogite breccia (after
2701 Angiboust et al., 2012a).

2702 e) Inferred restoration prior to subduction highlighting the discontinuous nature of the
2703 Alpine oceanic lithosphere (see § 2.2.1). In addition to shear zones formed at ~80 km
2704 depth (as testified by the presence of eclogite brecciation), some initial sedimentary

2705 and/or magmatic contacts were reworked or may have guided deformation during
2706 subduction.

2707

2708

2709 **Fig. 9**

2710 a) Characteristic shape of P-T paths for subducted alpine units. For oceanic
2711 fragments: Engadine (E; after Bousquet et al., 1998, 2002); Valaisan Petit Saint
2712 Bernard (VSB; Bousquet et al., 2002); Cottian Alps (lower, middle and upper units;
2713 Agard et al., 2001a; Plunder et al., 2012; see Fig. 4); Monviso (MV; Angiboust et al.,
2714 2012a; Locatelli et al., 2018); Zermatt-Saas (Groppo et al., 2009; Angiboust and
2715 Agard, 2010). P-T paths for the continental Internal Basement Complexes are shown
2716 for comparison (Dora Maira UHP: after Chopin and Shertl, 1999; Groppo et al., 2007;
2717 Gran Paradiso: Manzotti et al., 2015).

2718 b) Synthetic pressure-time paths of subducted Alpine fragments. Note the contrast
2719 between the early and late subduction period, with no fragments recovered for the
2720 first one. Pressure estimates compiled from the literature and available on request
2721 (see also Berger and Bousquet, 2008, Agard et al. 2009, 2018; Rebay et al., 2018).
2722 Since only rare studies provide closely tied P-T and age, average P-T and time
2723 estimates for peak burial had to be averaged independently. Circle size is indicative
2724 of the number of available age constraints: there are for example at least fourteen
2725 instrumentally well-constrained estimates for the peak burial of Zermatt-Saas area,
2726 north of the Aosta valley (Lu-Hf on garnet: Lapen et al., 2003; Herwartz et al., 2008;
2727 Skora et al., 2015; Bücher et al., 2020); Sm/Nd on garnet: Bowtell et al., 1994; Amato
2728 et al., 1999; Skora et al., 2015; Ar/Ar on phengite: Gouzu et al., 2006; U/Pb on
2729 zircon: Rubatto et al., 1998; Rb/Sr: Barnicoat et al., 1995; Skora et al., 2015).
2730 Constraints on the exhumation path are comprised in the thicker segment. Fewer
2731 studies and ages are available for Monviso (Monié and Philippot, 1989; Duchêne et
2732 al., 1997; Cliff et al., 1998; Rubatto and Hermann, 2003; Rubatto and Angiboust,
2733 2015). Hatched gray boxes refer to exhumation constraints for metasediments
2734 (Agard et al., 2002). Abbreviations as in figure 3c.

2735 c) Schematic tectonic evolution across the Liguro-Piemont domain of the southern
2736 Western Alps (after Agard et al., 2002), from the subduction of oceanic lithosphere
2737 onto continental subduction and finally collision. This evolution, along profile B-B'
2738 (Fig. 7a), is used as a template to compare and evaluate subducted-related tectonic

2739 contrasts along the alpine orogen (see § 4.2, 4.3 and 6, and Figs. 11-14).
2740 Exhumation stages and shear senses (D2,D3) after Agard et al. (2001a) and Plunder
2741 et al. (2012). Similar shear senses were reported by Ghignone et al. (2020). Note the
2742 tectonometamorphic contrast between the S units and MUM units: the latter show
2743 higher P-T values, faster exhumation velocities (Fig. 9a), larger coherent tracts of
2744 mafic units, lithostratigraphic features ascribable to OCT in several locations, and
2745 burial and exhumation during the final stages of the subduction process, a few Ma at
2746 most before the internal crystalline massifs (Fig. 9b). In a broader orogenic
2747 perspective, the Alpine belt can be seen as the result of the imbrication of three
2748 successive, different scale accretionary/decoupling systems: oceanic (between the S
2749 and MUM units), crustal (between continental sediments and deeper subducted
2750 crust), and finally lithospheric (e.g., indentation by the Ivrea body during collision, as
2751 shown by the last step in the figure).

2752

2753

2754 **Fig. 10**

2755 Comparison of P-T estimates for all Alpine subducted oceanic fragments, grouped by
2756 locality, with diagnostic data worldwide (Agard et al., 2018). For the sake of
2757 comparison, P-T estimates shown here are those listed in Agard et al. (2018). Values
2758 for the Central and Eastern Alps, not considered then, are those cited in the text. All
2759 localities align along or close to the subduction P-T gradient for mature subduction.
2760 This observation also allows to rule out significant overpressure in the Alps, since it
2761 would engender variable P/T ratios in the rock record (see additional arguments in §
2762 6.1). Maximum pressures largely differ along strike and in particular no deeply buried
2763 rocks are recovered east of the Simplon/Leponine Central Alps (save possibly for
2764 the small Lanzada fragment: Figs. 12a,c).

2765

2766

2767 **Fig. 11**

2768 a) Idealized restoration of the subduction configuration in the Western Alps during the
2769 Paleocene, at ~60 Ma, after subduction and partial exhumation of the Sesia micro-
2770 continental sliver. The section is a composite one since the Sesia Zone is projected
2771 here laterally onto the Helminthoid Flysch-Monviso traverse (section B-B'; Figs. 1a,
2772 7a). This figure is to be compared with figures 3c, 9c and 14. Particular attention was

2773 devoted to respecting the scales of the units and their distances from one another.
2774 No vertical exaggeration. Tectonic contacts formed during oceanic stages are
2775 featured in grey whereas subduction-related ones are shown in black.

2776 b-d) Tectonic evolution towards the end of oceanic subduction, specifically for the
2777 southern western Alps (i.e., Sector A; Maurienne to Queyras; § 4.3; Figs. 13,14).
2778 Uncertainties concern the age of underplating of the upper S units, or the exact age
2779 of peak burial for Dora Maira, most likely between 40 and 35 Ma (§ 3.3). The
2780 evolution considers peak burial at 46-45 Ma for Monviso (Fig. 9b; see text) and ~ 38
2781 Ma for Dora Maira. Given convergence velocities on the order of 1 cm/a (§ 2.3), the
2782 detachment of the Lago Superiore slice of the Monviso massif (Figs. 6a,8) and part of
2783 its exhumation relate to the entrance of the Briançonnais micro-continent into
2784 subduction. This is even clearer for sector B i.e. for the broad Zermatt-Saas area, as
2785 shown by figure 9b, with the entrance of Gran Paradiso and Monte Rosa.

2786

2787

2788 **Fig. 12**

2789 a) Geological map of the Central Alps (after Schmid et al., 1996, 2004; Wei and
2790 Froitzheim, 2001). Same colors as in Fig. 1a. Maximum temperatures outline the
2791 collisional overprint across the Valais domain (after Wiederkehr et al., 2011).

2792 b) Simplified section across D-D'.

2793 c) Compilation of P-T paths for the Central Alps (see text for references). Light blue
2794 color paths and corresponding stars correspond to localities of the Valais domain
2795 shown in Fig. 12a (see Wiederkehr et al., 2011).

2796 d) Paleogeographic restoration of the Central Alps region shortly after the rifting of
2797 the Liguro-Piemont domain (after Froitzheim et al., 1996; Mohn et al., 2011) showing
2798 key locations of the ocean-continent transitional domain, e.g. the Malenco exhumed
2799 sub-continental mantle, Margna-Sella extensional allochthons and Platta oceanic core-
2800 complex.

2801 e) Idealized restoration of the subduction configuration in the Central Alps during the
2802 Paleocene, at ~60-55 Ma, after subduction and partial exhumation of the Margna-
2803 Sella micro-continental sliver. The exact timing of subduction/exhumation of Malenco
2804 and the Avers (and Lanzada) units are not known with precision (see text for details)
2805 but lie in the range 60-40 Ma. Compare with Fig. 11a.

2806

2807 **Fig. 13**

2808 a) Distribution of the metamorphic facies of all subducted Alpine oceanic domains.
2809 Sectors A-D are defined solely on the basis of marked contrasts in the history of
2810 subducted fragments (see § 4.3 for details). Sector boundaries are indicative (and
2811 therefore drawn as straight lines) since they were certainly deformed by later
2812 collision.

2813 b) Same as a) for sectors A-C featuring the Internal Basement Complexes and the
2814 Sesia Zone: an obvious correlation exists (i) between the spatial extent of the mid-
2815 Penninic internal Briançonnais IBC and the location of deeply buried - yet recovered -
2816 subducted oceanic fragments, and (ii) between the Sesia Zone and sector B (see
2817 text).

2818 c) Similar map with Helminthoid flyschs, Préalpes, External crystalline massifs and
2819 the entire Briançonnais domain for comparison. Note the match between sector B
2820 and the Préalpes or Ivrea body (after Zhao et al., 2015, 2020). Transect C was
2821 strongly affected by continental collision in its western part, which may suggest
2822 further subdivision of this domain.

2823

2824 **Fig. 14**

2825 Idealized view of the Alpine subduction zone at ~40 Ma, showing the relative location
2826 of all fragments discussed in the text. Compare with figure 3c (same abbreviations).

2827 Further work could help relate these lateral contrasts to inherited structures
2828 (Variscan- or rifting-related), differences in incoming material impacting subduction
2829 (e.g., sediment input, magmatic production) or differential kinematics. See text for
2830 details.

2831

2832 **Fig. 15**

2833 Conceptual view of the subducted interface as inferred from the Alpine example, i.e.
2834 for a slow-spreading, discontinuous oceanic domain with a P/T gradient typical of
2835 mature subduction.

2836 a) Inset: key 'ingredients' of the subduction factory, emphasizing mechanical aspects
2837 (i.e. long- and short-term coupling) and fluid release. The dashed area corresponds
2838 to figure b). More generally this zone is mechanically decoupled in the long-run but
2839 transiently coupled/blocked at times, since the plate interface contact steps down into

2840 the slab to strip pieces from it (i.e., the recovered subducted fragments now exposed
2841 in the orogen). Adapted from Agard et al. (2018).

2842 b) Close-up view onto the plate interface. The discontinuous crust and part of the
2843 mantle are sliced off the slab and become the MUM units, while metasedimentary S
2844 units (attesting to a shallower transient stepping-down of the plate contact into the
2845 slab) are commonly underplated preferentially at ~30-40 km depth, near the down dip
2846 end of the seismogenic zone. Deeper underplating also occurs in the southern
2847 Western Alps (middle and upper S units, from the Maurienne to Queyras; Figs. 7c,
2848 11). Note that 'underplating' is loosely used in the literature as synonymous for the
2849 detachment of metasedimentary units from the slab and possible plastering below
2850 the upper plate, but the mechanics and triggering of this process are probably not
2851 different from that detaching MUM units (save for the depth of the décollement).
2852 Metasedimentary slices, however, seem to return more slowly to the surface (Fig.
2853 9b). Detachment of tectonic slices/fragments probably takes place along former
2854 tectonic discontinuities (shown in grey as for figure 11; see Figs. 8c,e) and along
2855 newly formed ones (shown as black). The latter case can be demonstrated in
2856 Monviso, for example, with shear zones formed at intermediate-depth and bearing
2857 evidence for past brittle events (yellow stars; most likely earthquakes), or in Lanzo
2858 (past earthquakes marked by pseudotachylites).

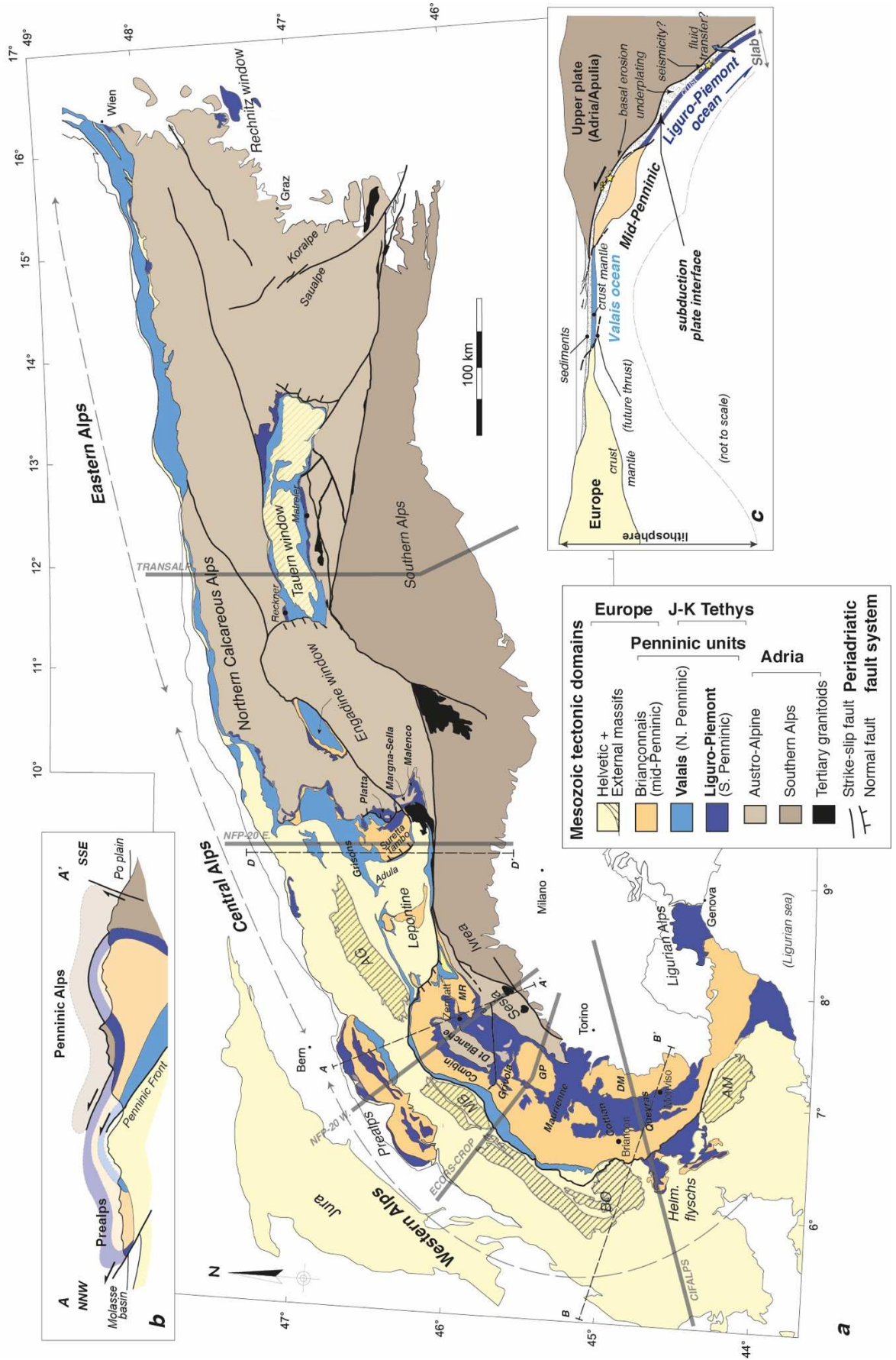
2859 A number of studies have dealt with element/fluid transfer across and along the
2860 interface/channel, to characterize fluid composition and provide some assessment of
2861 fluid migration. It is hoped that the present sketch will prove useful to set back future
2862 observations. So far, however, no proven fragment from the mantle wedge has been
2863 recovered in the Alps, and none that would have been paired with a deep tectonic
2864 slice from the downgoing slab. This is a major limitation for the assessment of
2865 effective element/fluid transfer to the mantle wedge and extrapolation to sub-arc
2866 depths.

2867

2868

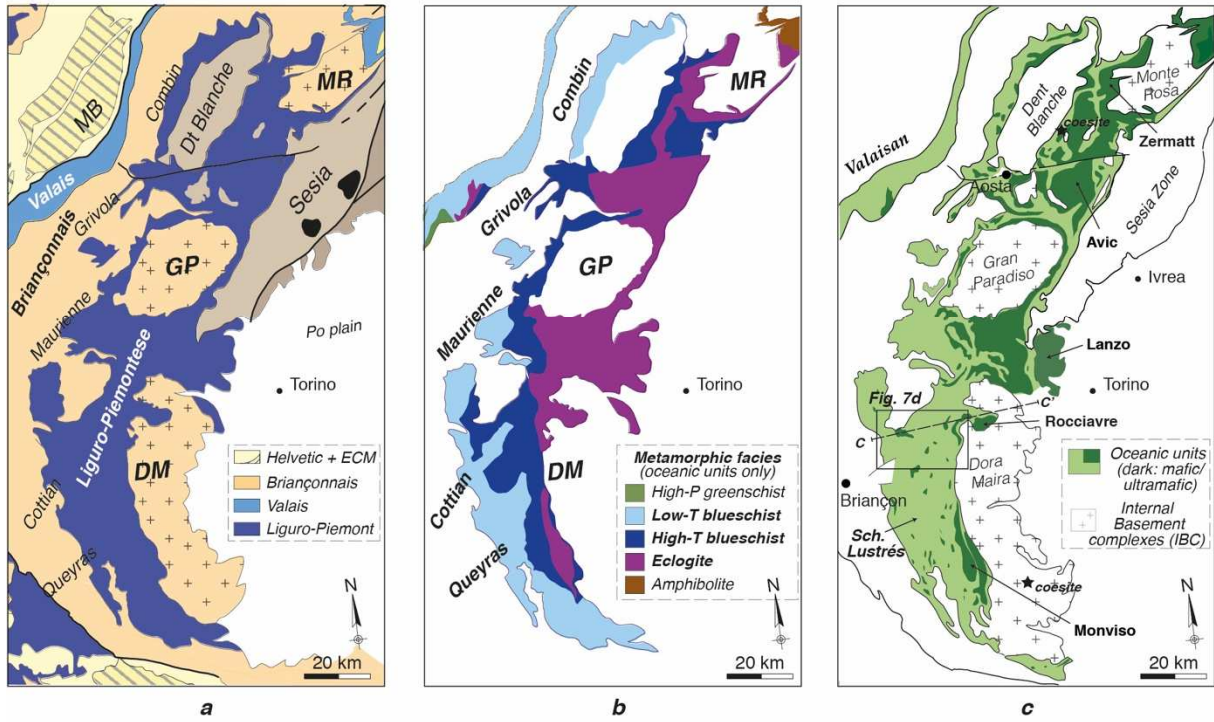
2869

Fig. 1



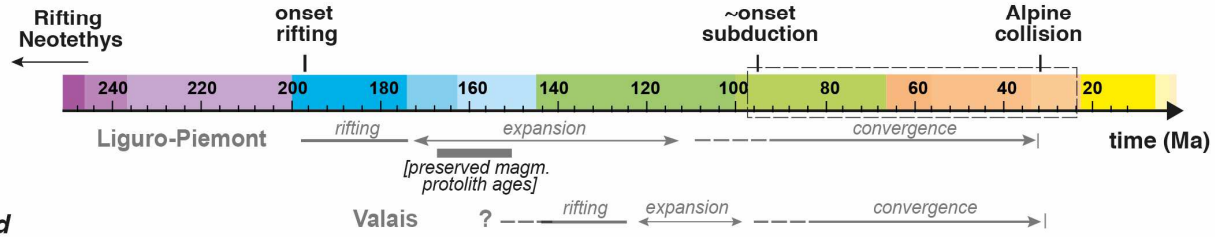
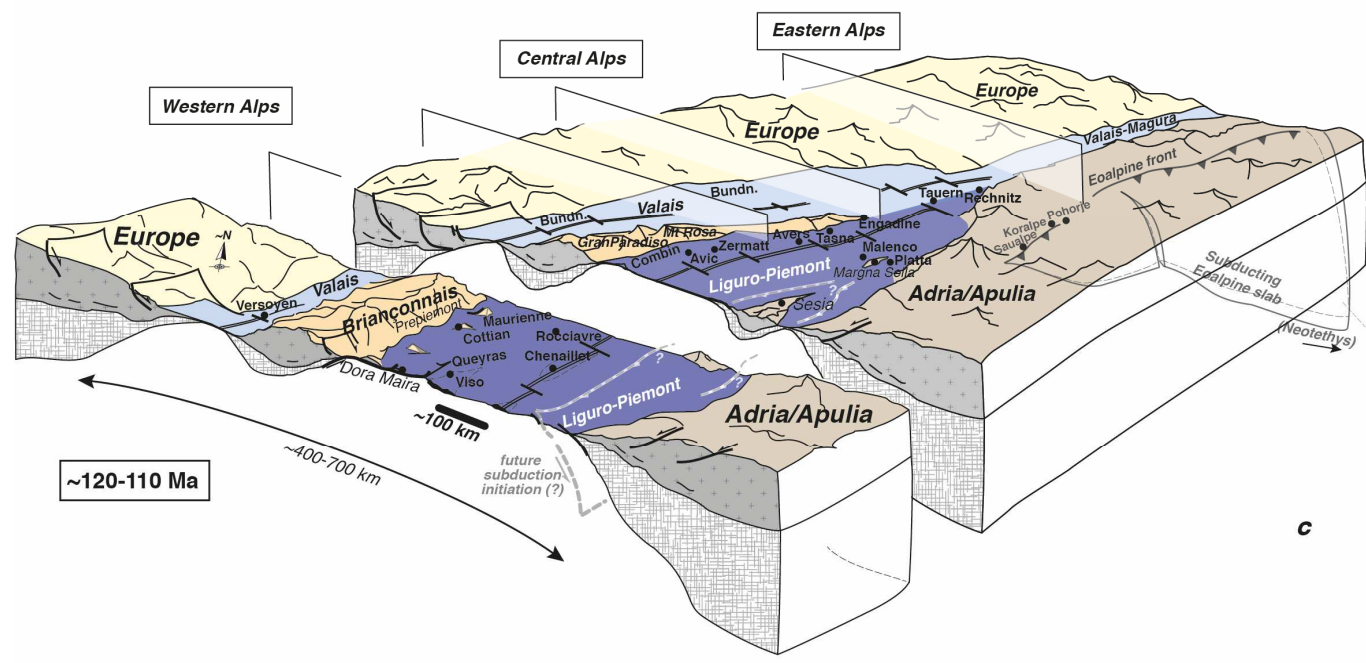
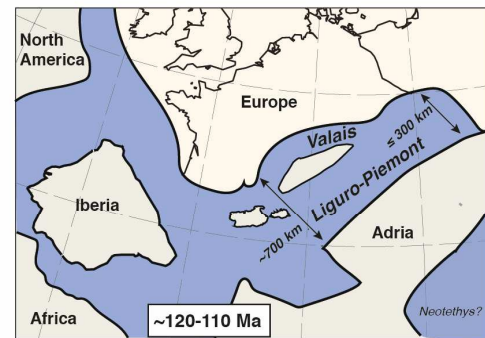
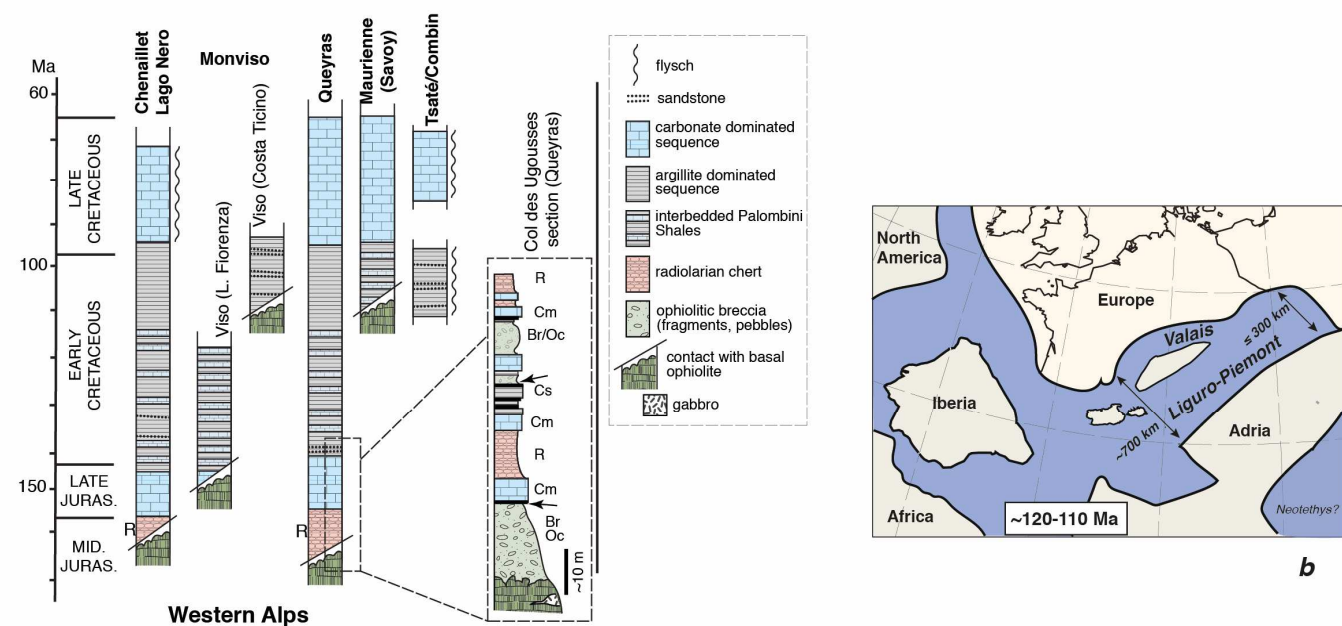
2870
2871

Fig. 2



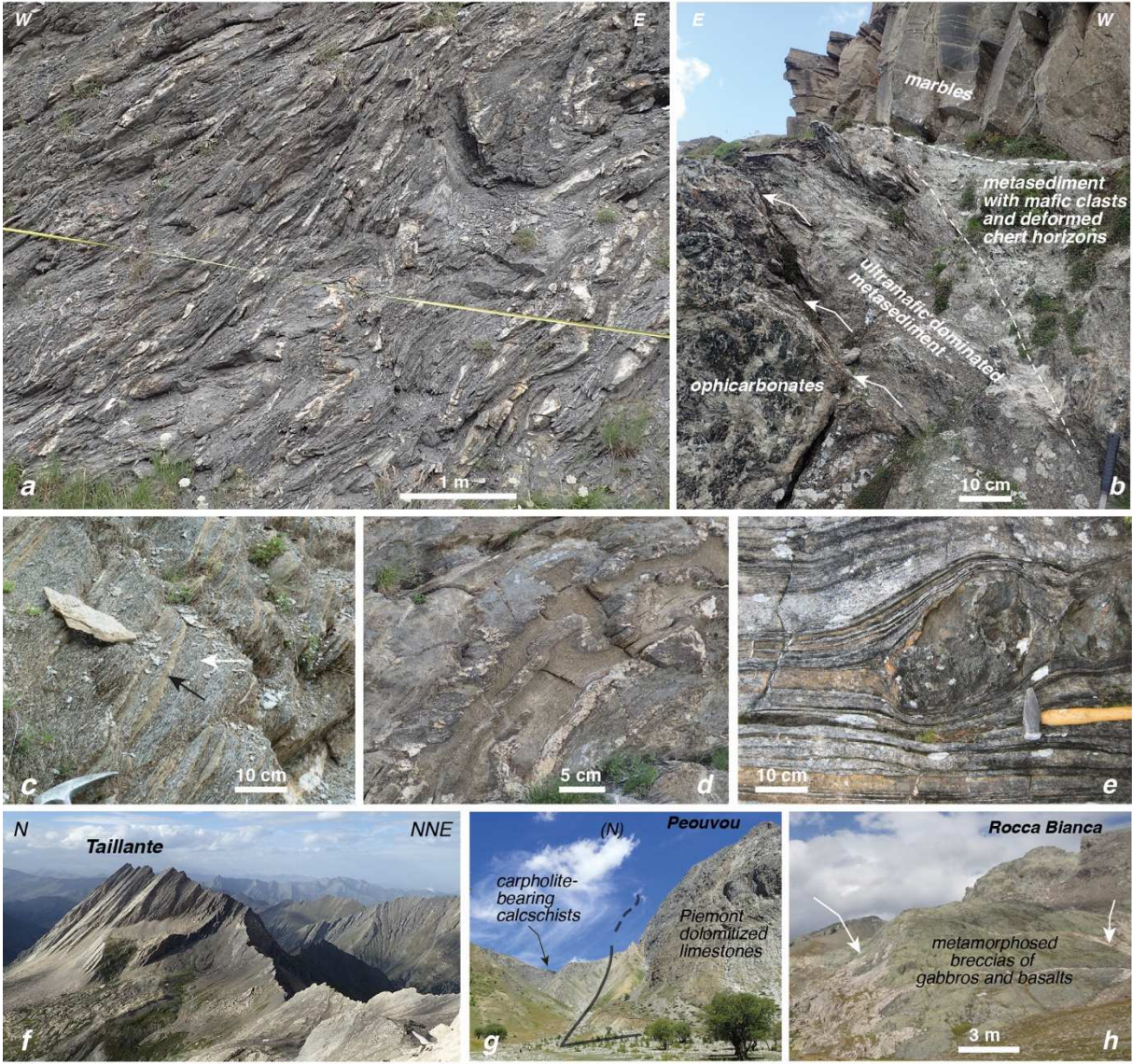
2872

Fig. 3



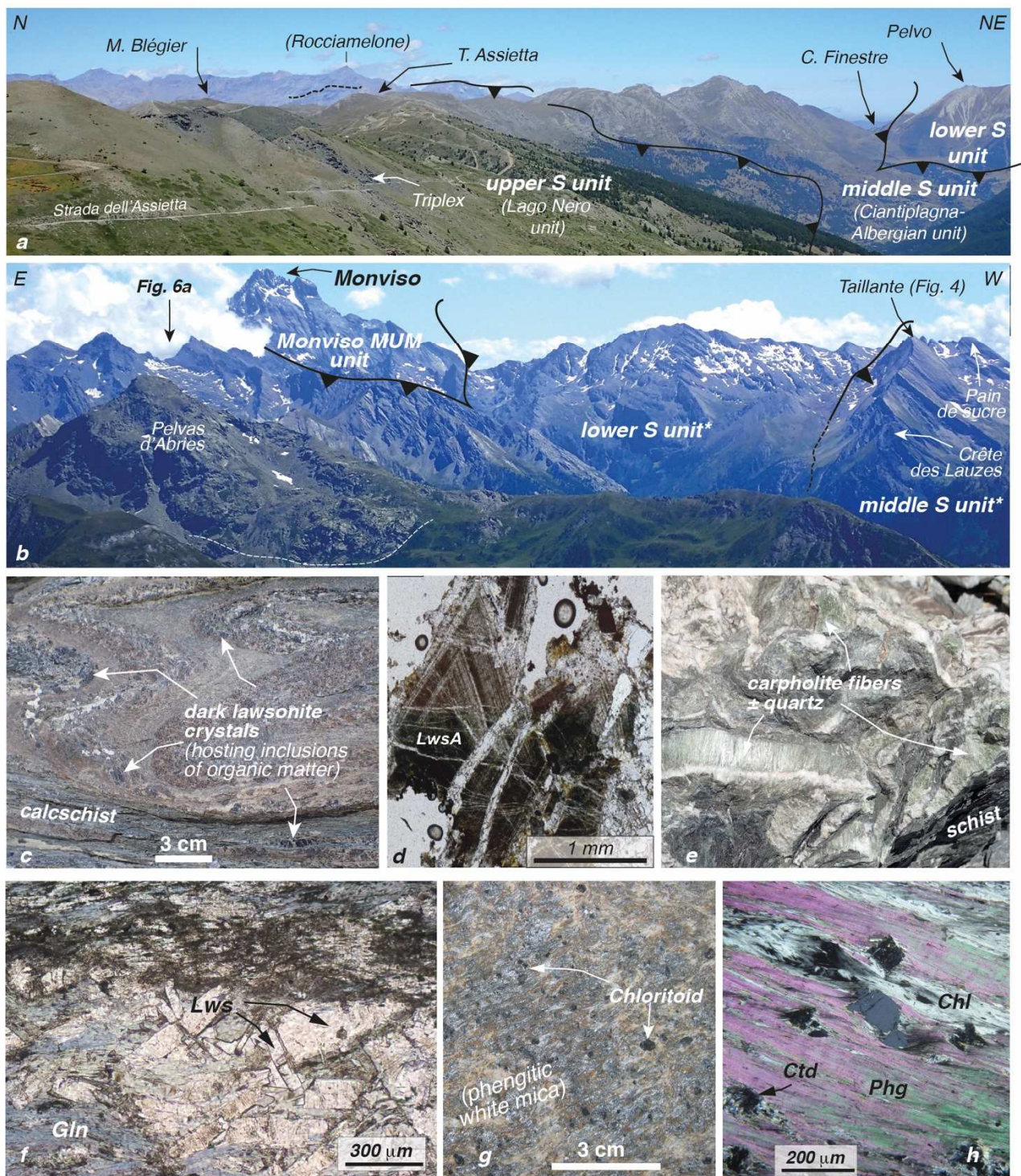
2873
2874

Fig. 4



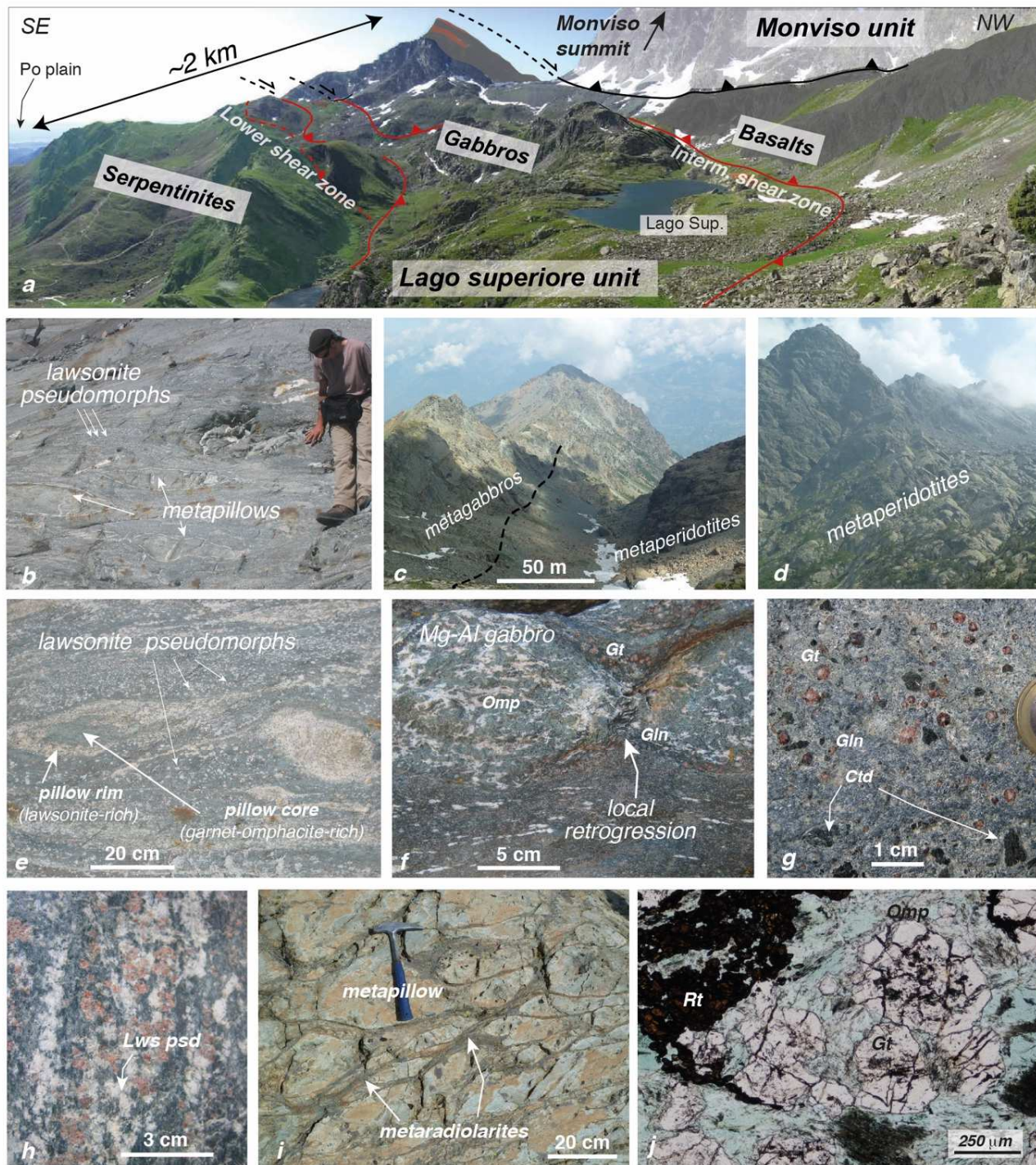
2875
2876

Fig. 5



2877
 2878

Fig. 6



2879
2880

Fig. 7

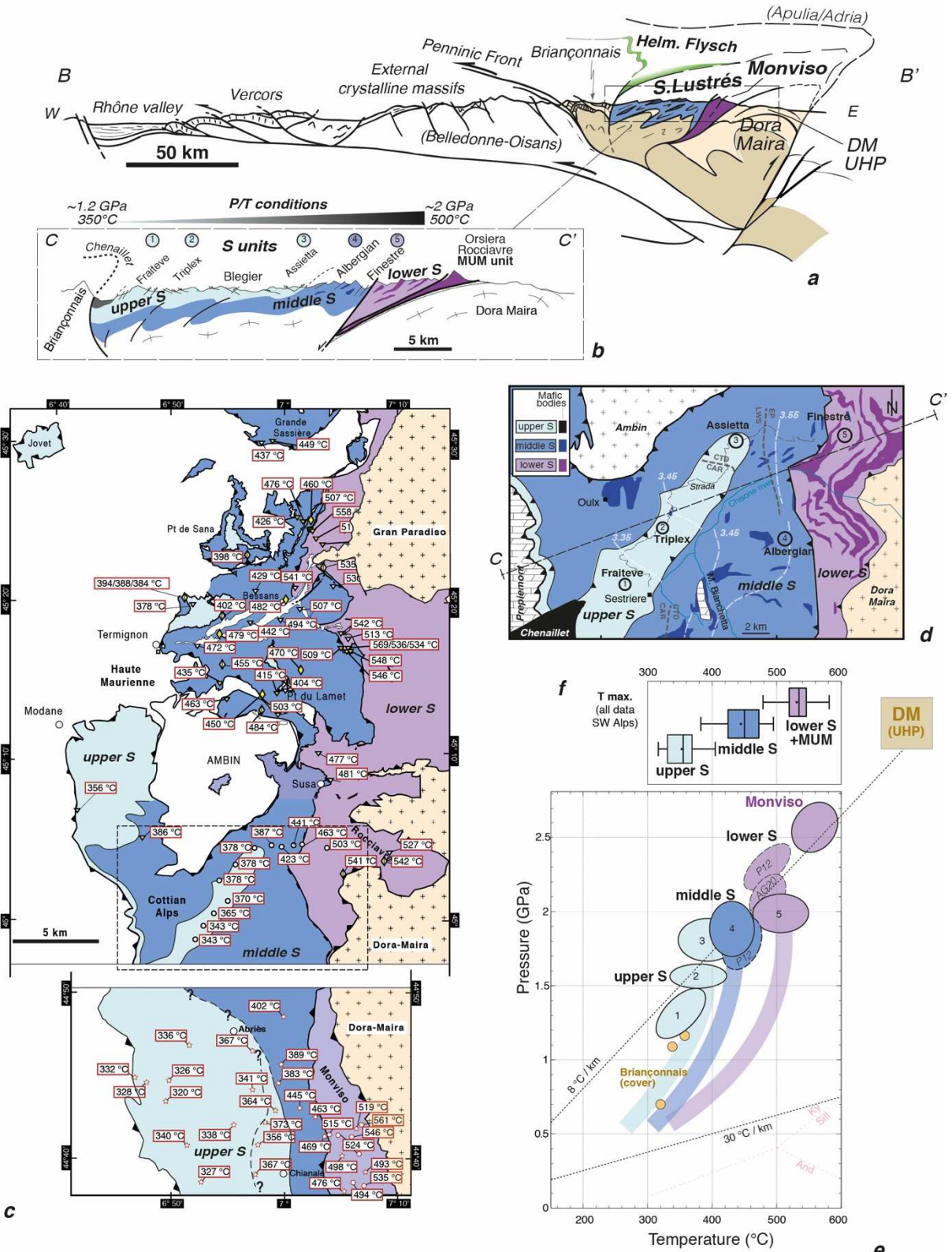
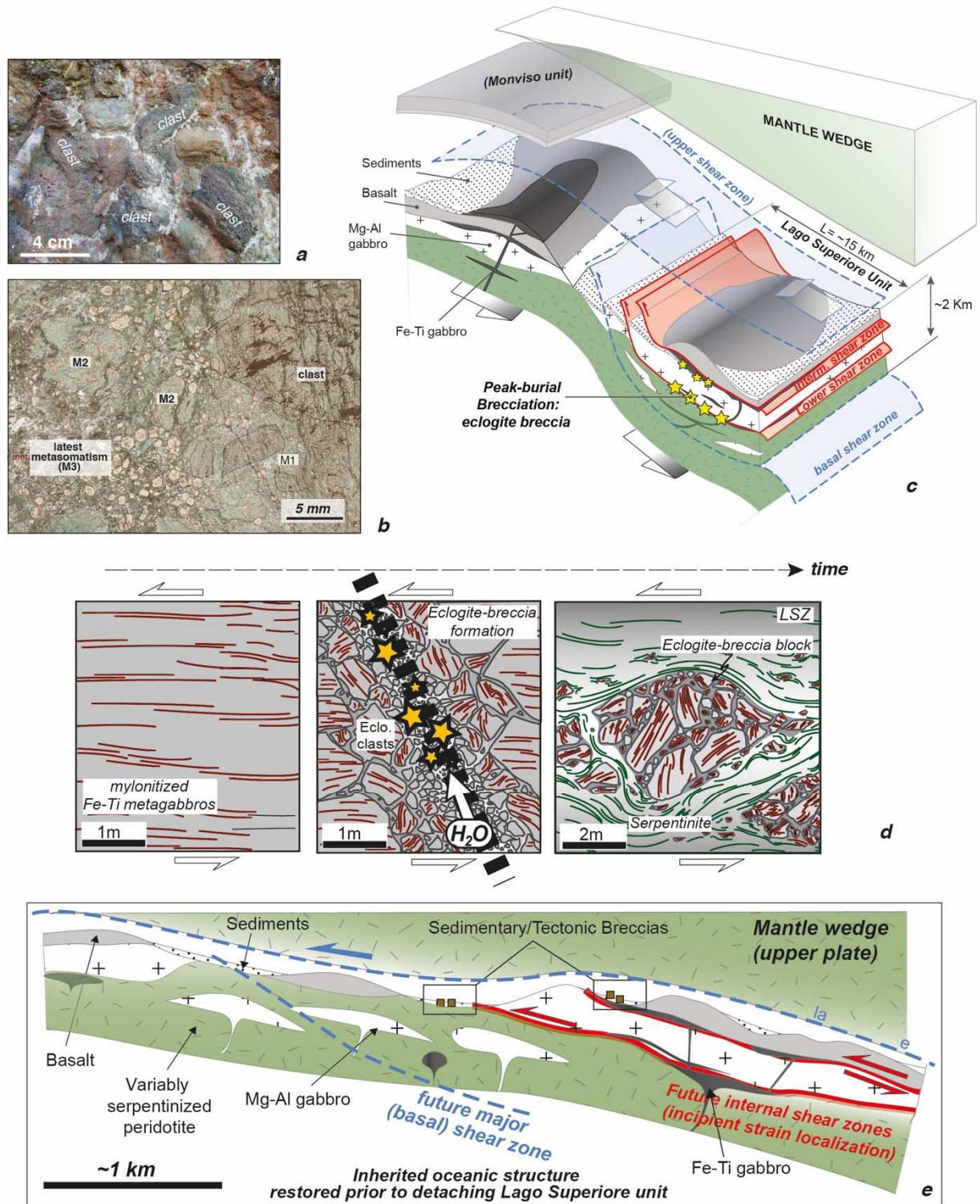
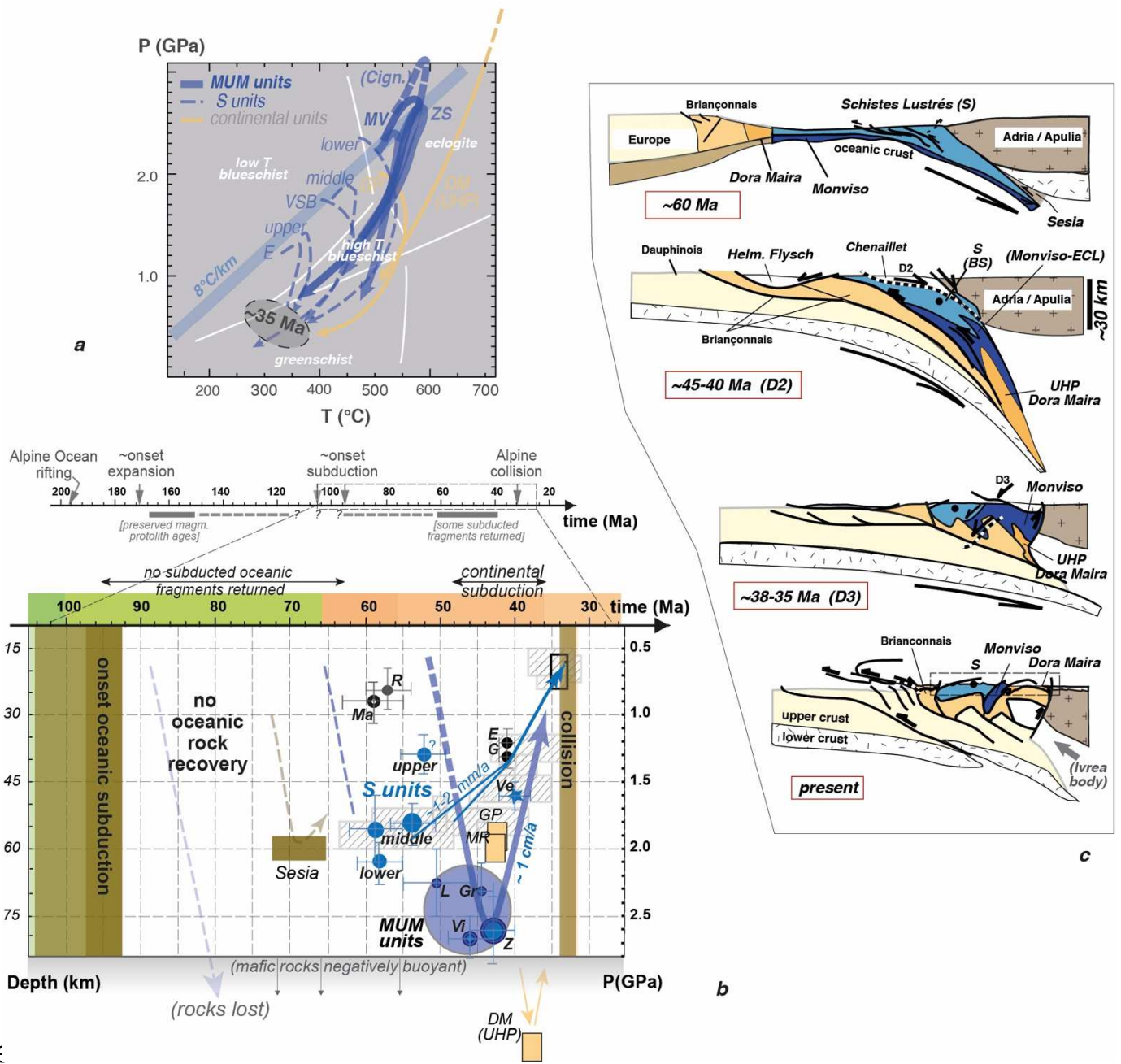


Fig. 8



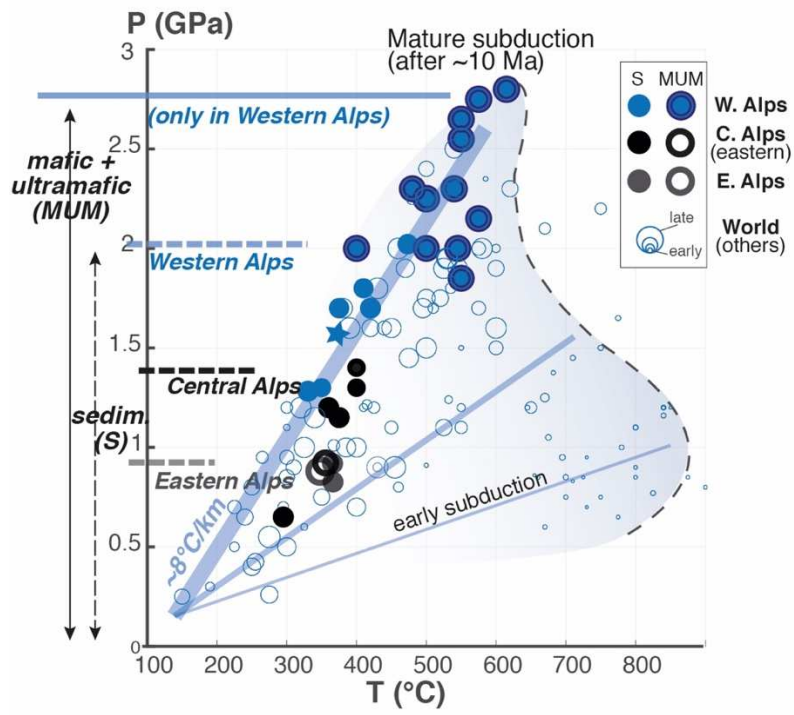
2882

Fig. 9



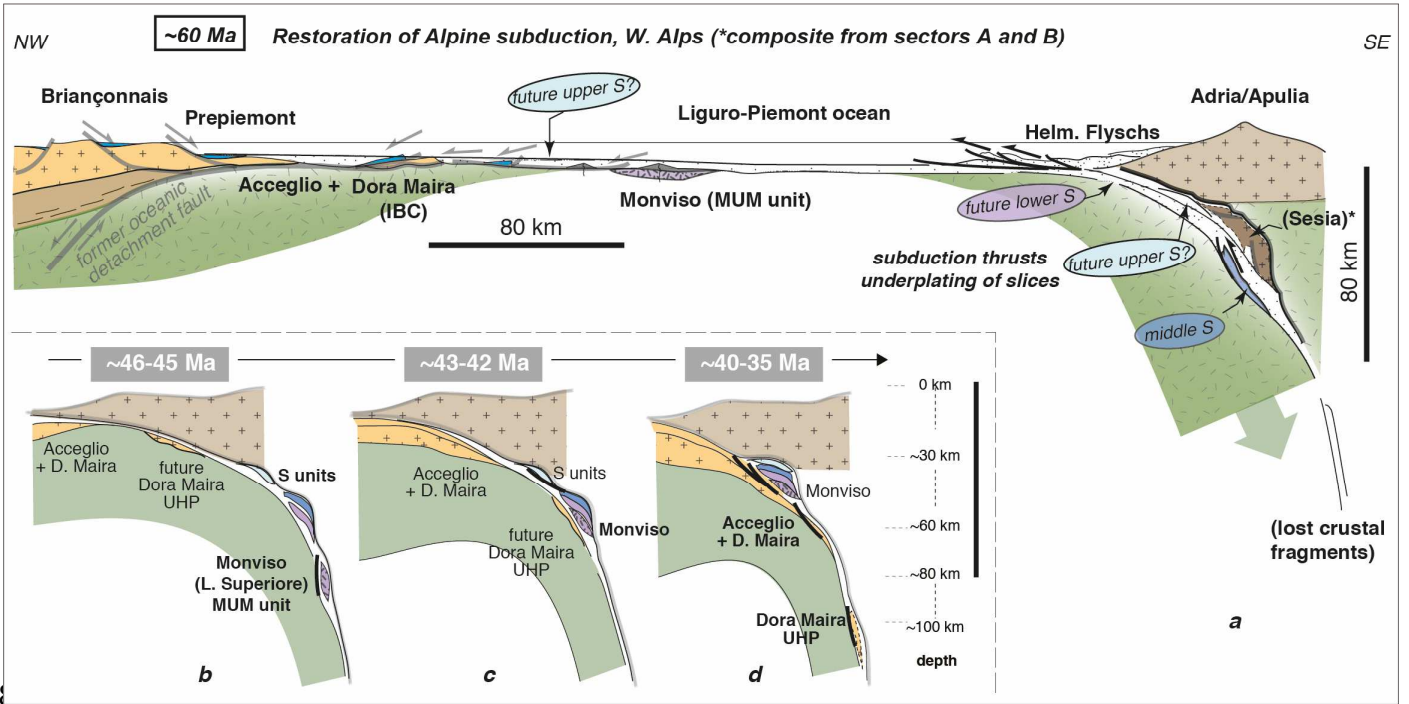
288:
 2884

Fig. 10



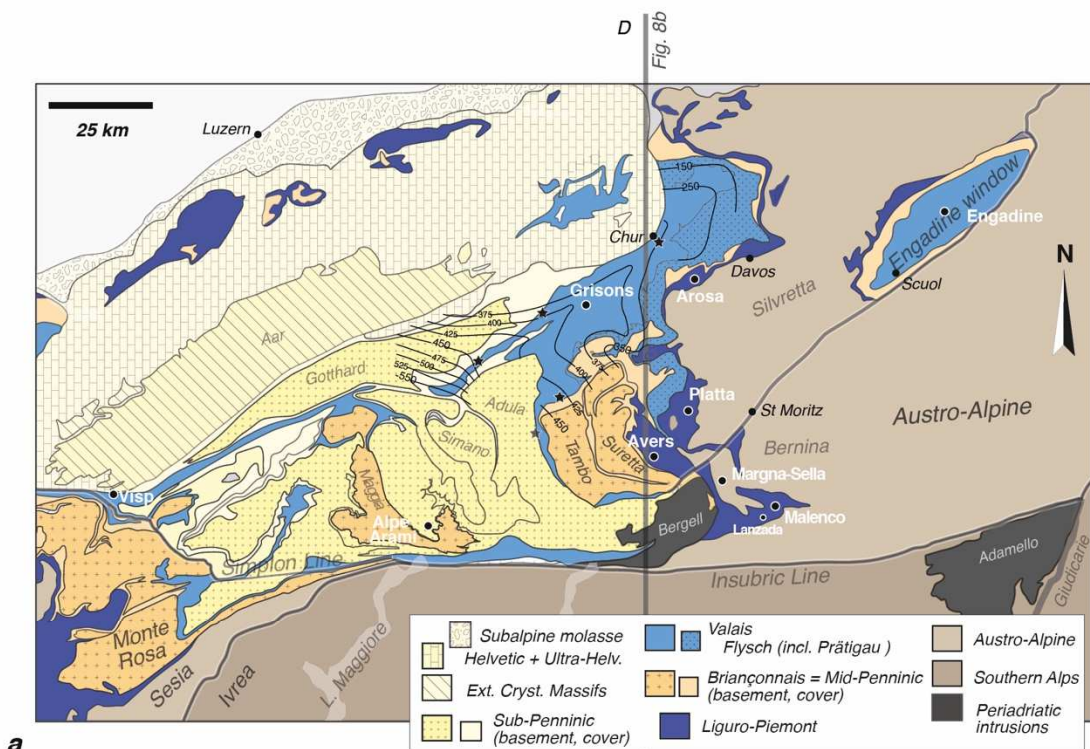
2885

Fig. 11

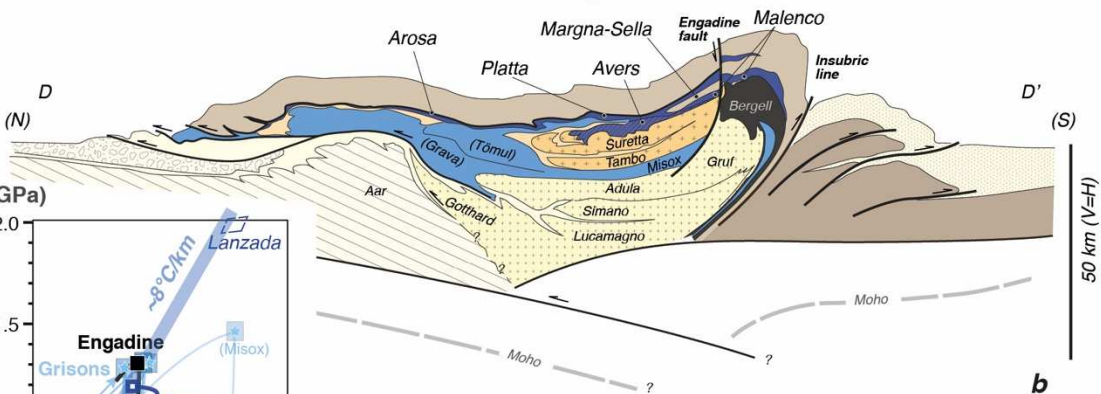


288
2887

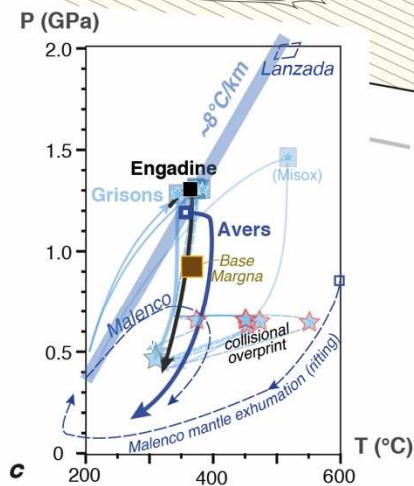
Fig. 12



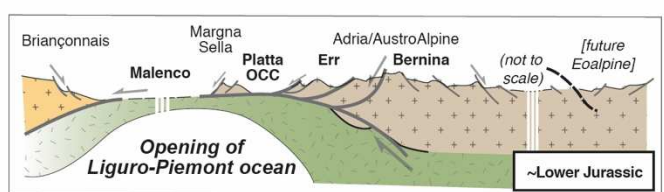
a



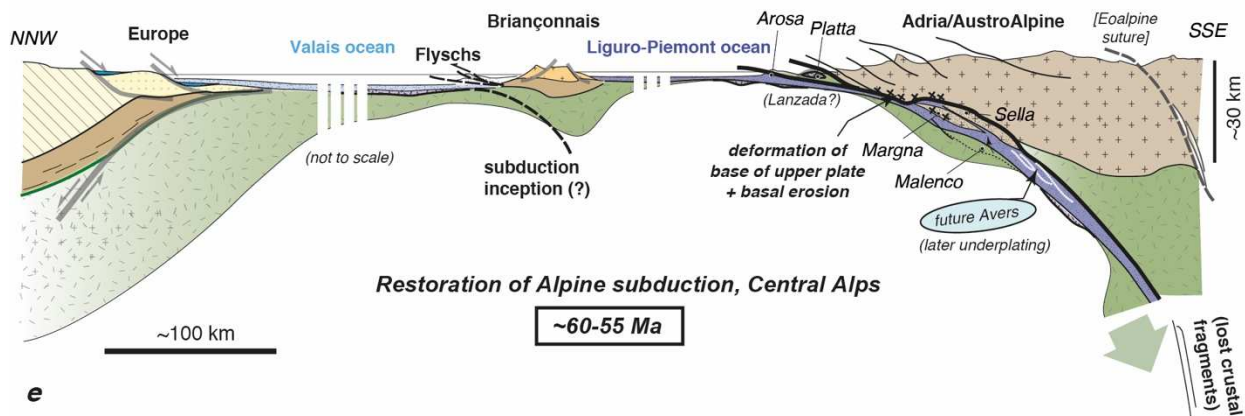
b



c



d



e

Fig. 13

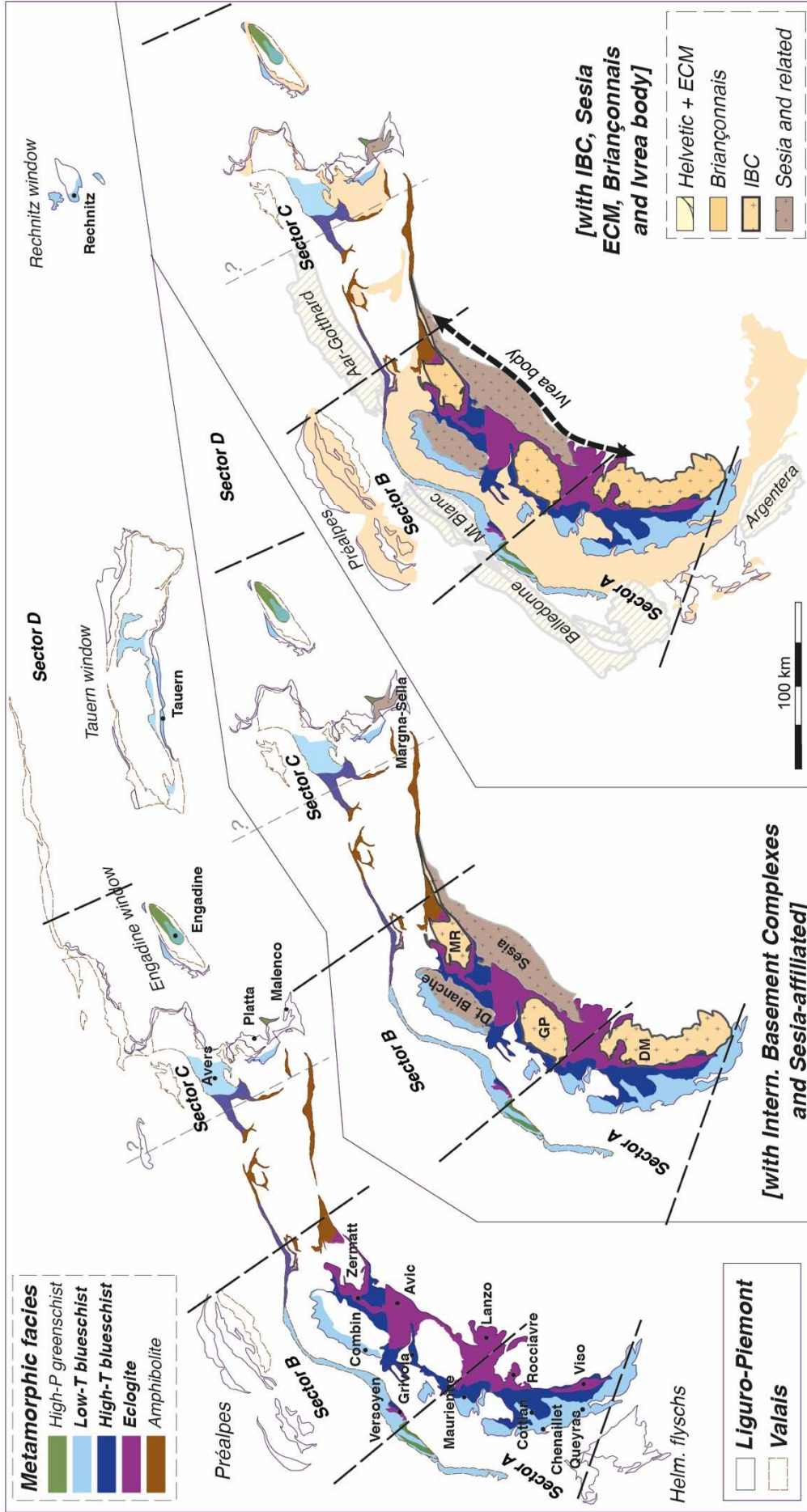


Fig. 14

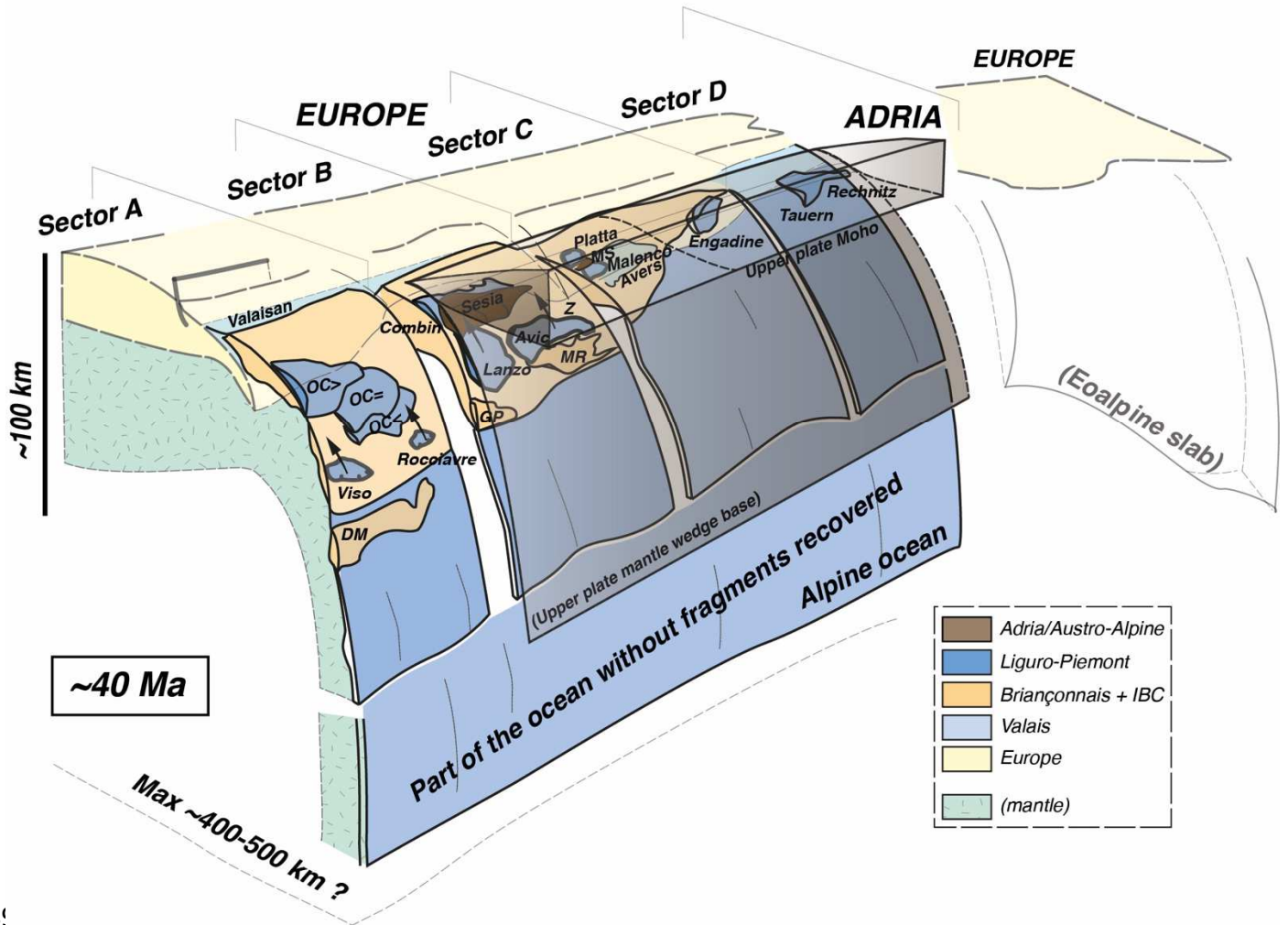
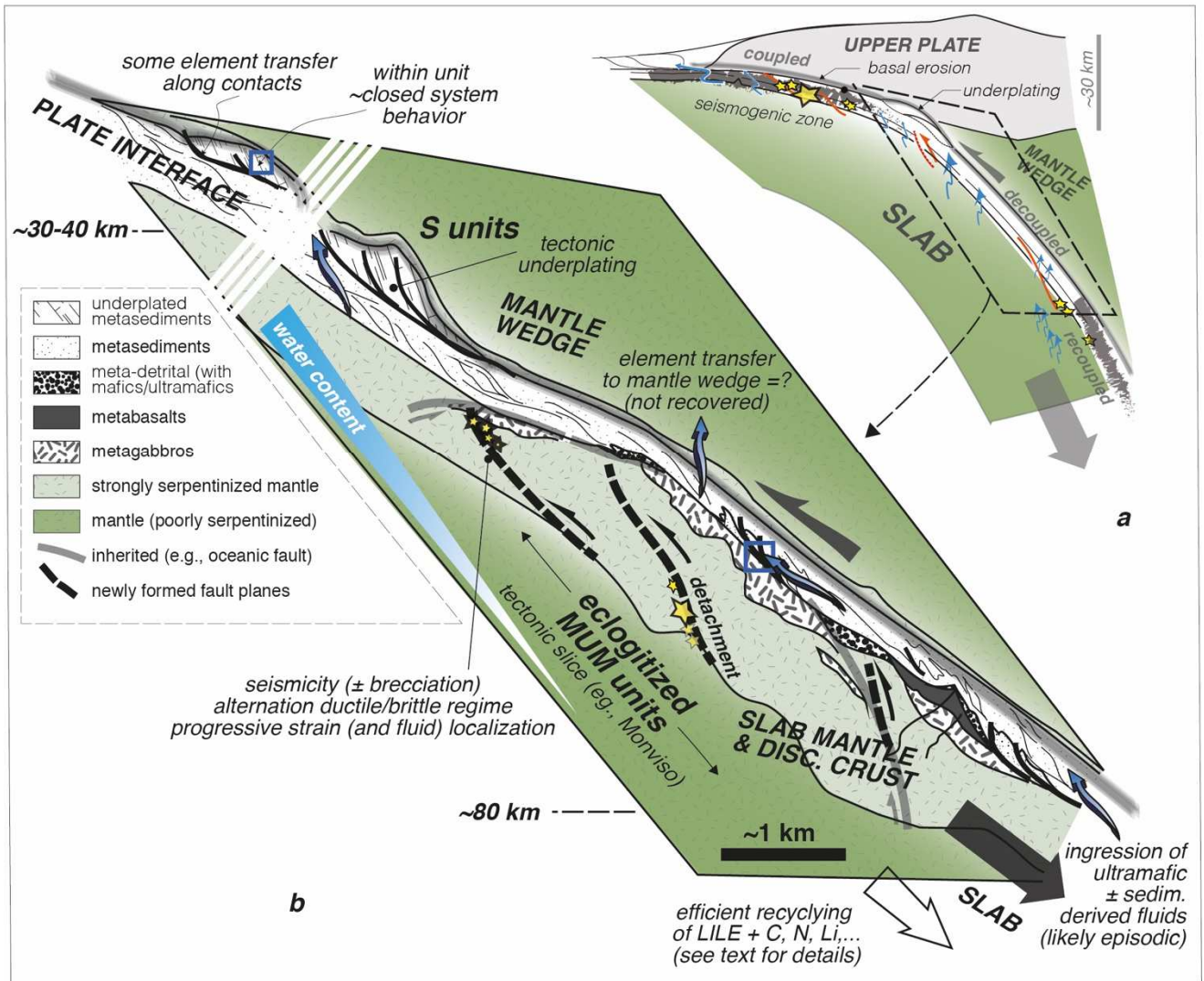


Fig. 15



2891
2892

2893

2894